Forensic Applications of Infrared Spectral Imaging

by

Katherine Bojko

A thesis submitted for the degree of

Doctor of Philosophy (Science)

University of Technology, Sydney

February 2008

Certificate of Authorship and Originality

I certify that the work in this thesis has not previously been submitted for a degree nor has it been submitted as part of requirements for a degree except as fully acknowledged within the text.

I also certify that the thesis has been written by me. Any help that I have received in my research work and the preparation of the thesis itself has been acknowledged. In addition, I certify that all information sources and literature used are indicated in the thesis.

Production Note:
Signature removed prior to publication.

Katherine Bojko (nee Flynn)

21st February 2008

Acknowledgements

There are many people who gave me advice, assistance, support and encouragement throughout my PhD research, and to all of you I offer my most sincere thanks.

I would like to offer my particular thanks to both of my supervisors for their guidance, ideas, advice, encouragement and involvement in many ways in my project. A big thankyou goes to Brian Reedy for your initial project idea and for your involvement in numerous ways throughout the research ... I could not have asked for a more dedicated supervisor and I thank you for everything you have done over the past five years. Thankyou to Claude Roux for encouraging me to do a PhD in the first place, without your encouragement I may not have ventured down this path. Thank you to both of you for the time spent providing feedback on my work.

I would like to acknowledge all the people who have helped me in different ways throughout my PhD research, whether it be providing me with samples or sharing their knowledge and providing assistance in using equipment. Thanks goes to Katie McBean for your help with the ESEM imaging of bicomponent fibres, and to David Royds (AFP), Thomas Biermann (BKA), Steffen Dillinger (BKA), and the Trevira Fibre Company for providing me with bicomponent fibre samples. I would like to thank Ed Bartick (FBI/Suffolk University) for sending me fibre literature and allowing us access to his infrared library database. I would also like to thank Phillip Maynard for allowing me to use the paint samples collected during his 1996 study, and for his assistance in using various equipment in the forensic laboratories. Thanks also go to Jacki Stitt, Jim Brandi, and Brenda Woods from the AFP, for

answering my many questions involving document analysis and trace evidence analysis.

During the intersecting lines research there were a number of times where I required assistance from others. I would like to thank the 'anonymous' document examiners who volunteered their valuable time in examining the blind samples using techniques regularly employed in casework. Thanks also to one document examiner in particular for your time taken to provide feedback on the research in general, and on the draft of the journal article on this research. I would also like to thank Liz Chan, Mark Tahtouh, Alison Beavis, Lisa Mingari, Christie Wallace-Kunkel, Fiona Burger and Matt Foot for either preparing my blind samples or providing me with materials for the intersecting lines work. Thanks also Mark for building a new macro-ATR clamp when the other one broke!

Partway through my research I decided to convert to part-time study, and began employment with the NSW Police Force. I would like to thank my colleagues and the NSW Police Force for supporting my PhD in kind by allowing me study time each week, as without this assistance it would have been a whole lot longer before I finished.

A huge thankyou goes to my fellow PhD buddies who have made the PhD journey all the more enjoyable (even if you did make the PhD take longer than it would have otherwise if there had been no "board/bored" meetings and especially UNO)! You

are a fantastic bunch and I will miss you guys! I hope we can keep in touch and I wish you all the best for your future.

Finally I would like to thank my family for their continual support and encouragement throughout this PhD, and for believing I would get there in the end ... eventually! To my husband Nick, thank you for putting up with all the time I've spent studying ... for the six years we have known each other I have been studying for all but about 3 months. I thank you for all your love, support and encouragement over the years.

Table of Contents

List of Figures

List of Tables

List of Publications

Types of Publication	Number	Reference
Papers Published in Refereed Journals	3	[1,2,3]
Oral Presentations at Conferences	5	[4, 5, 6, 7, 8]
Poster Presentations at Conferences	6	[9, 10, 11, 12, 13, 14]

1. Flynn, K., O'Leary, R., Lennard, C., Roux, C., Reedy, B. J. "Forensic Applications of Infrared Chemical Imaging: Multi-Layered Paint Chips" Journal of Forensic Sciences 2005;50(4):832-41.

2. Flynn, K., O'Leary, R., Roux, C., Reedy, B. J. "Forensic Analysis of Bicomponent Fibers Using Infrared Chemical Imaging" Journal of Forensic Sciences 2006;51(3):586-596.

3. Bojko, K., Roux, C., Reedy, B. J. "An Examination of the Sequence of Intersecting Lines using ATR-FTIR Spectral Imaging" Accepted for publication in Journal of Forensic Sciences, 2008.

4. Flynn, K., Reedy, B. J., Roux, C., Tahtouh, M., O'Leary, R., Lennard, C. "Forensic Applications of Infrared Chemical Imaging" Presented at the 17th International Symposium on the Forensic Sciences, Australian and New Zealand Forensic Science Society, Wellington, NZ March 2004

5. Flynn, K., Reedy, B. J., Roux, C. "Determining the Sequence of Intersecting Lines Using Infrared Chemical Imaging" Presented at the 17th Meeting of the International Association of Forensic Sciences, Hong Kong, China August 2005.

6. Reedy, B. J., Flynn, K., Tahtouh, M., Burger, F., Roux, C. "Infrared Chemical (Hyperspectral) Imaging: Applications in Forensic Sciences" Presented at the 17th Meeting of the International Association of Forensic Sciences, Hong Kong, China August 2005.

7. Reedy, B. J., Flynn, K., Tahtouh, M., Burger, F., Rutlidge, H., Kalman, J., Doble, P., Roux, C. "Forensic Applications of Infrared Chemical Imaging" Presented at the 6th Australian Conference on Vibrational Spectroscopy, Sydney, Australia September 2005.

8. Flynn, K., Roux, C., Reedy, B.J. "Further Forensic Applications of Infrared Spectral Imaging" Presented at the 18th International Symposium on the Forensic Sciences, Australia and New Zealand Forensic Science Society, Fremantle, WA, Australia April, 2006.

9. Flynn, K., Reedy, B. J., Roux, C., Lennard, C. "Applications of Infrared Chemical Imaging to Questioned Document Examinations" Presented at the 17th International Symposium on the Forensic Sciences, Australian and New Zealand Forensic Science Society, Wellington, NZ March 2004.

10. Flynn, K., Reedy, B. J., Roux, C., Lennard, C. "Examination of Line Crossings by Infrared Chemical Imaging". Presented at the 57th Annual Meeting of the American Academy of Forensic Sciences, New Orleans, LA, USA February 2005.

11. Flynn, K., Reedy, B. J., Roux, C. "Infrared Chemical Imaging of Bicomponent Fibers" Presented at the 17th Meeting of the International Association of Forensic Sciences, Hong Kong, China August 2005.

12. Flynn, K., Reedy, B. J., Roux, C. "Determining the Sequence of Intersecting Lines Using Infrared Chemical Imaging" Presented at the 6th Australian Conference on Vibrational Spectroscopy, Sydney, Australia September 2005.

13. Flynn, K., Reedy, B. J., Roux, C. "Infrared Chemical Imaging of Bicomponent Fibers" Presented at the 6th Australian Conference on Vibrational Spectroscopy, Sydney, Australia September 2005.

14. Tahtouh, M., Flynn, K., Walker, S., Roux, C., Reedy, B. J. "FTIR spectral imaging applications in trace evidence" Presented at the National Institute of Justice (NIJ)/Federal Bureau of Investigation (FBI) Trace Evidence Symposium, Clearwater Beach, Florida, USA August 2007.

Abstract

Fourier transform infrared (FTIR) spectral imaging is emerging as an exciting new tool in forensic analysis. This technique is capable of simultaneously collecting thousands of infrared spectra using an array detector, thus yielding both spectral and spatial information with extremely fast collection times. The aims of this research were to examine potential forensic applications of FTIR spectral imaging, in particular in the physical evidence area.

Infrared spectral images of multilayered paint chips have been successfully obtained, with the chief advantage over conventional infrared analysis being that thousands of infrared spectra are collected in a few minutes across the whole paint sample. As with conventional infrared spectroscopy, chemical species can be identified from their spectra, but there are also a number of different ways to make multi-component spectral (and hence chemical) comparisons between two samples easy to visualise and understand. Infrared spectral images of two paint chips being compared side-by-side can be viewed as a "movie", in which each frame is an intensity map of the two samples at a given wavenumber (frequency) value. In another approach, the spectra in the image files are classified into chemically similar groups, resulting in a "cluster" image that makes it possible to simultaneously compare all of the layers in two paint chips.

Bicomponent fibres are a special class of fibres that comprise two polymers of different chemical and/or physical properties. In over 50% of the bicomponent fibre

samples analysed, infrared spectral imaging was able to spatially resolve two spectroscopically distinct regions when the fibres were examined side-on. The technique provided characteristic infrared spectra of each component and images which clearly illustrated the side-by-side and sheath-core configuration of these components in the fibre. It was possible to prepare and image a cross-section of one of the fibres, but in general the preparation and analysis of fibre cross-sections proved very difficult. A number of infrared sampling techniques were investigated and spectral imaging results were compared with those obtained using conventional fibre microscopy techniques.

Attenuated total reflectance (ATR) FTIR spectral imaging was shown to be successful for determining the sequence of heterogeneous line intersections produced using ballpoint pens and laser printers. By imaging at the particular frequencies corresponding to the functional groups specific to the ballpoint pen ink and toner materials, it was possible to form spectral images showing their spatial distribution. It was possible to determine whether the ink was above or below the toner, by examining whether there was a gap present in the ink spectral image at the point of intersection with the toner. Blind tests were performed and the results obtained using ATR-FTIR spectral imaging were directly compared to those obtained by experienced forensic document examiners using methods regularly employed in casework. ATR-FTIR spectral imaging was shown to achieve a 100% success rate in the blind tests, whereas some incorrect sequence determinations were made by the forensic document examiners when using traditional techniques. The technique was

unable to image ink-jet printing, gel pens, roller ball pens and felt-tip pens, and was also unable to determine the sequence of intersecting ballpoint pen lines.

Overall, infrared spectral imaging was shown to be a successful technique for analysing multi-layered paint chips, bicomponent fibres and determining the sequence of intersecting ballpoint pen and toner lines. In the past five years, there has been a significant increase in the number of reported forensic applications of infrared spectral imaging. It is anticipated that this technique will continue to grow in importance as a tool for forensic scientists over the next decade, and that infrared spectral imaging will find a regular place in forensic laboratories.

CHAPTER 1:

Introduction

Chapter 1: Introduction

Forensic science is broadly defined as the application of science to law. There are a wide range of evidence types that can be encountered such as glass, paint, DNA, fingerprints, fibres, drugs and questioned documents. Consequently, there is also a very wide range of instrumentation and analysis techniques that are employed in forensic analysis. With technology continually evolving, it is important that forensic scientists explore new developments that may prove to be superior to techniques currently in use in forensic laboratories. This is vital to ensure that the most informative techniques, providing both timely and reliable results, are used. Chemical imaging is one such new development and is emerging as an exciting new tool for forensic scientists. This research evaluates the technique of infrared spectral imaging, a significant technological advancement, and explores the potential it holds for forensic analysis.

1.1 Infrared Spectroscopy

1.1.1 What is Infrared Spectroscopy?

Infrared (IR) spectroscopy is a widely used analytical technique which allows for the molecular (and hence chemical) characterisation of materials. Infrared spectroscopy is an extremely versatile technique as both qualitative and quantitative information can be obtained from a sample, and the technique has the capability to analyse samples in either the gaseous, liquid or solid form. The technique of infrared spectroscopy is based on the vibrations of the atoms of a molecule and the interaction of infrared light with matter. The infrared region of the electromagnetic spectrum

spans from 12,800 to 10 cm^{-1}, and can be further subdivided into the near-infrared (12,800 – 4000 cm^{-1}), mid-infrared (4000 – 200 cm^{-1}) and far-infrared (200 – 10 cm^{-1}) regions (1). The mid-infrared region is the most commonly used spectral range for analytical applications, and is the range examined throughout this research project.

As mentioned above, the technique of infrared spectroscopy is based on the vibrations of atoms within molecules. A molecule does not consist of atoms fixed rigidly in place. Rather, its atoms are constantly moving due to various types of vibrations. There are two main categories of vibrations, these being stretching and bending. When atoms are undergoing a stretching vibration, the interatomic distance along the axis of the bond between the two atoms is continuously changing (i.e. the bond length is changing). The stretching vibration can be either symmetric or asymmetric. A bending vibration occurs when the angle between two bonds is changed. The four types of bending vibrations are scissoring, rocking, wagging and twisting (1, 2).

When infrared radiation is passed through a sample, an infrared spectrum is obtained by determining what percentage of radiation is absorbed by the sample at particular energies or frequencies. A sample will only absorb incoming radiation of the same frequency as a vibration of part of the molecule. An infrared spectrum is a graphical representation of the vibrational modes of a sample, and by examining the frequencies where infrared radiation has been absorbed, and what percentage of incident radiation is absorbed, it is possible to identify the molecular structure of a sample, and also determine how much is present (as the amount of incident radiation

absorbed is directly proportional to the amount of compound present, among other things) (2).

1.1.2 Forensic Applications of Infrared Spectroscopy

Infrared spectroscopy is a widely-accepted technique for the analysis of many types of forensic samples. There are a number of advantages of the technique including its ability to provide both qualitative and quantitative chemical information, the sampling versatility, and the ability to rapidly analyse a sample, often with little to no sample preparation. There are a number of ways infrared spectroscopy is used for forensic analysis, from identifying the composition of an unknown material to comparing the composition of two materials to determine if they could potentially be from the same source. There have been a number of review papers covering the use of infrared spectroscopy in forensic analysis (3-7).

The development of Fourier Transform Infrared (FTIR) spectroscopy, and the coupling of microscopes with infrared spectrometers, has led to a great increase in applications in forensic science, due to the enhanced speed, sensitivity and selectivity of the technique. Prior to the development of Fourier Transform IR, dispersive IR spectrometers were generally useful for the analysis of bulk samples such as drugs (7). The coupling of a microscope and FTIR spectrometer, together known as FTIR microspectroscopy, has the great advantage that microscopic-sized samples can be analysed, with little to no sample preparation required. The development in sampling accessory technologies, such as diffuse reflectance accessories, diamond anvil cells (DACs), and attenuated total reflection (ATR) accessories, has also helped

to make FTIR microspectroscopy one of the most useful and versatile techniques in a forensic laboratory. The sampling accessories used throughout this PhD research are further discussed later in this chapter.

There is a wide range of evidence types that can be analysed using FTIR spectroscopy including, but not limited to, paint (8-13), fibres (14-19), drugs (20, 21), explosives (22), documents (e.g. inks, toners, paper) (23-29), adhesives (29, 30), soil (31) and drugs in hair (32, 33). Further information regarding FTIR analysis of the forensic evidence types examined throughout this PhD can be found in Chapters 2-4.

Most forensic laboratories have at least one FTIR microscope. To assist in identifying unknown materials, a wide range of infrared library databases have been established such as the Georgia State Forensics Drug Library, the Synthetic Fibers Library, the Toronto Forensic Library and the Hummel Polymer and Additives Library. One of the most recent advances in FTIR analysis in forensic science has been the development of field-portable FTIR instruments, such as the TravelIR®, which means that analysis can be conducted in real-time at a crime scene (34). The other major advancement in FTIR technology is the development of FTIR spectral imaging, which has been largely unexplored for the analysis of forensic evidence.

1.2 Chemical Imaging in Forensic Science

Chemical imaging is emerging as an exciting new tool for forensic analysis. Broadly speaking, chemical or hyperspectral imaging is the ability to map the spatial distribution of chemical species across a sample surface. It allows for the visual enhancement of the sample and the chemical identification of its components. Since spectroscopy is one of the most important tools for identifying and quantifying chemical species, a chemical (hyperspectral) image is usually constructed by collecting multiple spectra in the frequency (ν) or wavelength (λ) range of interest in an array across the sample. The resulting dataset consists of intensity values at each position in an $x \times y \times \lambda$ datacube (Fig. 1.1). The data can be represented and analysed in a number of different ways. It can be visualised as a spectrum at each pixel in the image, or as series of $x \times y$ images, one for each wavelength value collected in the spectrum. The latter visualisation represents the simplest form of chemical imaging, since a particular wavelength may correspond to a spectral band of a specific molecule, and thus an image at this wavelength will selectively map the distribution of that molecule across the sample.

The very large three-dimensional datasets collected by most chemical imaging instruments contain a wealth of information that is not always accessible using the simple visualisations mentioned above. For this reason, multivariate statistical techniques are often employed to reduce the data and/or classify the spectra, and thus form more informative images than the raw data.

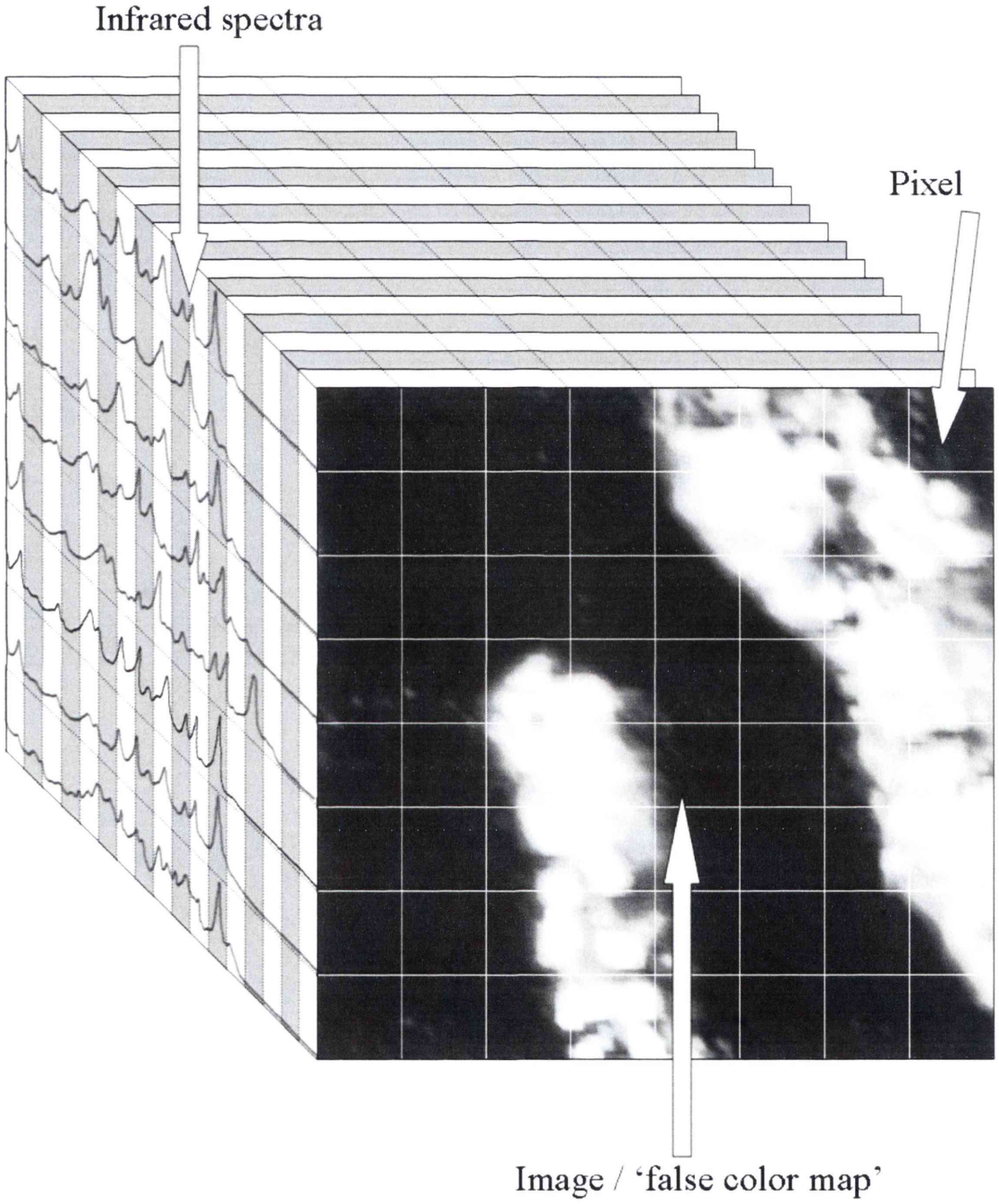

Figure 1.1: *Diagrammatic representation of 'datacube' generated by focal plane array (FPA) detector (reproduced with permission from Reference (35))*

The potential of chemical imaging in forensic science has been apparent since instrumentation became available in the late 1990s. Some of the techniques currently available include UV-visible/fluorescence imaging (36), near infrared (NIR) imaging (37), Raman mapping and imaging (38), mid-infrared mapping and imaging (39), and compositional mapping using electron microprobe analysis (40, 41). All of these techniques can, in theory, be applied in forensic situations. Infrared and Raman mapping (as distinct from imaging) are now the poor relations of chemical imaging in that they require the point by point acquisition of spectra across the sample, an extremely time-consuming process. However, technological improvements in the areas of array detectors, liquid crystal tunable filters, infrared interferometers and computing power in recent years have meant that true mid-infrared and Raman chemical imaging systems are becoming available to the forensic scientist (35).

Chemical imaging in the visible and NIR spectral regions is currently being investigated to gain improved contrast and discrimination in the imaging of fingerprints, paints, tapes and adhesives, inks and firearm propellants (36, 42, 43). Raman chemical imaging has been explored for the forensic analysis of synthetic fibres and condom lubricants (44, 45). Overall the findings have shown that chemical imaging offers forensic scientists several key advantages, such as the ability to display both visual and spectral (hence chemical) results side-by-side, and in ways that are easier for lay persons (such as jurors) to understand. Chemical imaging is also a non-destructive analysis for many of the evidence types examined, thus preserving the evidence for future analyses, and it also offers the advantage of reduced sample preparation, reducing the risk of contamination (43).

Infrared spectral imaging and Raman spectral imaging have enormous potential in forensic science because of their greater chemical specificity compared with UV-visible spectral imaging techniques. This specificity comes from the sheer abundance of narrow, highly resolved bands in the vibrational spectrum of even relatively simple molecules, and the fact that these bands correspond to particular functional groups of the molecules. As a simple example, the UV-visible spectrum of a colourless polymer may contain as few as one or two broad UV absorptions that may do little to distinguish the polymer from similar or even quite dissimilar materials. The addition of a coloured dye to the polymer may introduce one or two broad absorptions into the visible region of the spectrum, but the ability to spectroscopically distinguish this sample from others with similar colouration (especially those identically dyed) is limited.

The vibrational (mid-infrared or Raman) spectra of the polymer will, however, usually contain at least several (but often dozens of) sharp bands corresponding to specific structural components of the molecule that enable it to be differentiated even from closely related structures. Infrared (or Raman) spectra can be used to precisely identify materials in a heterogeneous sample; when collected in the form of an image, the spectra can be used to map the spatial distribution of the different chemical components of the sample to a resolution of around 15 μm (for mid-infrared imaging) or better (Raman imaging) (46).

1.3 FTIR Spectral Imaging

1.3.1 Development of FTIR Spectral Imaging

Prior to the development of FTIR spectral imaging, a process called infrared mapping was employed to obtain spatially resolved chemical information from a sample. This process involves the sequential point-by-point acquisition of individual spectra across a sample surface, using a computer-controlled motorised stage. This technique suffers from a number of drawbacks. Infrared mapping is inefficient for very small samples or those which are smaller than the detector element, and the spectrum obtained of the sample will contain excess noise (as only a small part of the detector is receiving an IR signal, yet noise results from the entire detector). To overcome this problem, apertures can be used to restrict the data collection from a smaller area, however this will reduce the amount of infrared signal passing through, and in turn will reduce the signal-to-noise ratio of the acquired data. To obtain spectra with an adequate signal-to-noise ratio, it is recommended that apertures should only be used to reduce the sampling area to as small as a ~ 20 μm x 20 μm square (47). Aperture sizes of less than 20 μm approach the wavelength of the infrared light being used, and so the spectral range which can be observed is reduced with decreasing aperture size (19). Another major drawback of infrared mapping is that the time taken to map a sample can be extremely long (hours, or even days) (48).

The limitations encountered in IR mapping have largely been overcome with the development of FTIR spectral imaging, which employs a focal plane array (FPA) detector. A FPA detector contains a large number of discrete detectors (or pixels) laid out in a grid pattern. FPA detectors were originally developed for astronomical

or military purposes (such as heat seeking missiles or night-vision for aircraft or vehicles), and due to the military interest their availability was initially restricted for classified projects (49, 50). It was not until 1995 that the first commercial mid-IR spectral imaging instrument was available. This instrument utilised a indium antimonide (InSb) 128 x 128 pixel FPA detector, but this detector only allowed for data to be collected in the spectral region of 4000 – 2000 cm^{-1} (51). In 1997, Digilab released a mid-IR spectral imaging system which employed a mercury-cadmium-telluride (MCT) FPA detector, which can collect data from the spectral region of 4000-900 cm^{-1} (49). Several types of FPA detectors have been developed, with a wide range of detector sizes, from 16 x 16 up to 1024 x 1024 pixels (although the cost increases substantially with the larger arrays). Some infrared imaging instruments employ 'linear' array detectors, as opposed to 'focal plane' array detectors. A 'focal plane' array detector consists of a grid (i.e. more than one row and column) of detector pixels, whereas a 'linear' array detector consists of a single row of detector pixels. Systems using a linear array detector are generally cheaper, however a smaller area is imaged. To obtain a larger image using a linear detector, it is necessary to stitch together multiple images, and instruments using this technology have been referred to as a hybrid of imaging and mapping (52). The term 'focal plane' in FPA refers to the fact that the array detector is positioned at the focal plane of the microscope, and effectively a 'snapshot' of the sample is projected onto the array detector. Further details on the various detectors available can be found in Kidder et al (50).

At present, the most common mid-IR detector used for spectral imaging is the 64 x 64 pixel MCT FPA detector, which is the detector employed in the instrument used throughout this research (50). This detector contains 64 x 64 discrete detectors (or pixels) laid out in a grid pattern. Each pixel detector is capable of collecting a spectrum from an individual small area on a sample. Using this array detector, 4096 spectra can be obtained simultaneously in the form of an image, with one spectrum recorded for each pixel, therefore allowing both spectral and spatial information to be obtained from a sample in a short period of time. This is in contrast with conventional infrared spectroscopy, where only one spectrum can be collected at a time. In approximately the same amount of time taken by a conventional spectrometer to collect a single spectrum, this relatively new technology can simultaneously collect thousands of spectra using an array detector, and thus map the spatial distribution of chemical species across a sample. The image data collected can be thought of as a three-dimensional datacube, which contains vertical (x) and horizontal (y) spatial dimensions, and a spectral frequency domain (z) (see Fig. 1.1) (35). In other words, at every point (x, y) on the sample, an infrared spectrum is collected (z). There are a number of different ways that the data can be visualised, including selecting a particular point on the sample and obtaining the infrared spectrum at that location, or forming images ("false colour maps") based on the spectral intensity at particular frequencies. In the latter case, the data can be viewed as a series of images, with one image at each wavenumber resolution unit.

A number of parameters can be used to form spectral images including peak height, peak area, or ratios of areas or heights at different frequencies of interest. A false

colour map is formed by assigning an arbitrary colour to each pixel according to the intensity of the particular parameter selected. Most commonly, a scale from high intensity red to low intensity blue is used (the scale used throughout this research), but other options such as greyscale are available. By imaging at frequencies corresponding to the vibrations of chemical functional groups, the spatial distribution of different chemical components in the sample can be seen.

As discussed previously, in IR mapping experiments the spatial resolution will typically be limited to around 20 μm, and the process involves the use of apertures to physically restrict the data collection area. However, in IR spectral imaging, as there are 4096 discrete detectors each of which collects a spectrum from an individual small area on the sample, there is no such need to use apertures, and the spatial resolution is effectively determined by the wavelength of the light and the pixel size of the FPA detector. In a typical image dataset, the spatial resolution varies depending upon the wavelength chosen to form the image. Previous studies have demonstrated that a spatial resolution of approximately 16 μm can be achieved using transmission FTIR imaging, and, with micro-ATR imaging, a higher spatial resolution of around 5 μm is possible (46). The spatial resolution in micro-ATR imaging is dependent on the refractive index of the ATR crystal material employed. In general, the higher the refractive index of the ATR crystal, the better the spatial resolution achieved, but this advantage is offset by a reduction in the field of view. Further information regarding spatial resolution can be found in Chan and Kazarian (53). It should be noted that the macro-ATR accessory used in this research does not

yield this magnification effect because of the angle at which the light passes through the crystal.

It can clearly be seen that there are a number of advantages of infrared spectral imaging, including the ability to simultaneously collect thousands of spectra from a sample, and thus collect both spectral and spatial information in rapid analysis times. The technique can achieve higher spatial resolution than conventional IR analysis, and another advantage is that analysis is often non-destructive, therefore allowing a sample to be retained for further analysis. There are a number of ways the technique can be used, including obtaining spatially-resolved chemical information from a single sample or it can also be used to rapidly collect chemical information from multiple samples (50).

1.3.2 General Applications of Infrared Spectral Imaging

There have been numerous applications reported for infrared spectral imaging covering a broad range of areas. Infrared spectral imaging has found widespread applications in the polymer and materials industry. One such application is the analysis of several polymer layers in a cross-section of a multi-layered laminate (54, 55). This application demonstrates the high spatial resolution possible as polymer layers can quite often be very thin. Another key advantage of infrared spectral imaging that is clearly demonstrated with the polymer laminate studies is that both spectral and spatial information can be obtained from across the whole sample in rapid analysis times. By selecting frequencies specific to each of the polymer materials, it is possible to form images showing the distribution of each of the

polymer layers and to also chemically identify the materials present. Infrared imaging allows for any contaminants within the polymer layers to be identified, and is used for quality control purposes (39). There are several other polymer applications including the study of semicrystalline polymers and their blends, polymer liquid systems, polymer liquid crystal systems and determining phase diagrams, and further information on these applications can be found in (39).

Another key area where infrared spectral imaging has been shown to have wide-ranging applications is in the biomedical and biological fields, including the visualisation of silicon leakage in breast tissue from silicon gel implants (56), cancer detection (57, 58), lipid analysis in obesity research (59), pharmaceutical tablet content analysis and the real-time study of drug diffusion (60, 61), hair cross-section analysis (46), and bone analysis (62) among others. Infrared spectral imaging has also been shown to have agricultural applications, for example the technique has been used to study the quality of wheat kernels (63). Infrared spectral imaging has also been used to study an embedded paint cross-section from Rembrandt's famous painting *Portrait of a Standing Man*, painted in 1969, for art conservation and historical purposes (64). As can be seen, there has been a significant number of disciplines where infrared imaging has been shown to be useful, and further applications can be found in Kidder et al (50) and Bhargava and Levin (65). One area where research has been lacking is that of potential forensic applications.

1.3.3 Forensic Applications of Infrared Spectral Imaging

FTIR spectral imaging instrumentation has been commercially available since 1995, but at the commencement of this PhD research in 2003, there was extremely little published work regarding its use in forensic analysis. At the beginning of 2003, there were no published journal articles on forensic applications of infrared spectral imaging, and only a small number of conference abstracts.

One of the earliest reported forensic applications of infrared spectral imaging was for the imaging of latent fingerprints, presented at the International Association of Forensic Sciences (IAFS) conference by Bartick et al in 2002 (66). This work involved obtaining FTIR spectral images of untreated latent fingerprints which had been deposited on aluminium-coated glass microscope slides (which were specifically chosen for their reflective surfaces). The same authors also presented further research into this area at the Federation of Analytical Chemistry and Spectroscopy Societies (FACSS) annual meeting in late 2002, in which they demonstrated they were able to use FTIR spectral imaging to detect and form images of an explosive material, RDX, which was contained within a latent fingerprint deposit (67).

In 2002 - 2003, there were a number of presentations at the Pittsburgh Conference on Analytical Chemistry and Applied Spectroscopy (PITTCON) from Chris Brown and his colleagues at the University of Rhode Island. Their work focused on the use of IR spectral imaging to compare the ageing of vein and capillary blood (68, 69). Their other study focused on the analysis of official baseballs' collected from

ballparks over a time frame of 1963 to 2000. The Rhode Island State Crime Laboratory launched an investigation into whether the official baseballs chemical makeup and relative compositions had changed over the years. Infrared spectral images were taken from various parts within the dissected baseballs, and the tests showed that the chemical makeup and relative compositions of the baseballs had changed over the years, corresponding to a mechanical improvement in the balls (70).

It was not until January 2005, almost a decade since the first commercial FTIR spectral imaging instrument was available, that the first journal article was published on the use of infrared spectral imaging for forensic purposes. This study by Tahtouh et al concerned the detection and enhancement of latent fingermarks (35). In this study, FTIR spectral images of untreated latent fingermarks on glass microscope slides and also on an infrared reflective (metal oxide-coated) microscope slide were successfully collected, and showed clear ridge detail. The authors noted that the success of this experiment relied upon the fact that the background surfaces chosen did not contain vibrational peaks which would interfere with the peak used to form the images of the fingerprints (C-H stretching vibration). Many typical surfaces encountered in forensic investigations, such as polymer and ceramic surfaces, would typically contain their own C-H stretching vibrations that would interfere with those from the untreated fingerprint deposits. Tahtouh et al also investigated the use of a common fingerprint development technique, where the fingerprints are fumed using ethyl cyanoacrylate (superglue), prior to FTIR spectral imaging. The reasons for choosing this particular fingerprint technique was that ethyl cyanoacrylate contains a

C≡N (nitrile) functional group, which should be isolated and unique to the developed fingerprint (i.e. is unlikely to be a vibrational peak found in common background surfaces, and therefore should not have any interference from the background). Unfortunately, they found that this peak disappears during polymerisation. Nevertheless, they were still able to image the cyanoacrylate-fumed fingerprints using a carbonyl (C=O) peak, and successfully applied the technique to the imaging of treated prints on an Australian polymer banknote, a surface on which it is extremely difficult to develop fingerprints using standard fingerprint development techniques due to its highly-coloured and complex background pattern.

The majority of articles published over the past few years on forensic applications of infrared spectral imaging have focused on fingerprint evidence. Crane et al (2007) reported on the capability of FTIR spectral imaging to image unprocessed latent fingerprints on a variety of porous and non-porous surfaces including trash bags, a soda can, duct tape, copier paper, cigarette butt paper, a U.S. dollar bill and a postcard (71). The authors did note that in some instances the latent fingerprints were already slightly visible on the surfaces, but improved visualisation was obtained through FTIR spectral imaging. Crane et al also recovered some trace evidence, a blue fibre, from within one of the latent fingerprints. They noted the importance of imaging untreated latent fingerprints, since if any fingerprint development techniques had been used, the fibre may have been obscured or lost during the treatment, or otherwise contaminated with the chemical reagents used for fingerprint development, thus altering its own IR spectrum. The blue fibre was not analysed *in situ*, and was removed for single-point FTIR analysis. The authors also explored various data

processing methods for imaging the fingerprint ridge pattern on the various backgrounds including one of, or a combination of, the following methods: basic infrared spectroscopic band intensities, addition and subtraction of band intensity measurements, principal components analysis (PCA) and second derivative band intensities (71).

Tahtouh et al (2007) reported further findings and method optimisation techniques for FTIR spectral imaging of latent fingerprints on various surfaces (72). In this study they demonstrated the ability of the technique to successfully image cyanoacrylate-fumed fingerprints on aluminium drink cans, which often contain varied printed background patterns. The authors presented a systematic methodology for optimising the instrumental settings for each type of surface, and with the new optimised settings, were able to improve the collection times for imaging treated fingerprints on Australian polymer banknotes to around 4 hours for an image measuring 2.24 x 2.24 cm, as opposed to around 18 hours using the original un-optimised settings. Attempts to image fingerprints on porous surfaces, including white A4 copier paper, various masking tapes, and thermal paper which had been developed using standard fingerprint reagents such as ninhydrin or 1,2-indanedione were unsuccessful. The cellulose constituents from the paper background swamped any peaks that may have been present from the fingerprint, and as such FTIR spectral imaging was unable to isolate any vibrational peaks which could be used to form images of the fingerprint ridges. In most of the fingerprint studies reported, the authors have all noted that the location of fingerprints is known prior to FTIR spectral imaging. In a case scenario, the location of fingerprints in most instances

will not be known, and Tahtouh et al (2007) have proposed the use of visible and UV light sources as a tool to locate fingerprints prior to FTIR spectral imaging (72).

Kazarian and colleagues at Imperial College London have published several articles relating to FTIR spectral imaging of latent fingerprint residues, and also the detection and characterisation of trace materials within the fingerprints (73-76). Ricci et al (2007) demonstrated for the first time the ability of FTIR spectral imaging to image latent fingermarks which were collected from various surfaces including a door handle, a mug handle, a curved glass surface and a computer screen, using gel lifters commonly used at crime scenes (BVDA Gelatine Lifter and Dycem Gel Print Lifter) (74). They found that both types of gelatine lifts contained several infrared bands which could mask the spectral bands of the fingerprint residue. They recommended the use of an ATR-FTIR spectral imaging approach with a variable angle ATR accessory as a means of reducing spectral interference from the gel lifts (74). Ricci et al also investigated the use of *in situ* ATR-FTIR spectral imaging to characterise the components found in latent fingerprint residues, in which a fingerprint is placed directly onto the ATR crystal surface. They explored the effects that ageing and environmental changes, such as temperature change, had on the composition of the latent fingerprint residue. It is hoped through further studies that FTIR spectral imaging analysis of the composition of the fingerprint residues may assist forensic investigators in deciding the best fingerprint detection method to use (based on exactly what components are left in the fingerprint residues) (75).

Another reported use of FTIR spectral imaging is the detection of trace amounts of drugs. Chan and Kazarian reported the use of FTIR spectral imaging using a macro-ATR crystal to study drug traces directly from the surface of a finger (trapped between the fingerprint ridges), following the handling of a drug. Using this method they could characterise the drug material, and also view the distribution of the drug on the surface of the finger (76). Ricci et al followed on from this work and showed that drug traces could be imaged directly within tape-lifts collected from a crime scene, and also directly from the surface of a newspaper that had previously been contaminated with drug particles (73). The advantages of this approach are that the polydimethylsiloxane (PDMS) tape-lift removes the traces of drugs from surfaces non-destructively, allowing for further analysis of the drug samples, and also the ability to detect trace materials directly upon a person's hands may assist in linking a person to a specific act by showing the presence of trace materials directly upon them e.g. drug traces, explosives (73).

Ricci et al (2007) explored the use of a combined technique of FTIR spectral imaging and desorption electrospray-ionisation ion-trap mass spectrometry (DESI MS) to analyse counterfeit anti-malarial tablets (77). FTIR spectral imaging using a micro-ATR crystal was shown to be able to successfully non-destructively detect and characterise all of the components within the tablets, and DESI MS was used to confirm the chemical identities of the components. It was also possible to form FTIR spectral images showing the spatial distributions of the materials.

In summary, there have only been a handful of forensic applications reported for FTIR spectral imaging, and all of these fall into the broad categories of fingerprint analysis or drug analysis. There are still many other unexplored forensic applications, especially in the area of physical evidence. These are addressed in this PhD research.

1.3.4 Infrared Spectral Imaging Instrumentation Used Throughout This Research

The instrumentation used throughout this research project is the Digilab (now Varian) Stingray II Imaging system, which is comprised of an FTS7000 FTIR spectrometer, coupled to a UMA600 infrared microscope fitted with a Lancer 64 × 64 MCT FPA detector (as shown in Fig. 1.2). Images and spectra are collected and processed in the first instance with Digilab Win IR Pro software. The FPA detector can be either mounted on the microscope or can be physically moved across to the large sample accessory.

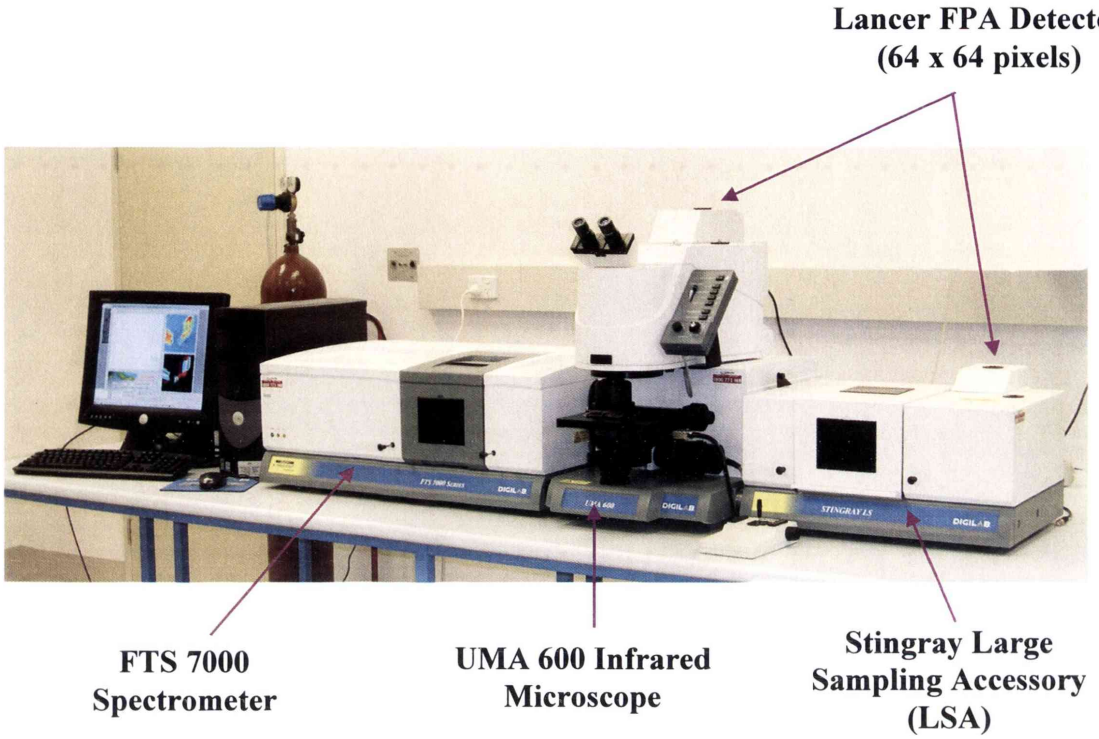

Figure 1.2: *Digilab Stingray Infrared Imaging System.*

1.3.5 Infrared Sampling Techniques Used Throughout This Research

1.3.5.1 Transmission Methods

Transmission analysis is the traditional method of obtaining an infrared spectrum, and involves infrared light passing through a sample. A sample will partly absorb the infrared radiation passing through it, and therefore reduce the intensity of the transmitted beam. Transmission analysis can be used to study samples in liquid, gaseous or solid forms (2). As this PhD research only examines solid samples, discussion will be limited to the infrared transmission analysis of solid samples. Ideally a sample should be no thicker than 10 - 20 μm for transmission analysis so that enough infrared radiation can be transmitted through the sample (19). For many samples, which may be too strongly absorbing or too thick to transmit infrared radiation, some type of flattening or reduction in sample thickness will be required

prior to transmission analysis. Some of the available methods include using a microtome to cut thin sections of a sample; a metallic roller or a diamond anvil cell can also be used to exert pressure on a sample to flatten it to a suitable thickness for transmission analysis. The use of a microtome and metallic roller are described further in Chapters 2 and 3.

A micro diamond anvil cell (DAC) consists of two diamond windows (anvils) which are embedded in the centre of two triangular steel plates. The steel plates contain guide pins which assist in the correct alignment of the two diamond faces. A sample is squeezed between the two diamond windows and flattened prior to analysis. Once a sample has been flattened to a suitable thickness for transmission analysis, the sample can either be analysed between the two diamond faces or, more commonly, a sample will be analysed through only one half of the diamond anvil cell. Diamond is a suitable material as it is extremely hard and can easily be used to exert enough force to flatten a sample. However, care must be taken not to apply too much force so as to flatten a sample into a thin smear or to destroy or alter the crystallinity within a sample. Diamond is an appropriate material for infrared transmission analysis as it is transparent in the important infrared fingerprint region and also in the visible region, thus allowing visual observation of the sample within the DAC. Advantages of the technique include the minimal sample preparation involved, and that only minute quantities of materials are required for analysis (3, 19, 78).

1.3.5.2 Reflectance Methods

Reflectance methods can be divided into two main categories, external reflectance and internal reflectance measurements. External reflectance measurements are those in which the infrared beam is reflected directly from the sample surface, and can be further subdivided into specular reflectance, in which the reflected angle of incident radiation is equal to the angle of incidence, and diffuse reflectance, in which the incident radiation is reflected in many different directions. In order for the infrared radiation to be reflected from a surface, the sample surface itself must be reflective or consist of a thin layer on a reflective backing (e.g. a thin coating of paint on a metallic surface) (2).

Internal reflectance measurements can be made using an attenuated total reflectance (ATR) accessory, in which an ATR crystal is placed in direct contact with the sample. The detailed theory of ATR analysis is covered elsewhere (79), therefore only a brief explanation will be given here as to why it is considered a surface-preferenced technique. Under the right conditions, the IR beam undergoes an internal reflection within the ATR crystal. Even though the IR beam is completely reflected at the internal interface, part of the radiation's electrical field penetrates a small distance into the sample material; this penetrating field is often referred to as the evanescent wave. The distance the evanescent wave penetrates into the sample depends on a number of factors, including the refractive index (RI) of the ATR crystal material and of the sample. The depth of penetration (d_p) can be calculated using the following equation:

$$d_p = \frac{\lambda}{2\pi n_1 [\sin^2 \theta - (n_2/n_1)^2]^{0.5}}$$

where λ is the wavelength, θ is the angle of incident radiation, n_1 is the refractive index of the ATR crystal and n_2 is the refractive index of the sample (52). A major advantage of ATR analysis is that often only minimal or no sample preparation is required, due to the fact that the depth of penetration of IR light into the sample is not influenced by the thickness of the sample (61).

There is a variety of materials that can be used in an ATR cell, including germanium (RI = 4.0), zinc selenide (RI = 2.4) silicon (RI = 3.4) and diamond (RI = 2.4). As can be seen from the equation above, the higher the refractive index of the ATR crystal material, the lower the depth of penetration of infrared radiation will be into the sample. The choice of ATR crystal material will depend on many factors such as the desired penetration depth of the infrared radiation, whether the crystal material needs to be able to analyse a rough sample (e.g. diamond is extremely strong and does not scratch easily, however zinc selenide will easily scratch), whether it is desirable to view the sample through the ATR crystal (e.g. silicon and germanium are optically opaque) and also cost, as a diamond ATR crystal can be extremely expensive.

In this research project, there are two ways in which ATR analysis can be performed using the Digilab Stingray IR imaging instrument. It is possible to conduct micro-ATR analysis using the infrared microscope and a slide-on ATR crystal. Using a slide-on germanium hemispherical ATR microscope objective (Harrick Scientific SplitPea), it is possible to collect an image size of around 80 μm x 80 μm with a

spatial resolution of approximately 5 μm. For analysing larger samples, it is possible to conduct macro-ATR imaging in the large sampling accessory using a Harrick Scientific FastIR™ single reflection horizontal ATR accessory. Using this particular accessory with a zinc selenide ATR crystal, it is possible to collect an image size of 3.0 x 2.3 mm, with a spatial resolution of around 44 μm. The use of macro ATR crystals for collecting infrared spectral image data was pioneered by Chan et al, and a number of specially built ATR accessories have been demonstrated which can image areas from 1 mm^2 to ~ 16 mm^2 (53, 60, 80). Some reported applications of macro-ATR FTIR spectral imaging include the study of the distribution of excipients within pharmaceutical tablets and the direct detection of drug particles on the surface of a person's finger (60, 76). Macro-ATR FTIR spectral imaging, with its ability to image larger fields of view, is an extremely promising tool for forensic analysis, and its use in examining line crossings on questioned documents is further discussed in Chapter 4.

1.4 Project Overview

The focus of this research project is to explore the potential of FTIR spectral imaging for use in forensic analysis in the physical evidence area. Three forensic evidence types are examined, including the analysis of two types of trace evidence, multilayered automobile paint chips (Chapter 2) and bicomponent fibres (Chapter 3). Analysis of these types of physical evidence can assist a criminal investigation by establishing a link between a person and a crime scene, between two persons, and so on. The ability to use these types of transfer evidence to show an association stems

from Locard's exchange principle, which, in essence, states that 'every contact leaves a trace'. It is expected that infrared spectral imaging will offer a number of advantages over traditional infrared micro-spectroscopy for the analysis of paint and bicomponent fibres, including increasing the confidence in results obtained due to the large amount of chemical data obtained with imaging, as opposed to the small number of averaged spectra with conventional analysis. As both spectral (chemical) and spatial (visualisation) information is obtained with infrared spectral imaging, it theoretically should be able to simultaneously analyse all components within a multi-layered paint chip and bicomponent fibre, at a higher spatial resolution than is achievable using conventional infrared transmission analysis. Another anticipated advantage is that the user gains an overview of the chemical composition of the entire sample and thus can observe features that would not be detected in single-point measurements.

The third application explored is the use of FTIR spectral imaging as a new technique for determining the sequence of intersecting lines on questioned documents (Chapter 4). Infrared spectroscopy had not previously been used to examine the order of intersecting lines. As infrared spectral imaging is capable of simultaneously obtaining both chemical information from a sample and visualising its components, it should be possible to form infrared spectral images of the various materials used to produce line crossings on documents, and should be possible to observe a reproducible pattern when one line crosses over another line. A key advantage of infrared spectral imaging, if successful, for this type of application is

that images would be formed based on chemical differences in the sample, and would be an objective and non-destructive method of analysis.

Overall, this research project explores the advantages and limitations of infrared spectral imaging for the analysis of three different types of forensic evidence. Further detailed project aims are outlined in Chapters 2-4.

CHAPTER 2:

Forensic Analysis of Multi-Layered Paint Chips Using Infrared Spectral Imaging

Chapter 2: Forensic Analysis of Multi-Layered Paint Chips Using Infrared Spectral Imaging

2.1 Introduction

2.1.1 Forensic Paint Evidence

A paint film consists of three main components, namely binder, pigment and fillers. Paint is extremely prevalent in our society and can occur as forensic trace evidence in a number of ways, for example, in cases involving road accident investigations such as hit-and-runs, where paint may be transferred from the automobile onto the victim's clothing, and also in break and enters, where paint may be transferred onto the tools used during the burglary.

Paint evidence is frequently encountered by forensic laboratories, and samples may be received as smears or intact paint fragments, possibly consisting of multiple layers. When a paint sample is received at the forensic laboratory, an initial optical examination is conducted and physical characteristics such as colour, layer sequence, layer thickness, surface and layer features, contaminants and weathering are examined. A physical fit between a 'known' sample and 'questioned' sample would then be attempted. A physical fit is a very powerful method of showing whether two paint chips have the same origin. Many paint examinations will also include the comparison of the colour and shade of the paint layers. Visible microspectrophotometry is an objective method of colour comparison that is often used during paint examinations. If no physical fit is shown, and there are no significant differences found between the two paint chips in the initial visual

examination or the colour comparison by visible microspectrophotometry, then a chemical examination of the materials within the paint chips would be conducted. The techniques chosen depend on the type and amount of paint sample available (e.g. chip, smear, minute vs. larger quantities). Examples of techniques that can be used include FTIR spectroscopy, pyrolysis gas chromatography (PGC), scanning electron microscopy-energy dispersive X-ray analysis (SEM-EDX), X-ray fluorescence (XRF) and X-ray diffraction (XRD) (81).

2.1.2 Infrared Microscopy in Forensic Science: Paint Chips

With optical microscopy and visible microspectrophotometry, infrared spectroscopy is one of the most commonly used techniques in the analysis of paint, yielding information on the identity and relative concentrations of major binder, pigment and filler components (11, 82). This information can be used in two ways: for example in a hit-and-run case, it may provide an investigative lead by identifying the make and model of the automobile by comparison with database spectra; secondly, if there is reference material available from a suspect car, then the chemical information can be analysed and compared to determine whether the paint materials could have a common origin (13).

Numerous sampling techniques have been reported in the literature for the infrared analysis of paint chips, including transmission (9), reflection (12, 83), attenuated total reflection (ATR) (13), transflection (84), and diffuse reflectance (DRIFTS) (10). Transmission experiments often involve the use of microsampling accessories such as the diamond anvil cell (85). In general, transmission analysis is preferred over

reflection analysis, even if it does require more sample preparation time (11). Drawbacks with reflection analysis include poor signal-to-noise ratio, spectral distortion (e.g. derivative-shaped peaks due to anomalous dispersion effect) and problems encountered with reproducibility (11). Band shifts of up to 30 cm^{-1} have also been reported for reflection spectra relative to the corresponding transmission spectra (83). Transmission spectra are therefore more easily compared with reference databases, which are generally compiled using transmission data. Reflectance spectra can be useful in certain circumstances, however, such as for the analysis of trace smears of paint on tools or paint embedded in fabric, which may be difficult to remove and manipulate (12, 13). High quality infrared spectra of individual paint layers can be collected using an attenuated total reflectance (ATR) microscope objective, but the ATR analysis of multi-layered samples is still tedious and difficult as it requires the separation of the individual paint layers.

The development of infrared microscopy has enabled the analysis of the very small paint samples that are often received by forensic laboratories, and has meant that the separation of each individual layer prior to analysis is no longer necessary because apertures can be used to limit the analysis area to one layer at a time (11). For transmission analysis, this requires that a thin cross-section of the paint layers be prepared, generally by embedding the paint chip in a suitable resin and using a microtome to cut sections 1 – 10 μm in thickness (9).

Numerous different embedding media have been suggested for paint chips prior to infrared analysis, including wax (86), gelatine (water-soluble) (9), polyesters (87),

and cyanoacrylates (88). The ideal properties of a resin medium were originally outlined by Derrick et al, and modified for forensic analysis by Chang et al to include:

(i) curing at room temperature without shrinking;

(ii) not reacting with or infiltrating the sample; and

(iii) being easy to microtome (86, 89).

In a recent study, seven different embedding methods were evaluated for their use on forensic automotive paint evidence. Overall, the best results were obtained using a fast-epoxy resin, but infiltration problems were minimised with the use of wax (89).

A method that avoids the use of any resin material was proposed by Van der Weerd et al (90). This involves doubly polishing a paint chip embedded in a KBr pressed pellet. Drawbacks include the potentially lengthy trial and error nature of the method, the inability to determine the final thickness, and the destruction of the majority of the paint evidence. An advantage is that no specialised equipment, such as a microtome, is required.

Whether the paint layers are separated prior to analysis, or embedded and microtomed, very thin paint layers, such as thin base coats (12 – 20 μm), can cause difficulties. The manual separation of thin layers is obviously problematic; small sample sizes and/or incompletely separated layers may result. The sequential analysis of layers in a transverse-sectioned paint chip usually requires the use of an aperture, which allows the isolation of a small area of the sample. Aperturing has the

disadvantages of reduced signal to noise (necessitating longer collection times) and the limiting of the spectral range to wavelengths smaller than the size of the aperture (13). With both methods of analysis, it may also be possible to overlook a layer, if two adjacent layers are similar in appearance. If each layer of a multilayered paint chip is analysed individually, this will be a fairly time-consuming process, particularly for chips from older cars that have been repainted and repaired numerous times (91). In one actual case study reported by Zieba-Palus, an automobile paint sample was reported to have nineteen layers (92). However it should be pointed out that for paint chips analysed in cross-section, most infrared microscope software enables the automated sequential collection of spectra from user-designated points on a visible light image of the sample, thus reducing operator time.

2.1.3 Infrared Spectral Imaging for Paint Analysis

Infrared spectral imaging readily suggests itself as a powerful method for discrimination within evidence types such as paint chips, because it simultaneously delivers chemical and spatial information about the sample. For example, infrared spectral imaging has been applied to paint cross-sections in order to investigate art restoration work conducted on one of Rembrandt's paintings (64). However, this analysis was carried out in reflection mode, which led to poor signal-to-noise and the introduction of spectral artefacts caused by specular reflection, necessitating the subsequent use of the Kramers-Kronig transform, a mathematical correction algorithm. For the purposes of identifying various materials used to restore the art work, this sampling method was satisfactory; however, transmission analysis is preferred in forensic work, as previously noted.

2.1.4 Overall Aims

In this chapter, the potential of infrared spectral imaging is investigated, with and without associated multivariate analysis techniques, in forensic identification and classification studies, using automobile paint chips as an example. In addition, for the specific case of paint chip analysis, many different embedding media and sampling techniques are evaluated. A new method is proposed for the preparation of samples prior to analysis by infrared microscopy/imaging.

2.2 Materials and Methods

2.2.1 Sample Details

Eight multi-layered and multi-coloured paint chips of varying quality were obtained from a previous study on automotive paint (see Table 2.1 for details) (93). These paint chips were collected from insurance car yards and had 4-8 layers each. The samples were set in a relatively soft medium such as paraffin (Paraplast®, Oxford Labware) or Fimo (014 Transparent, Eberhard Faber) prior to transverse sectioning using a Leica RM2165 motorised microtome. Paint chip sections of 5-10 μm thickness from a given sample were allowed to separate or fall out of the embedding medium, and were then carefully laid onto a bed of spectroscopic grade potassium bromide (KBr, Merck) powder in a dye. The KBr powder and paint chip sections were then pressed into a conventional 13 mm diameter disk, using a press. Individual paint chips were selected for imaging if they remained flat (unfolded) and parallel to the surface of the disk after pressing.

A variety of other resins were tested including Serifix (Struers), cyanoacrylate (Selleys Fix 'N' Go Supaglue), Spurrs embedding resin (soft formulation, ProSciTech), and a UV-curable resin (Loctite). It was necessary to reduce the amount of hardener by half in the Serifix recipe to obtain a resin of suitable hardness for microtoming. Paint sections of 5 – 10 μm thickness were microtomed and placed on a KBr plate for imaging.

To determine whether the resins were infiltrating the paint chip samples, each individual layer in the paint chips was physically separated and analysed according to the current procedure used by the Australian Federal Police (94). The paint chip samples were viewed under a stereomicroscope and thin sections of the surface of the paint were cut away using a scalpel. A very thin slice of the paint was cut from the centre of the layer and then placed in a diamond anvil miniature cell (DAC) (High Pressure Diamond Optics, Inc.). The slice of paint was flattened in the diamond anvil cell, and then the top anvil was removed prior to analysis. The sample was then analysed using the FTIR microscope, and a single-point spectrum was obtained with 256 co-added scans at 8 cm^{-1} resolution. A background spectrum was obtained through the vacant diamond anvil cell. The remainder of the paint layer was then scraped away to reveal the next layer, and the entire process above repeated until all layers in each of the paint chips were sampled and analysed.

PAINT CHIP	QUALITY	NUMBER OF LAYERS	LAYERS	APPROX. THICKNESS OF LAYER (µm)
# 36 Red Ford Telstar 1982 Front mudguard	Good	5	Dark grey Light grey Red (thinner) Yellow Red (thick)	40 28 33 77 50
# 264 Red BMW 320i 1984 Front mudguard	Good	5	Dark grey Light grey Red Maroon Red	28 70 40 17 90
# 218 Red Daihatsu Charade 1988 Door	Fairly Good	4	Dark grey Light grey Red Clear	16 35 22 44
# 211 Red Ford Laser 1982 Front mudguard	Slightly crumbly	7	Silver Red Black Green Red Green Red	16 22 16 44 22 55 22
# 64 Black Ford Laser 1986 Front mudguard	Very crumbly	8	Blue Brown Black Brown Red Brown Black Clear	90 18 20 22 65 16 20 16
# 442 White Toyota Corona 1984 Front mudguard	Good	4	Grey White Grey White	20 50 30 55
# 221 Red Toyota Corolla 1982 Bonnet	Slightly crumbly	4	Green Red Green Red	55 50 75 35
# 462 White Mazda 323 1986 Rear mudguard	Slightly crumbly	4	Purple Red White Clear	40 28 36 20

Table 2.1: *Paint sample details*

2.2.2 Infrared Spectral Imaging

Infrared spectral imaging of the paint chips in the KBr medium was carried out using a Digilab Stingray system, comprised of an FTS7000 FTIR spectrometer, coupled to a UMA600 infrared microscope fitted with a Lancer 64 × 64 focal plane array (FPA) detector. Images and spectra were collected and processed in the first instance with Digilab Win IR Pro software (version 3.4.2.025). All samples were imaged in transmission mode using either the normal field of view, in which each individual image tile is approximately 350 x 350 μm in size, or the expanded field of view (EFOV) setting, which produces an image tile of approximately 700 × 700 μm in size. Within each image datacube, absorbance spectra were collected at 8 cm^{-1} resolution, using 64 or 256 co-added scans. The spectral range collected was 900-4000 cm^{-1}, with the lower value being determined by the limit of the FPA detector. Background image files were collected from vacant areas of the KBr disks/plates. Some samples were also imaged in reflectance mode, with most parameters similar to those for the transmission experiments, except that (i) background images were collected from infrared-reflective metal oxide-coated glass slides (Kevley Technologies), and (ii) a minimum of 1024 co-added scans was often required to obtain a reasonable signal-to-noise ratio.

2.2.3 Cluster Analysis

Classification of infrared spectral images was carried out in specialist spectral imaging software packages, ENVI 4.0 (Research Systems Inc.) and Cytospec 1.05.10 (www.cytospec.com), which were also used to preprocess the spectra. Hierarchical cluster analysis (HCA) was carried out in Cytospec using the D-values distance

method and Ward's algorithm for clustering. The D-values distance is calculated according to:

$$C_{SR} = \frac{\sum_i (S_i - \bar{S})(R_i - \bar{R})}{\sqrt{\sum_i (S_i - \bar{S})^2}\sqrt{\sum_i (R_i - \bar{R})^2}} \qquad [i = 1 \cdots M]$$

where C_{SR} is the correlation coefficient (the 'distance' between two spectra, $\boldsymbol{R}$ and $\boldsymbol{S}$, in the datacube), and the spectra $\boldsymbol{R}$ and $\boldsymbol{S}$ are represented by 1-dimensional vectors of absorbances at M frequency values, and $\bar{\boldsymbol{S}}$ and $\bar{\boldsymbol{R}}$ are the mean values for each vector. A qualitative description of the clustering algorithm is given in the results and discussion section (refer Section 2.3.3). Prior to the HCA analysis, spectra were truncated to a spectral range of 1000-2000 cm^{-1} (leaving just the fingerprint region which contains most of the discriminating power of an infrared spectrum) and then converted to their second derivatives and normalised in the spectral domain. Supervised classification of images was carried out in ENVI using the Mahalanobis distance method to classify spectra as members of user-defined "regions of interest". The Mahalanobis distance is calculated according to

$$d_{SR} = \sqrt{(S - R).\boldsymbol{C}^{-1}.(S - R)'}$$

where d_{SR} is the distance between the two spectra $\boldsymbol{S}$ and $\boldsymbol{R}$, and $\boldsymbol{C}$ is the variance-covariance matrix of the variables. A qualitative description of how the Mahalonobis distance method is implemented in ENVI is given in Section 2.3.3. Spectra were preprocessed as for HCA, except that spectra were further truncated to meet the requirement that they contain fewer variables than pixels defined in each region of interest.

2.3 Results and Discussion

2.3.1 Sample Preparation Considerations

As mentioned earlier, the preparation of multi-layered paint samples for infrared microscopic analysis is not straightforward. In order to access all of the advantages that spectral imaging offers in the analysis of this type of evidence, cross sections must be prepared. For reflected light analysis, whether visible or infrared, the cross sections can be prepared simply by cutting a mounted or unmounted sample with a scalpel or a microtome. However, since in most cases the quality of (non-ATR) infrared reflection spectra will not be adequate for identification or discrimination purposes, the sample must be prepared as microtomed sections thin enough for transmission analysis. The choice of mounting resin is critical, and the chief conclusion that can be drawn from the literature surveyed in the introduction is that no single resin material is ideal for all infrared microscopy applications. In fact, the results obtained in this study lead to the conclusion that few of the embedding resins or waxes commonly used for optical and electron microscopy are suitable for infrared microscopy; many epoxy and polyester resins are designed to infiltrate the sample, so are immediately undesirable here, while paraffin waxes do not adhere sufficiently to the sample, allowing it to fall out after sectioning. Some epoxy resins require curing at elevated temperatures, and actually dissolve paint samples. It was found in this study that the Spurrs resin (epoxy-based) and cyanoacrylate either partially or completely dissolved the paint samples, therefore making these resins unsuitable for embedding forensic paint samples.

In order to avoid interference with sample spectra, the ideal resin for embedding samples prior to sectioning for infrared analysis would have either no infrared spectrum, or a very simple spectrum with a very small number of absorption peaks. Few carbon or silicon-based polymers with appropriate physical properties meet this criterion; the paraffin waxes do seem ideal from this point of view, but have other drawbacks as mentioned above. The traditional medium for embedding samples prior to macroscopic infrared analysis has been the halide salts, such as sodium chloride (NaCl) and potassium bromide (KBr). These are transparent to infrared radiation above characteristic low wavenumber frequencies, and are usually mixed with powdered sample and pressed in a dye into a pellet or disk. The efforts of Van der Weerd (95) to capture paint chips in KBr sought to take advantage of the non-interfering nature of KBr, but seem unnecessarily laborious and difficult.

The method outlined in the experimental section for embedding paint chip sections in KBr has potential for defeating most of the problems identified here for other methods. The use of a low melting point paraffin (or similar material such as Fimo) in which to embed the paint chip for sectioning obviates problems of infiltration, dissolution and spectral interference. The paraffin sets in minutes, after which time the sample can be readily microtomed. The tendency of the thin sections of paint to fall out of the microtomed paraffin slices is now treated as an advantage, because a clean transfer can be made to the KBr prior to pressing. Although it might be considered that the "liberated" paint section could be used "as is" for infrared microscopy, it was often found to be too delicate to handle and/or not sufficiently flat for imaging analysis. This overall method has been found to work well for

multilayered paint chips of reasonable quality, but is not recommended, for obvious reasons, for samples with a tendency to separate or crumble easily. Care must also be taken to avoid smearing of paraffin across the paint surface when microtoming.

Other resins found to be satisfactory for embedding paint samples include the Serifix and UV-curable resin (which must be used with a high powered UV source to allow for complete and rapid curing). However, for older, more porous paint samples, the resins were found to have infiltrated the samples, as spectral bands due to the resins could be seen in spectra of the paint layers. The older samples were also found to fall apart and crumble when microtomed in these resins.

2.3.2 Infrared Spectral Images

Infrared spectral imaging was found to be a powerful technique for analysing multi-layered paint samples. There are a number of advantages of infrared imaging over conventional infrared microscopy as applied to the analysis of multilayered samples such as paint chips. These include: (i) the simultaneous collection of spectra from all layers at once, so that only a single experiment is required in order to (potentially) identify all of a sample's components; (ii) potentially hundreds of spectra are collected from each layer of the chip, a feature that greatly increases confidence in any conclusions drawn, and lends itself to multivariate classification techniques; and (iii) any (potentially characteristic) inhomogeneities present in the layers can be revealed. The ability to detect inhomogeneities present in the paint layers would be of particular interest to those studying works of art e.g. conservators and art historians, perhaps looking to determine the authenticity of a historic painting, or to

study restorative work that has been carried out over the years. With single-point infrared analysis of paint cross-sections it is also necessary to use apertures to restrict the sampling area to each individual paint layer in the cross-section, and this can lead to reduced signal-to-noise ratios and also the limiting of the spectral range to wavelengths smaller than the size of the aperture. Infrared spectral imaging has the advantage that it does not require apertures and obtains spectra from across the whole of the paint chip cross-section. By avoiding the use of apertures, infrared spectral imaging also significantly reduces the risk of missing an adjacent paint layer that may appear to be visually similar, but which is chemically different.

As mentioned earlier, infrared spectral imaging data can be visualised in a number of ways. In one mode, single-point spectra can be extracted from any pixel in any layer in the paint sample and then classified or submitted for a spectral library search as would be done for conventional infrared spectral data. In a more powerful representation of the dataset, it can be viewed as a series of images produced by mapping the spectral intensity, at any given wavenumber value, across the field of view. These images can be based on the simple spectral intensity (e.g. absorbance) at a single wavenumber value, or they can be formed using the integrated intensity under a spectral peak that represents a chemical component of the sample. In either case, the spatial distribution of a chosen chemical component can be displayed, using either a greyscale or a "false" colour scale (e.g. red for high through to blue for low) to indicate intensity.

Figures 2.1(a) and 2.1(b) show, respectively, the visible light image and an infrared spectral image of a five-layer automotive paint chip (Ford Telstar, chip #36). Figures 2.1(c) to 2.1(g) show characteristic infrared spectra from each of the five layers. Using the flowcharts, tables and spectra in references (11) and (13), the paint types in the layers can be identified as follows: (c) epoxy enamel with clay extender; (d) and (e) polyester-melamines; (f) acrylic urethane with clay pigment extender; and (g) acrylic urethane. The infrared image was formed using integrated spectral intensity under a peak centred near 1606 cm^{-1}, which corresponds to a C=C stretch of the aromatic bisphenol ring in the epoxy resin (c, layer 1). This choice permits all five layers to be seen together, because of the contrast yielded by the different intensities at that frequency in the corresponding layers (blue indicating low intensity, red indicating high), even though only one layer contains that precise functional group. By itself, this image could be more informative than the visible light image (if it revealed a previously undetected layer); in any case, it represents only a tiny fraction of the information available in the entire infrared image datacube. Multivariate techniques for better accessing the entirety of this information are discussed in the next section, but one simple way to visualise more of the information is to view a "movie" constructed using the full sequence of spectral images across the spectral range. As the movie plays, different chemical components of a heterogeneous sample, such as a paint chip, are highlighted sequentially. This capability can be used to make very powerful comparisons between two samples, such as a paint chip from a hit-and-run scene and one from a suspect vehicle. The two infrared images, collected under identical conditions, can be joined side-by-side. If the two paint chips are from the same source, each frame of the resulting movie

will show the corresponding layers of the two chips behaving identically to each other (in terms of intensity patterns) at every wavenumber value across the spectrum. Figure 2.2 shows four frames of such a movie. With a colour intensity scale, this is a particularly powerful way of highlighting the similarities and differences between two paint chips. This representation is more easily understood by a layperson such as a jury member than a comparison of individual infrared spectra, a significant advantage for forensic evidence.

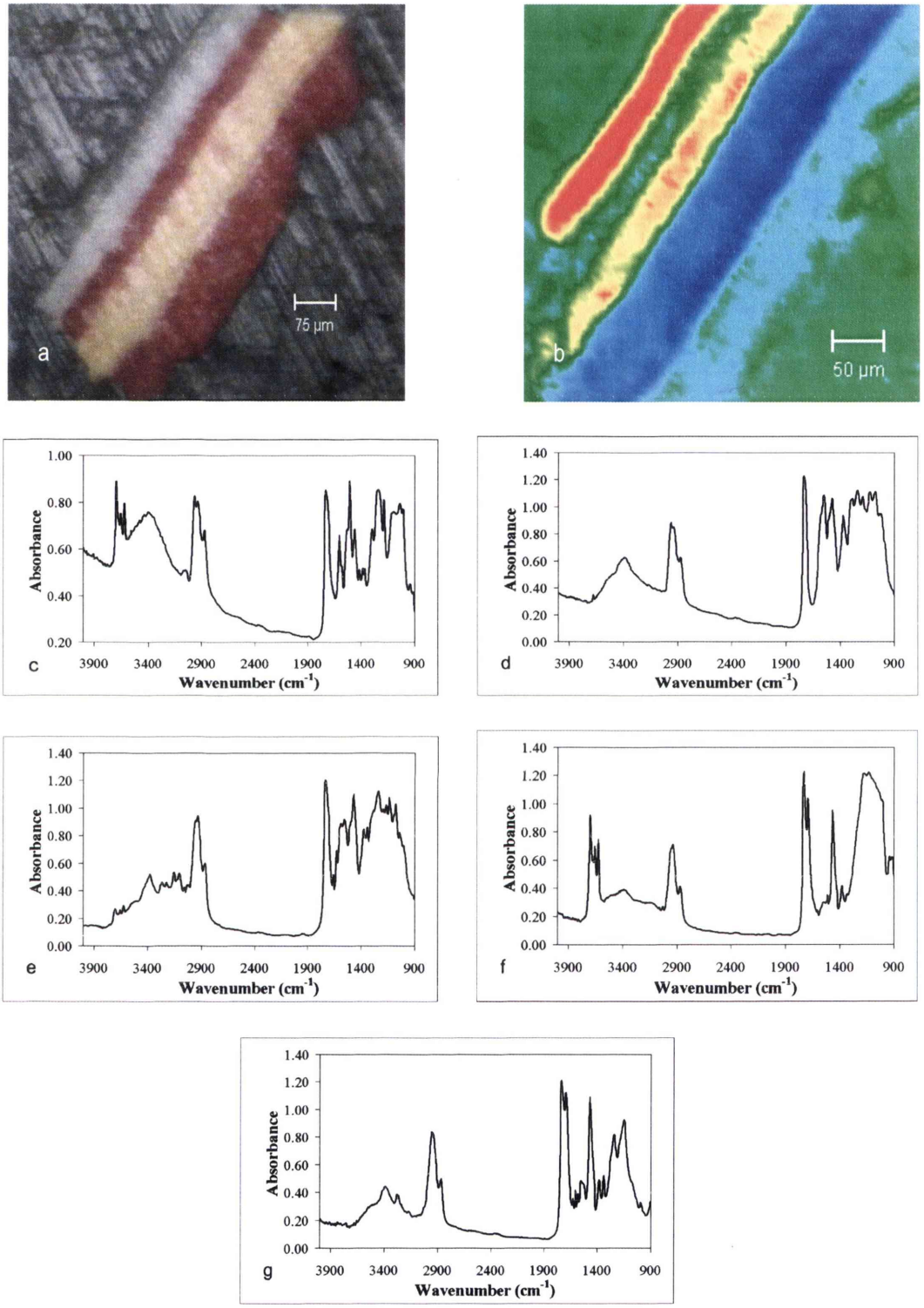

Figure 2.1: *a) Visible light image of paint chip #36*

b) FTIR spectral image of paint chip #36 at 1606 cm^{-1}

c) – g) Infrared spectra of paint layers 1-5

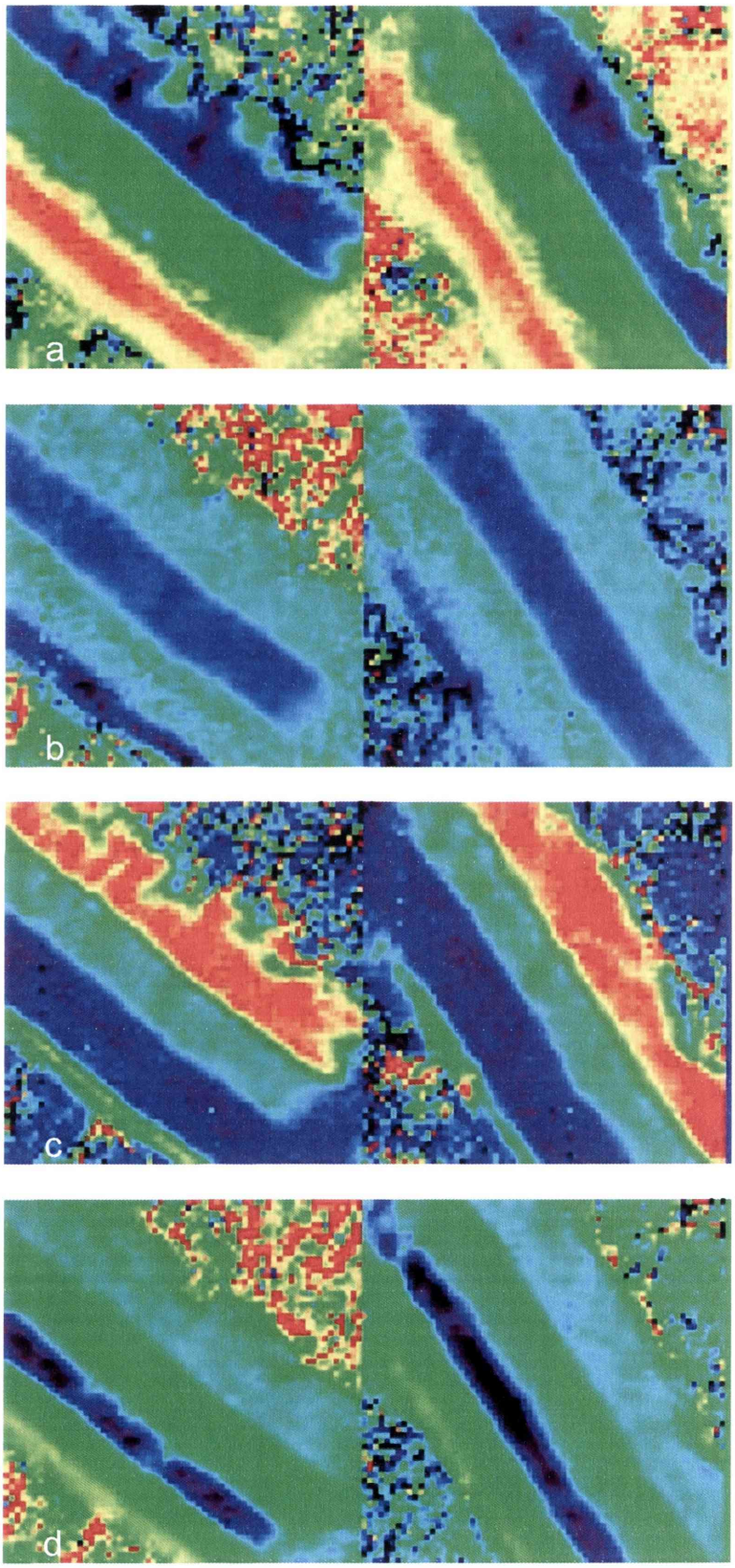

Figure 2.2: *a) – d) Four image frames captured at various wavelengths from movie comparing two paint chips from same source (#36)*

Most of the potential drawbacks of infrared spectral imaging correspond with those of conventional infrared spectroscopy, including the sample preparation issues discussed earlier in this chapter, and problems encountered when collecting data in reflectance mode. For certain samples, obtaining an acceptable signal-to-noise ratio in the spectra means longer acquisition times with the FPA detector compared to a conventional MCT infrared microscope detector (5-6 minutes for 256 scans, compared with less than 1 minute), but the extra time is small on an absolute scale, and the quantity of information collected in a spectral image is far greater, since it consists of 4096 spectra from across the whole sample. One imaging-specific disadvantage of infrared imaging systems as they are currently manufactured is that the spectral range at the low end does not extend below about 900 cm^{-1} (for the Digilab system used in our laboratory; 700 cm^{-1} for the Perkin Elmer Spectrum Spotlight), compared with about 600 cm^{-1} for an MCT detector on a conventional infrared microscope, and 220 cm^{-1} for a conventional infrared microscope equipped with cesium iodide (CsI) optics and a deuterated triglycerine sulfate (DTGS) detector. This means, for example, that some vibrations of inorganic components of a sample, such as some paint pigments, will not be observable using an array detector, as several inorganic pigments have the majority of their significant infrared absorptions occurring in the region below 700 cm^{-1}. Some additional infrared absorptions of common binders/resins also occur below 700 cm^{-1}, and will also be undetectable using an imaging system. Some examples of diagnostic infrared peaks of common binders/resins and inorganic pigments (that are undetectable using the Digilab imaging system used throughout this research) include styrene absorptions (760 and 700 cm^{-1}), an alkyd absorption (730cm^{-1}), benzoguanamine absorptions

(825, 789 and 710 cm^{-1}), an epoxy absorption (830 cm^{-1}), a melamine absorption (815 cm^{-1}), nitrocellulose absorptions (840 and 280 cm^{-1}), titanium dioxide (characteristic absorptions occurring between 700 – 350 cm^{-1}), magnesium (talc) absorptions (670, 465, 450, 420, 390 and 345 cm^{-1}) and barium sulfate absorptions (630 and 610 cm^{-1}) (13).

2.3.3 Cluster Analysis: Comparison of Spectral Images

Modern multivariate image analysis techniques are currently being used successfully in the classification of pixels in hyperspectral (chemical) image data in the disparate fields of remote sensing and cancer histopathology (57, 96). In remote sensing applications, spectral information (often consisting of just four visible or near infrared wavelengths) is used to accurately classify pixels in satellite and aerial images according to vegetation type, land use and mineral/soil types. A lot of published research has also been devoted to the classification of pixels in the infrared images of thin tissue sections. This type of work aims to use the very subtle differences in the infrared spectra of abnormal tissue to map the location of cancerous or potentially cancerous cells as an alternative to traditional staining techniques. Although the differences between the spectra of the different tissue types are very slight, the very large number (hundreds or thousands) of spectra involved mean that multivariate statistical techniques can be used to draw valid conclusions from the data. The application of these techniques to forensic samples such as paint chips actually poses less of a challenge because the differences between the infrared spectra of different paint layers are generally far greater than (say) the differences between normal and abnormal tissue from a human lymph node.

The statistical techniques that are used in the classification of hyperspectral or chemical images can be divided into two broad categories, supervised and unsupervised classification. Supervised methods rely upon information input by the operator when classifying pixels in an image, while unsupervised methods do not. Detailed descriptions of chemometric classification techniques can be found elsewhere (97), but here a brief summary and example is given, using infrared spectral images of paint chips, of how supervised and unsupervised classification techniques might be used in a forensic setting. While in the case of paint chips these approaches might seem unnecessary for, say, a comparison of two paint chips with the same sequence of ten brightly coloured layers, their value will be more apparent for more visually ambiguous evidence. Because the clustering techniques can assign a "false" colour to each chemically distinct region (cluster) in a spectral image, the resulting image represents a powerful way to make multiple chemical comparisons easy to understand for a layperson such as a juror.

When a forensic laboratory uses infrared spectroscopy to analyse a paint chip, the objectives are usually to identify the component paints as accurately as possible and/or to compare a paint chip from an unknown source (e.g. crime scene) with another from a known source (e.g. suspect vehicle). The former objective can best be accomplished by comparing spectra with those in infrared libraries. If a visible light comparison is inconclusive, a comparison of infrared spectra from corresponding layers of the two paint chips will provide information as to the chemical composition of the different layers. As mentioned earlier, one of the advantages of infrared spectral imaging over conventional infrared analysis in this

situation is that potentially hundreds of spectra from each layer of a paint chip can be collected in the same time it would take a conventional infrared microscope to collect one spectrum. Cluster analysis of the resulting spectra/image can identify and clearly display the location of all spectra that are classified as being "the same" (within certain limits) in the image of a paint chip, and, more powerfully, in the image of two paint chips that are being compared.

An example of an unsupervised cluster analysis technique is hierarchical cluster analysis (HCA) (97, 98). In this technique, the "distance" in multivariate space (a measure of similarity/dissimilarity) between each pair of spectra in an image is first calculated. Next, the two most similar spectra in the dataset are linked and placed into a group, or cluster, together. The distances between this group and each of the other spectra in the image are then calculated, and the linkage process is repeated, resulting in another spectrum being placed in a group, but at a lower level of similarity. This overall procedure is repeated until all of the spectra are in one group. The result of this sequential grouping process is a *dendrogram*, a tree-like structure that shows the stage at which each spectrum was grouped with other spectra (Fig. 2.3).

When followed in the reverse sense, the dendrogram can be used to identify ever-increasing numbers of clusters (with ever-increasing intra-cluster similarity) into which the spectra can be divided. Starting with all of the spectra grouped into one cluster (at the bottom of Fig. 2.3), the resulting image would be completely uniform. At the next step in similarity (moving up the dendrogram), the image can be divided

into two clusters; this shows all of the spectra in the image placed into either of two groups based on gross similarities/dissimilarities. For an object with a finite number of chemically distinct regions, the image can be divided into greater and greater numbers of clusters until such time as the resulting image has no further physical meaning.

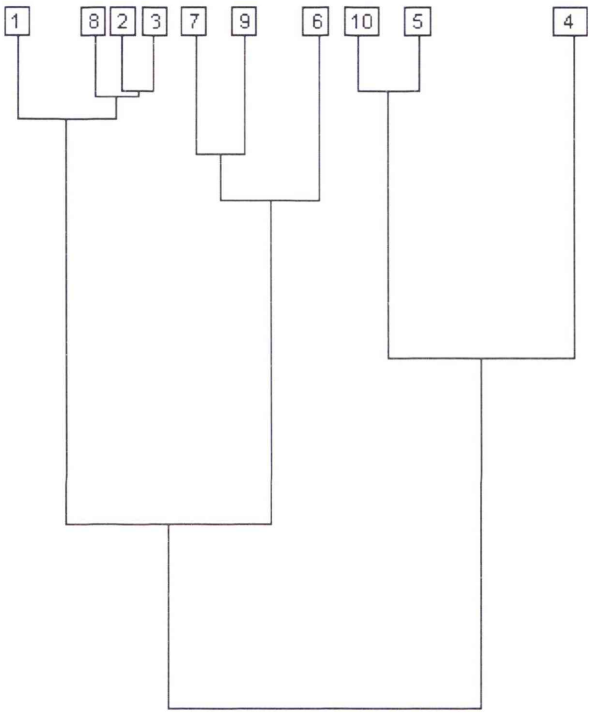

Figure 2.3: *Dendrogram result from a hypothetical hierarchical cluster analysis*

Figure 2.4 shows the results of HCA on the five-layer paint chip discussed earlier (Ford Telstar, chip #36). In Fig. 2.4(a), the first five clusters have been used to form the image, while in Fig. 2.4(b), the first six clusters are used. Since the visible light and raw infrared image analyses indicate that the chip has five layers, we would expect a maximum of six chemically distinct regions in the image (the five layers, assuming that they are all different from each other, plus the mounting material).

Indeed, the six clusters shown in Figure 2.4(b) do correspond to the five known paint layers and the mounting medium.

If there were more chemically distinct layers that had not been apparent in the visible or raw infrared images, an image based on seven or more clusters would show the location of such layers. On the other hand, if in reality there are no more chemically distinct regions in the sample, the addition of more clusters to the image will result in the subdivision of existing clusters into random or incoherently located pixels. This is illustrated in Fig. 2.4(c) where seven clusters have been used to form the image. The only change from Fig. 2.4(b) is that the areas corresponding to the KBr mounting material around the paint chip have been split into two clusters. Although some of these lie together near the edge of the chip, reference to the spectra at these pixels and to the visible image clearly shows that they lie outside of the physical boundaries of the chip. Images based on larger numbers (>7) of clusters serve only to strengthen the conclusion that Figure 2.4(b) is the most accurate representation of the location of the chemically distinct regions in the image, and that there are only six of these. Note that images based on several clusters above the "expected" number should always be examined, because a layer that has only subtle chemical differences from another may not be separated before other clusters (particularly those containing poor quality or low intensity spectra, such as those from pure KBr) start to break down into regions of different signal-to-noise (but with no chemical difference) or into physically meaningless shapes.

Figure 2.4: *Cluster images resulting from hierarchical cluster analysis (HCA) of paint chip #36 with a) five clusters b) six clusters and c) seven clusters.*

It is possible to 'mosaic' two paint chip images together, and conduct unsupervised hierarchical cluster analysis, as described above on the combined data. Figure 2.5(a) shows the visible light image of two 4-layered paint chips (Toyota Corona, # 442). Figure 2.5(b) shows the cluster image obtained with six clusters. In this example, there were two clusters that formed in the KBr medium before all four layers in the paint chips appeared as separated clusters, as there were only subtle chemical differences between some of the paint layers. Increasing the number of clusters above six only led to further clusters forming in the KBr mounting medium. It is also possible using the Cytospec software to conduct various 'quality' tests on the spectra prior to performing hierarchical cluster analysis. This includes testing for spectral signs of water vapour, testing sample thickness, signal-to-noise ratio, and a 'bad pixel' test (a tool which removes spectra originating from 'dead' pixels of focal plane array detectors). If the spectra in the images do not meet the specified 'spectral quality' criteria, they can be removed from the image prior to hierarchical cluster analysis, and those pixels will appear black in the cluster image. By conducting a sample thickness (total integrated intensity) test on the two paint chips mosaicked

together, it was possible to remove the spectra corresponding to the KBr mounting medium. Figure 2.5(c) shows the cluster image obtained when hierarchical cluster analysis was performed after the KBr mounting medium was removed through a sample thickness test and the 4-clusters obtained correspond to the layers found within each of the paint chips.

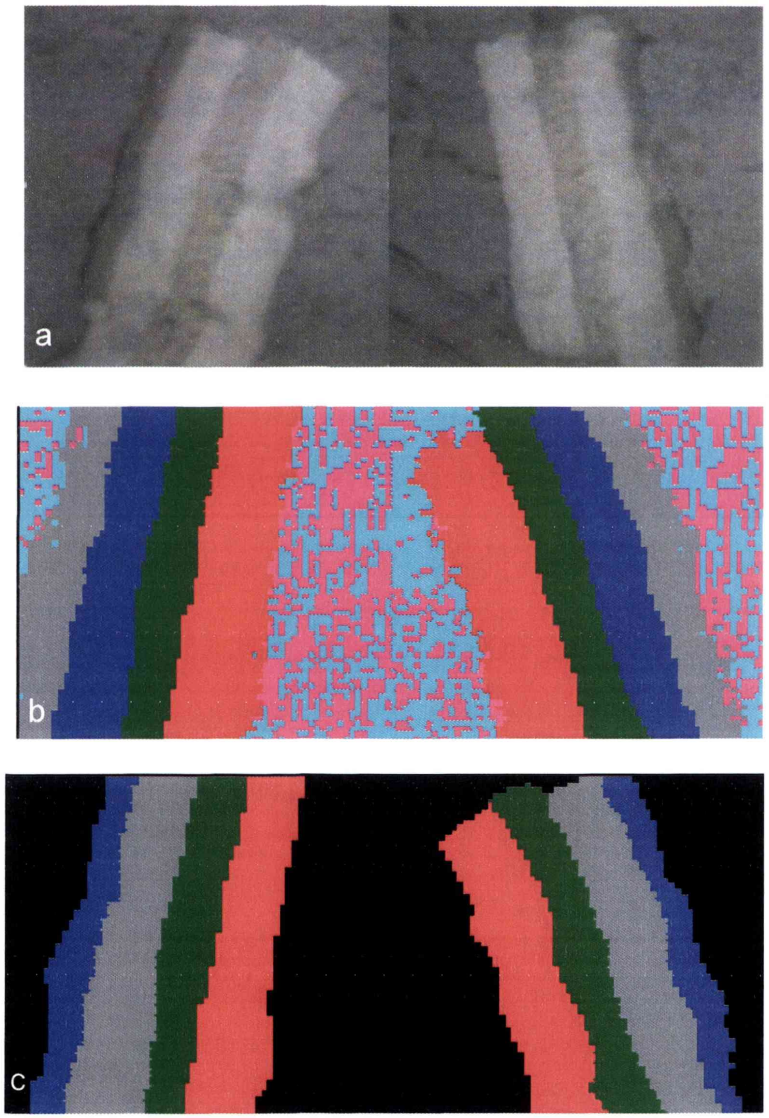

Figure 2.5: *a) Visible light image of two paint chips mosaicked together (# 442) b) Cluster image resulting from hierarchical cluster analysis (HCA) of paint chips with six clusters c) Cluster image resulting from hierarchical cluster analysis (HCA) of paint chips (with KBr spectra removed) with four clusters.*

Supervised image classification procedures implemented in the ENVI package require the user to indicate sets of pixels in an image (regions of interest, ROIs) that are known to represent chemically distinct areas of the image. The software is then able to classify the remainder of the pixels (spectra) in the image according to their similarity to spectra in these regions. This is done by calculating the distance (in multivariate space) between the average spectrum in each ROI and each of the unclassified spectra in the rest of the image. Spectra that lie within a specified maximum distance (threshold) of the average spectrum of a region of interest are classified as belonging to that region (cluster). In ENVI, the distance method that yielded the best results in this study for the classification of images containing paint chips was the Mahalanobis distance method (96).

This method is illustrated in Fig. 2.6, in which the two paint chips (BMW 320i, #264) are classified together using the ENVI supervised Mahalanobis distance classification routine. Figure 2.6(a) shows the visible light image of the paint chips and Fig. 2.6(b) shows the spectral image of the chips at 1492 cm^{-1} with pixels selected by the user in each of the six regions of interest in the left hand image only (the five layers apparent in visible light and infrared images, plus the surrounding KBr mounting material). Figure 2.6(c) is the resulting image when the software is allowed to classify all of the pixels in the combined image of the two paint chips.

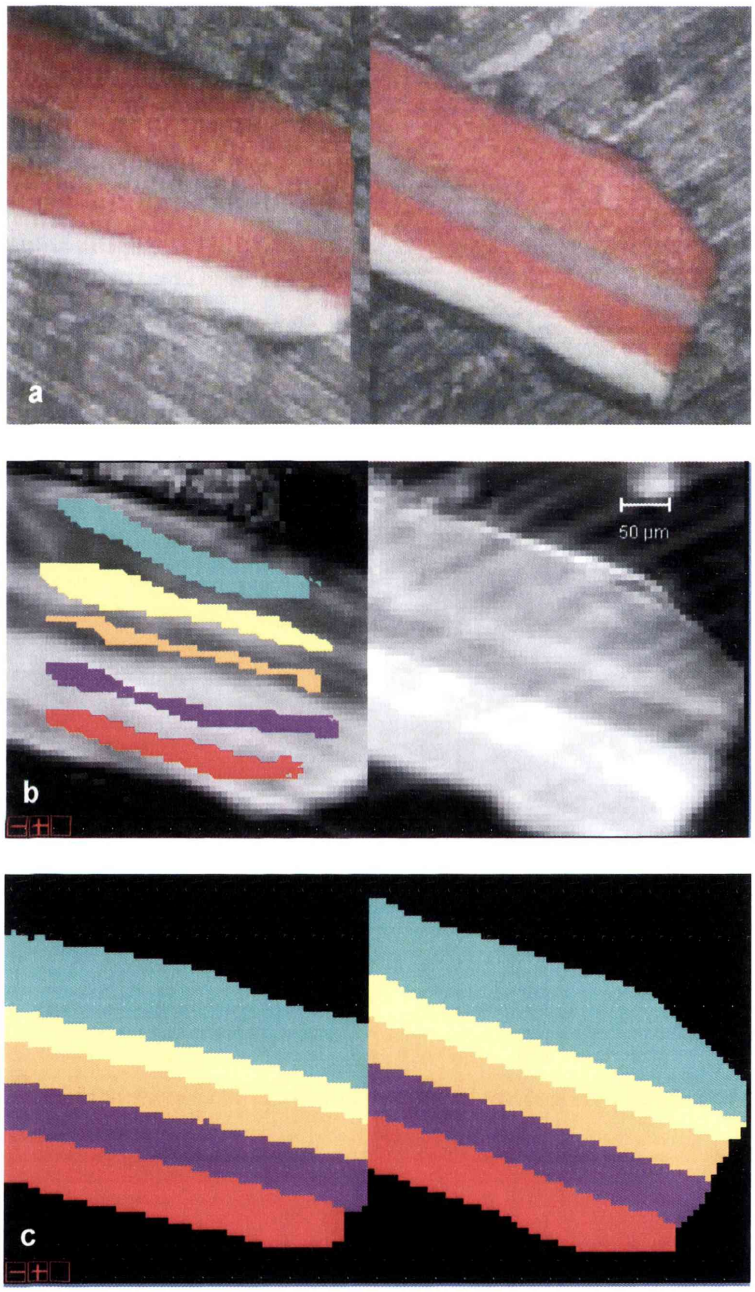

Figure 2.6: *a) Visible light image of two paint chips from the same source (#264, BMW 320i) b) Spectral image (1492 cm^{-1}) of the two paint chips with regions of interest (ROI) selected using ENVI. c) Resulting cluster image of paint chips using Mahalanobis distance classification method.*

A further example illustrating the ENVI supervised Mahalanobis classification method is shown in Fig. 2.7, in which two paint chips (Toyota Corona, #442) are classified together. The visible light image of the two paint chips (#442) is shown in Fig 2.7(a), which, despite its appearance, is a colour photo. From a visual inspection only, it could be incorrectly thought that layer 1 and 3 are the same paint, and layer 2 and 4 are the same paint, due to their similar appearance. Figure 2.7(b) shows the spectral image of the chips at 987 cm^{-1} with pixels selected by the user in each of the five regions of interest in the left hand image only (the four layers apparent in visible light and infrared images, plus the surrounding KBr mounting material). Figure 2.7(c) shows the resulting image when the software is allowed to classify all of the pixels in the combined image of the two paint chips. The characteristic spectra for each of the four layers are shown in Fig 2.7(d-g). Using the flowcharts, tables and spectra in references (11) and (13), the paint types in the layers can be identified as follows: (d) layer 1 - identified as acrylic-urethane, (e) layer 2 – identified as polyurethane with talc pigment extender, (f) layer 3 – identified as acrylic-melamine, (g) layer 4 – identified as acrylic-melamine with barium sulfate extender.

As with the HCA results, the fully classified images obtained using the ENVI supervised Mahalanobis classification method allows multiple chemical comparisons to be made rapidly at one glance, in a way that is very easy to understand. Of the two methods, HCA (as the unsupervised method) involves no subjective input from the operator, and so may therefore be preferred in forensic applications. However, the supervised classification procedure described here can be performed with a prescribed maximum spectral distance threshold that would specify mathematically

the greatest variation allowed between two spectra that are classified as representing the same chemical substance. This would confine the input from the operator to the selection of the regions of interest in the sample.

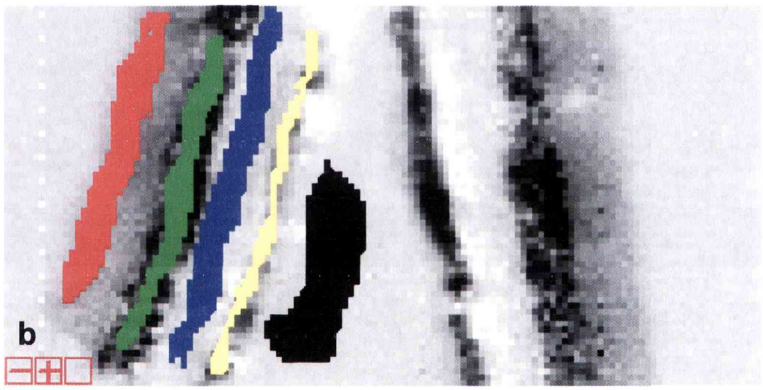

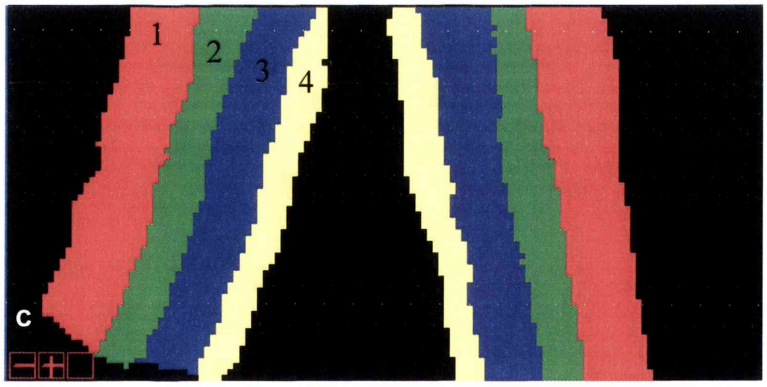

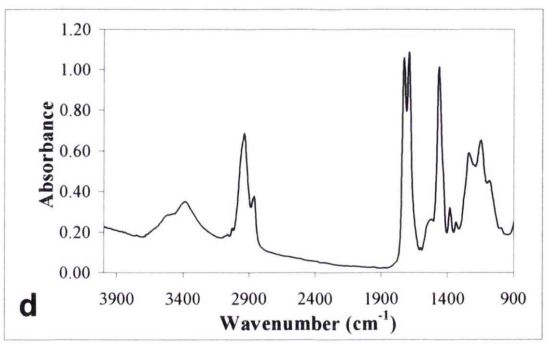

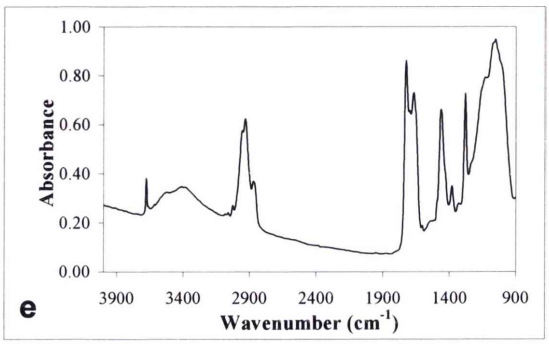

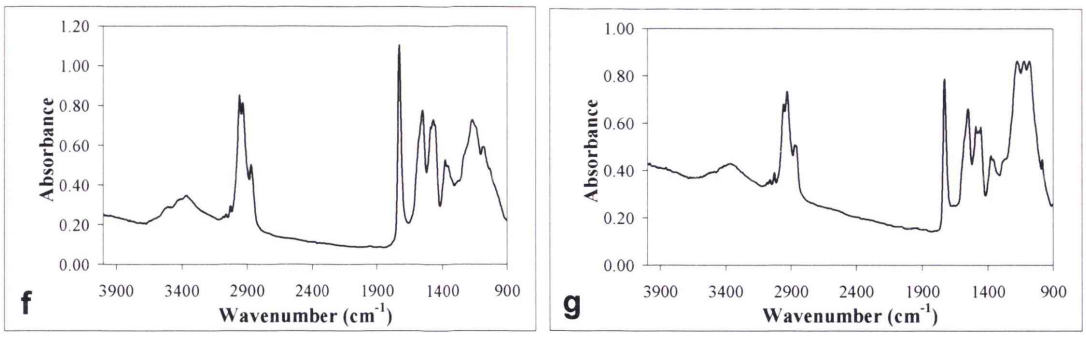

Figure 2.7: *a) Visible image of the two paint chips mosaicked together (#442) b) FTIR chemical image (using intensity at 987 cm^{-1}) of two paint chips showing selected 'regions of interest' c) results of Mahalanobis distance classification in ENVI, d-g) Infrared spectra of paint layers 1-4.*

It is worth pointing out that HCA is not the only unsupervised clustering technique, nor is the Mahalanobis distance the only supervised classification technique available. In Cytospec, HCA is the easiest unsupervised clustering technique to use, and some of the clustering techniques involve "fuzzy clustering", which allows a spectrum to be a member of more than one cluster simultaneously (something which may not be suitable for forensic applications). In ENVI, there are several other supervised classification techniques, but all require user input of thresholds which made them difficult to use objectively or successfully with this data. Both ENVI and Cytospec allow principal components analysis of these images in the spectral domain, but the resulting principal component images do not allow for a clear differentiation between the paint layers.

The first key advantage of using spectral imaging information in combination with multivariate techniques (or even simply displaying it as "movies") in the comparison

of heterogeneous samples for forensic purposes is that thousands of spectra are being compared with thousands of spectra, rather than one spectrum with one spectrum. In the case of paint chips, the *whole* of one sample can be compared with the whole of another in terms of chemical composition and the physical ordering of the chemical components. This dramatically reduces the chances of error when conclusions are being drawn from such comparisons. The second key advantage is that spectral imaging data (and the results of multivariate image classification) can be displayed in ways that make chemical differences and similarities between heterogeneous samples easy to visualise and understand. Importantly, both of these advantages can be exploited using any type of spectral imaging data, not just infrared spectral images.

2.4 Conclusions

Infrared spectral imaging has a number of important advantages over conventional "single-point" infrared spectroscopy with respect to the analysis of multi-layered paint chips. These advantages stem from the simultaneous collection of thousands of infrared spectra across the sample in a matter of minutes. Most importantly, the data can be used to visualise the spatial distribution of the different chemical components of a sample, an important advantage in comparison studies, since this spatial distribution (e.g. the ordering of layers) can itself be an important characteristic of a sample. Several different visualisation/comparison techniques are available: simple spectral imaging at fixed wavenumber frequencies, spectral image "movies" that allow two samples to be visually compared across the entire infrared spectrum, and cluster images, in which multivariate statistical techniques are used to group regions of the spectral image by similarity. These visualisation options make comparisons

using spectral imaging data easier for the layperson (such as a juror) to understand than a comparison of infrared spectra. Because the multivariate image analysis techniques compare hundreds or thousands of spectra in each sample, they also greatly reduce the chance of erroneous conclusions being drawn. Further extensive research into the use of multivariate image analysis techniques in forensic analysis needs to be conducted, with the work described in this chapter simply exploring the feasibility of using the techniques.

The main disadvantages of infrared spectral imaging are chiefly those of conventional infrared analysis, particularly those concerning sample preparation, although attempts were made to improve aspects of sample preparation in the work described in this chapter. When considering the practicality of using the sample preparation methods investigated in this study, one advantage is that they are only semi-destructive, and the paint sample is preserved for future analyses, such as scanning electron microscopy coupled with energy dispersive X-ray analysis (SEM/EDX), or micro X-ray fluorescence (XRF) spectrometry, for example. One key disadvantage is that in a forensic scenario, there will often only be small samples of paint samples to work with. Setting the sample in a resin without knowing whether the resin may infiltrate or dissolve the paint chip, or whether the paint chip is even sturdy enough to survive the microtoming process, is very risky, and even with all the advantages infrared spectral imaging offers, they may not outweigh the drawbacks encountered with the sample preparation required. For this reason, it is of key importance that a resin be developed that is suitable for embedding samples prior to infrared analyses, or that alternate sampling approaches be investigated, as

discussed further below. The infrared spectral range is somewhat restricted using a focal plane array detector (compared with conventional infrared detectors), and there is the requirement that the sample be flat.

2.5 Future Work Recommendations

There are a number of recommendations for future work that needs to be conducted. As indicated above, one of the greatest difficulties encountered in this work was that related to sample preparation, which affects both infrared imaging analysis and conventional single-point infrared analysis of multilayered paint chips. The majority of commercial resins available are not suitable for infrared analysis, and as such, there is need for the development of an embedding medium which meets the following requirements for infrared purposes:

- the embedding resin should completely infiltrate the sample so as to support the sample for sectioning
- the embedding resin must not react with or alter the sample in any way
- the embedding resin should be easily microtomed
- the embedding resin should have no infrared spectrum, or only a very small number of absorption peaks so as to eliminate or reduce any spectral interference.

Another sampling method which should be explored is micro-ATR imaging of the cross-sections of multilayered paint chips embedded in a resin block. The use of an ATR accessory, instead of transmission analysis, would avoid the need to cut thin cross-sections, allowing for the analysis of samples embedded in a resin block, and

therefore may be of use for analysing older, crumbling paint chips. Some problems envisaged with the micro-ATR technique include:

- a good degree of contact is required between the sample and the crystal, which may be problematic with the older paint chips,
- the requirement of a suitable embedding resin which will not contaminate the IR spectra of the paint layers, and
- the small sampling image area of approximately 80 μm x 80 μm may not be large enough to image an entire paint chip.

Nevertheless, it is still worthwhile investigating this sampling technique, as it may significantly reduce the time taken for sample preparation, and allow for imaging of samples which are unable to be imaged in transmission. Perkin Elmer released a new FT-IR Imaging ATR accessory in 2006 which allows for a larger area to be imaged. The ATR accessory contains a germanium ATR crystal with a 600 μm diameter sample area that can image a multi-layered sample a few hundred microns across. This accessory can also achieve a high spatial resolution of around 3 μm, which may overcome some of the problems described above for analysing multi-layered paint chips using micro-ATR imaging (99).

A feasibility study on the use of chemometric (multivariate) data analysis techniques was conducted, and showed promise. Further detailed investigation into the many available chemometric analysis methods needs to be explored, and the appropriate techniques validated for use in forensic comparisons of multi-component samples. Even though this research only explored the use of the chemometrics for multilayered paint chips, it is obvious that the multivariate image classification

(clustering) techniques should be applicable to the analysis of other types of multi-component forensic samples, and also to the analysis of analogous chemical imaging data collected from other parts of the electromagnetic spectrum, such as spectral images from the UV-visible and near-infrared regions.

Another conclusion from this work is that, although only one evidence type was examined in this particular study, it seems obvious that infrared spectral imaging should be investigated as a tool for the forensic analysis of other multi-component samples, as many of the same advantages should apply.

CHAPTER 3:

Forensic Analysis of Bicomponent Fibres Using Infrared Spectral Imaging

Chapter 3: Forensic Analysis of Bicomponent Fibres Using Infrared Spectral Imaging

3.1 Introduction

3.1.1 Forensic Fibre Evidence

Fibre evidence is frequently encountered in forensic investigations, and is an important class of trace evidence that can provide valuable information to support an association, such as between two people or between a person and a crime scene. Standard forensic examinations for man-made fibres consist of microscopic techniques such as visible light, polarised light and fluorescence microscopy, followed by microspectrophotometry. If, after that stage, two fibres are still indistinguishable, they are then examined by infrared spectroscopy, which is useful for identifying the fibre polymer type present, and then by dye extraction and analysis (19).

3.1.2 Bicomponent Fibres

In this chapter, a particular type of man-made fibres known as bicomponent fibres are examined. Bicomponent fibres are a special class of fibres comprised of two polymers of different chemical and/or physical properties existing within the same filament. They are produced to exploit properties not existing in either polymer alone. A number of different characteristics such as strength, lustre, shrinkage, dyeability and stability of the fibre are able to be altered by the choice of chemical components and the spatial configuration of these employed when manufacturing the fibre (100).

There are a number of different spatial configurations the two components may take on, with the most common examples shown in Fig. 3.1 (100, 101). This structure is employed to take advantage of the differing properties of each component; for example, the sheath material may be a more expensive material and contribute to lustre and dyeability, whereas the hidden core material may be chosen to reduce costs, have flame retardant properties, or add bulk and strength. Side-by-side fibres consist of two components divided lengthwise into two or more distinct regions. Side-by-side fibres are generally used as self-crimping fibres, based on the different shrinkage properties of each component (100).

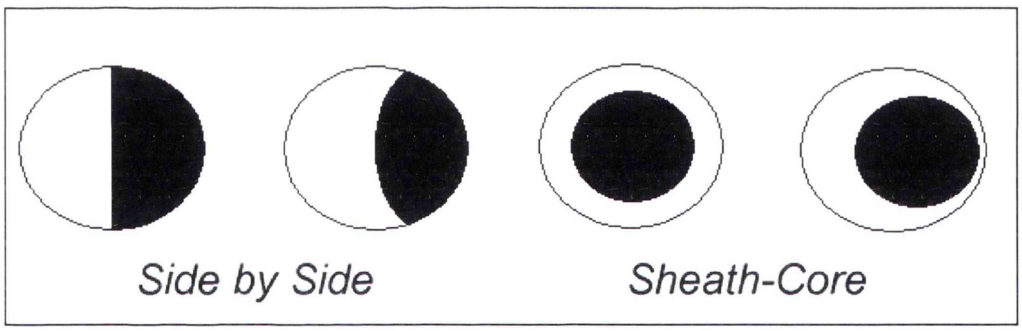

Figure 3.1 – Common configurations for bicomponent fibres.

The first commercial bicomponent fibre application was introduced by DuPont in the mid 1960s. This was a side-by-side hosiery yarn made from two nylon polymers that, on retraction, formed a highly coiled elastic fibre. In the 1970s, production of various other bicomponent fibres began in Asia. The first commercial use of sheath-core binding fibres was in carpets and upholstery fabrics. In 1998, Japan and Korea had the largest worldwide output of bicomponent fibres with a total of 90,700 metric tons produced annually. The annual production in the US market was around 27,200

metric tons, with Hoechst Celanese the largest US producer. The worldwide production of bicomponent fibres is only a fraction of the 25 million metric ton manmade fibre market, but with technological advances the producers are confident of a significant growth over the next five years or so (102). Bicomponent fibres can be found in many different products such as clothing (e.g. sportswear developed with water-absorptive properties), carpet, upholstery/mattresses, insulating materials and diapers (100, 103).

3.1.3 Bicomponent Fibres as Forensic Evidence

The greater the rarity and uniqueness of a fibre among the general population, the stronger the evidence will be. Bicomponent fibres have significant forensic value due to their relative scarcity in society, and the highly distinctive chemical/spatial configurations possible. There has been a small number of forensic studies conducted on bicomponent fibres. The first study by Grieve et al investigated a number of different techniques for recognising, characterising and comparing bicomponent acrylic fibres (14). The techniques examined included brightfield and polarised light microscopy, cross-sectioning, IR spectroscopy, and scanning electron microscopy (SEM). At the time of their study, it was reported that commercially-produced acrylic bicomponent fibres seemed to be exclusively of the side-by-side variety, and hence it was this configuration investigated in their work. Grieve et al recognised the need for further analytical techniques to be investigated due to the increased number of bicomponent fibres encountered in casework, and noted that in regular testing, the bicomponent nature of these fibres was often not being revealed, and hence their evidential value was not being completely recognised and exploited.

Grieve et al found that normal microscopic examination using brightfield and polarised light microscopy was not always effective in recognising bicomponent fibres. Only in instances where there was a difference in the delusterant concentrations between the two components of the fibres was it revealed that the sample was bicomponent using brightfield microscopy. Similarly, under polarised light, a slight birefringence difference between the two halves was the only indication that the fibres may contain slightly different polymers. However, many of the bicomponent fibres examined did not show variable birefringence. Cross-sectional analysis with examination by light microscopy and scanning electron microscopy were also found to be largely ineffective in recognising fibres as being bicomponent. Scanning electron microscopy only gave a clear indication that one out of the nine fibres studied was bicomponent, and cross-sectional analysis was only useful where there was a difference either in delusterant composition or colour variation between the two components.

Infrared spectroscopy was shown to be a more successful technique in recognising and characterising bicomponent fibres. Given that all the fibres studied were of the side-by-side variety, FTIR microscopy could be used to collect spectra of each half of the fibre to reveal the identity of the two polymers. A drawback to this approach in forensic casework, however, is that the structure of the bicomponent fibre might not be known prior to analysis.

Grieve et al concluded that the majority of acrylic bicomponent fibres encountered in their casework were recognised only if they had varying delusterant concentration, or

consisted of different-coloured components. For example, the techniques evaluated by Grieve et al failed to identify bicomponent fibres in an evidential garment known to contain Monsanto bicomponent acrylic fibres. Grieve et al also conceded that unless a fibre's bicomponent structure is microscopically obvious under transmitted light, bicomponent acrylic fibres may go unnoticed; no remedy was found for this in their studies.

Following this research, Tungol et al examined infrared spectroscopy for the analysis of sheath-core bicomponent fibres (16). They found through the use of apertures that, for flattened sheath-core bicomponent fibres, an infrared spectrum of the sheath component alone could be obtained at the edge of the sample, and a combined sheath-core spectrum could be obtained from the middle of the fibre sample. Through the use of spectral subtraction, a spectrum of the sheath material could then be obtained.

In a later study carried out by Cho et al (2001), both attenuated total reflection (ATR) and transmission infrared microspectroscopy were used for the qualitative analysis of bicomponent fibres (104). In this study, only sheath-core bicomponent fibres were examined. Cho et al demonstrated that with the use of both ATR and transmission techniques, spectral information could be obtained for both the sheath and core components of the fibre. As ATR is a surface-preferenced technique, it should in theory allow for the spectrum of the sheath component only to be obtained. Transmission analysis yields a combined spectrum of both the core and sheath components. Through subtraction of the two spectra, they were able to obtain a

spectrum mainly corresponding to the core material. Problems with this approach include the possibility of not obtaining a completely pure spectrum of each component, and also the shifts in peak frequency and intensity values that can occur with ATR analysis relative to transmission analysis. These shifts in frequency values may be problematic when obtaining the core spectrum, which involves subtracting an ATR spectrum (sheath) from the transmission spectrum (core and sheath), and could potentially lead to inaccurate results in identifying the core polymer type (19).

One major drawback with the infrared techniques described above is that the spatial configuration of the fibres, i.e. whether they are side-by-side or sheath-core, needs to be known prior to infrared analysis. This information is unlikely to be available in a forensic case scenario unless it is microscopically obvious. Ideally, a complete forensic analysis of bicomponent fibres should reveal both the chemical composition and the spatial distribution of the components present.

Infrared spectral imaging is a technique that may enable the complete characterisation of bicomponent fibres, as it allows for spatially resolved chemical data to be collected from a sample. By imaging at frequencies corresponding to the vibrations of chemical functional groups, the spatial distribution of different chemical components in the sample can be identified.

3.1.4 Overall Aims

In this chapter, infrared spectral imaging is investigated as a more suitable and informative technique to analyse bicomponent fibres than conventional infrared spectroscopy. Its main advantage is its ability to simultaneously collect hundreds to thousands of infrared spectra from across the whole sample to potentially reveal any inhomogeneity present in the sample, such as a second polymer component, without the need for any prior knowledge on the sample. Other conventional techniques (brightfield – polarised – fluorescence microscopy, scanning electron microscopy) are also applied in order to compare the value of infrared spectral imaging to more established techniques for the forensic examination of fibres.

3.2 Materials and Methods

3.2.1 Sample Details

Twelve bicomponent fibre samples, listed in Table 3.1, were obtained from two reference libraries, the Microtrace 'Forensic Fibre Reference Collection' (2001, USA) and the CTS Reference Collection of Synthetic Fibres (1987, USA), and from the Trevira Fibre Company (2005, Germany).

3.2.2 Conventional Testing

3.2.2.1 Microscopic Techniques

Fibre samples were mounted using a 50% glycerine/water mixture and examined using brightfield, polarised and fluorescence microscopy. A LEICA DMR Fibre Comparison Microscope was used to examine the fibres at 200x or 500x magnification. Photographs were taken using a LEICA MPS52 camera.

3.2.2.2 Environmental Scanning Electron Microscopy (ESEM)

The cross-sections of each fibre sample, embedded in either Serifix (polyester) or UV-curable resin (see below), were examined using a FEI XL30 environmental scanning electron microscope (ESEM) with a gaseous secondary electron (GSE) detector at magnifications ranging from 1000-5000x.

FIBRE	**MANUFACTURER**	**APPROX. DIAMETER* (μm)**
Cashmilon G4K	Asahi Chemical Co.	15
Acrilan B57	Monsanto	30
Acrilan B94	Monsanto	80
Monsanto X-24	Monsanto	20
Monvelle	Monsanto	35 - 50
Velicren Bicomponent	Snia	10
Beslon F040	Toho Rayon	20
Orlon 21	DuPont	25 - 30
Cantrece	DuPont	20
Creslan 68	American Cyanamid Co.	40
Dralon K	Bayer	25 - 30
Trevira 256	Trevira	30 - 35

* Diameter of unflattened fibre is given

Table 3.1: *Bicomponent fibre sample details*

3.2.3 Infrared Spectral Imaging

Infrared spectral imaging of the bicomponent fibres was carried out using the Digilab Stingray system described previously in Chapter 2. Unless otherwise specified, all samples were imaged using the "normal field of view", in which each individual image tile is approximately 350 x 350 μm in size. The spectral range collected was 900-4000 cm^{-1}, with the lower value determined by the limit of the FPA detector.

A number of different infrared sampling methods were employed to analyse each of the bicomponent fibre samples, including normal transmission analysis and two micro-sampling techniques, using a diamond anvil miniature cell (DAC) (High Pressure Diamond Optics, Inc.) or a germanium attenuated total reflectance (ATR) microscope objective (Harrick Scientific SplitPea).

3.2.3.1 Transmission

For transmission analysis, a single fibre was taped at both ends across a window cut out of acetate frames (EXP photocopier transparency sheets), and then flattened using a hand-held metallic roller (Kevley Technologies). The hand-held metallic roller surface was first 'roughened' using silicon carbide paper, to avoid producing a thin layer with a smooth surface, which can lead to interference fringing (19, 105). When analysing in transmission mode, absorbance spectra were collected at 8 cm^{-1} resolution, using 256 co-added scans. Background images were collected through air adjacent to the sample.

3.2.3.2 Diamond Anvil Cell (DAC) Accessory

A single fibre was placed between the two diamond faces and flattened to a suitable thickness for infrared transmission analysis. A slight rocking of the diamond cells was employed when flattening the fibres to avoid producing a thin flat film, and hence minimise interference fringing. The top half of the diamond anvil cell was then removed, and infrared analysis conducted through one half of the cell only, also to reduce interference fringing (19). Absorbance spectra were collected at 8 cm^{-1} resolution using 256 co-added scans. Background images were collected from vacant areas of one diamond face. Some problems were encountered with the analysis of the acrylic bicomponent fibres, with sloping baselines and interference fringing appearing in the infrared spectra obtained. In an attempt to overcome these problems, a drop of paraffin oil was occasionally added to the diamond anvil cell (see Results and Discussion).

3.2.3.3 Attenuated Total Reflectance (ATR) Microscope Accessory (Side-on analysis)

A single fibre was taped straight at both ends to a microscope slide, and analysed using a germanium hemispherical ATR crystal. To obtain infrared spectral images, the ATR crystal was placed in contact with the fibre sample and a contact alert system (SpectraTech) used to monitor the pressure applied. For ATR analysis, it was necessary to collect a higher number of co-added scans and, for absorbance spectra collected at 8 cm^{-1} resolution, at least 1024 co-added scans were required. Background images were collected from the vacant ATR crystal.

3.2.3.4 Cross-Sectional Analysis - Transmission

Cross-sectional analysis was also attempted for the fibres. The first method attempted was the analysis of thin cross-sections of the fibres in transmission mode. The fibres were first taped at both ends across a window in acetate sheeting, as described previously, to assist with positioning for sectioning and also to prevent the fibres from crimping (106). They were then set in a variety of resins including Serifix (Struers), Spurrs (ProSciTech) and a UV curable resin (Loctite). Multiple resins were tested due to difficulties in microtoming thin cross-sections in which the fibre sections remained during the microtoming process. Due to difficulties locating the colourless fibre cross-sections in the colourless resins, methyl violet 6B indicator (Searle Diagnostic) was used to dye the resins purple. Sections of 5-10 μm thickness were microtomed using a LEICA RM2165 motorised microtome. The fibre cross-sections were then placed on KBr plates and imaged in transmission mode as described previously. Background images were obtained from vacant areas of the KBr plates.

3.2.3.5 Cross-Sectional Analysis – ATR Analysis

A second method for obtaining spectral images of the fibre cross-sections was attempted due to the difficulties encountered with the microtoming and locating the fibres in the resins. This method involved setting the fibres in the resins as described above, but instead of obtaining thin sections by microtoming the samples, attempts were made to analyse the fibre cross-sections whilst still in the resin blocks using a hemispherical germanium ATR crystal. The microtome described previously was used to obtain a smooth flat surface, with the fibre cross-section visible at the surface

of the resin. The fibre cross-section was positioned so that it was in alignment with the centre of the ATR crystal, and then the ATR crystal was brought into contact with the fibre cross-section. Spectral images were obtained in reflection mode with 256 scans at 8 cm^{-1} wavenumber resolution. Background images were obtained through the vacant ATR crystal.

3.3 Results and Discussion

3.3.1 Conventional Testing

Varied results were obtained using conventional methods of analysis. None of the fibres exhibited any fluorescence and therefore fluorescence microscopy gave no indication as to whether or not the fibre samples were bicomponent.

Brightfield microscopy was found to be slightly more successful, and did allow for a few of the fibres to be identified as bicomponent. The clearest indications were seen for the Orlon 21 (DuPont) and Trevira 256 (Trevira) fibres, in which the two components could be easily distinguished due to the difference in delusterant concentration. The results for the Orlon 21 (DuPont) bicomponent fibre can be seen in Fig. 3.2, in which one half of the fibre appears transparent, while the other side contains brown speckles, due to the delusterant. Brightfield microscopy clearly demonstrates that this bicomponent fibre is of a side-by-side configuration. As can be seen in Fig. 3.3, brightfield microscopy reveals that the Trevira 256 (Trevira) bicomponent fibre is of a sheath-core configuration, with the delusterant only seen in the core component. A slight difference in delusterant concentration could also be seen for Monsanto X-24, revealing its side-by-side configuration. For the remainder of the fibre samples, there was no clear indication that the fibres were bicomponent.

In some of the samples, namely Monvelle (Monsanto), Velicren bicomponent (Snia) and Dralon K (Bayer), a faint division line could be seen down the middle of the fibre samples, indicating that the fibres could be side-by-side bicomponents (Fig. 3.4). In six out of the twelve samples examined, there was no indication using brightfield microscopy that these fibres were indeed bicomponent fibre samples.

Overall, polarised microscopy was not very successful in revealing the fibres as bicomponent. A slight difference in birefringence could be seen for Acrilan B94, with one half of the fibre appearing a paler aqua blue than the other. As with brightfield microscopy, a very faint division line could be seen down the middle of three samples, Velicren bicomponent (Snia), Orlon 21 (DuPont), and Dralon K (Bayer). Trevira 256 was the only bicomponent fibre that polarised microscopy clearly revealed as bicomponent. As can be seen in Fig 3.5, the polyethylene terephthalate (PET) core component appears as a bright white colour, compared to the much darker polyethylene sheath component. For seven samples, there was no indication that these samples were bicomponent fibres.

Figure 3.2: *Brightfield microscopy visible light image of Orlon 21 (DuPont) at 200x magnification.*

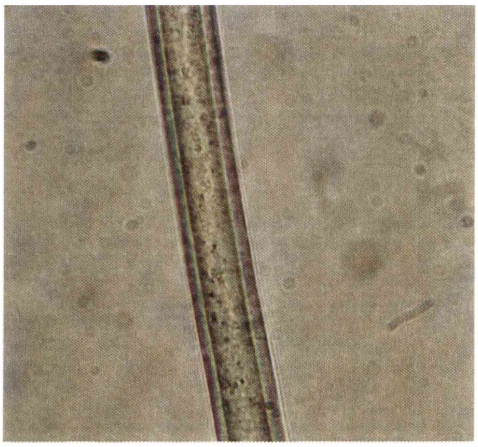

Figure 3.3: *Brightfield microscopy visible light image of Trevira 256 (Trevira) at 200x magnification.*

Figure 3.4: *Brightfield microscopy visible light image of Monvelle (Monsanto) at 200x magnification, showing faint division line visible down middle of sample.*

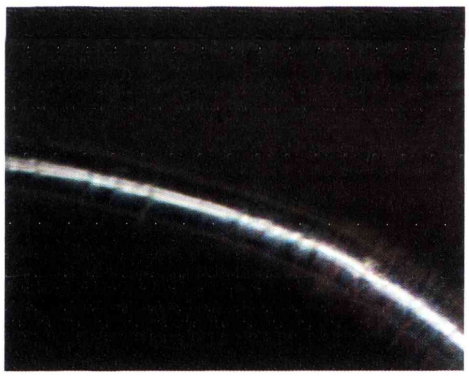

Figure 3.5: *Polarised microscopy image of Trevira 256 (Trevira).*

Environmental scanning electron microscopy was very successful in revealing Monvelle (Monsanto) as a side-by-side bicomponent fibre (Fig. 3.6). The two components could be clearly distinguished using this technique, and was the most successful result of all fibres tested. The technique was also successful in revealing Trevira 256 (Trevira) as a sheath-core bicomponent fibre, with the two components

visible in the ESEM images obtained (Fig. 3.7). For the remaining samples, there was either only a very faint dividing line that could occasionally be seen in the cross-section (possibly indicating side-by-side bicomponents) and that was not always visible across the whole diameter of the fibre, or there was no indication at all that the fibres were bicomponent.

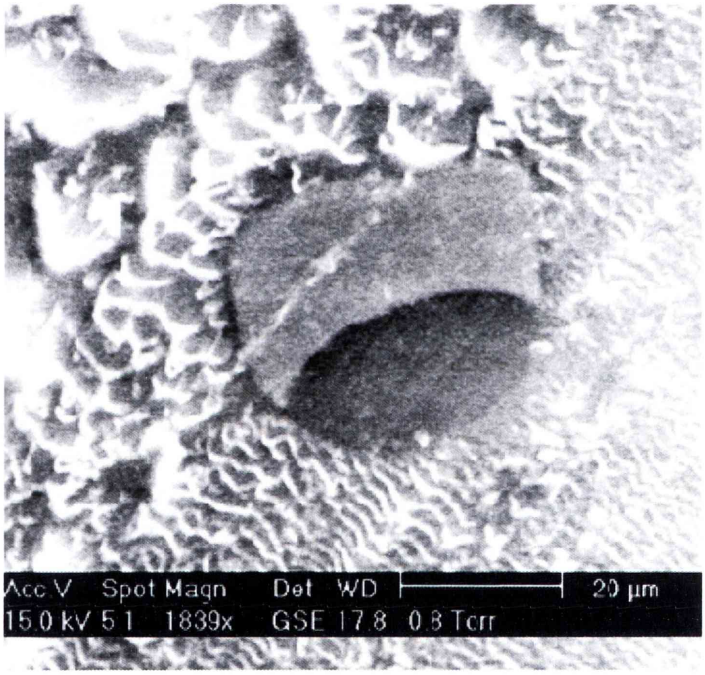

Figure 3.6: *Cross-section image of Monvelle (Monsanto) obtained using environmental scanning electron microscopy (ESEM).*

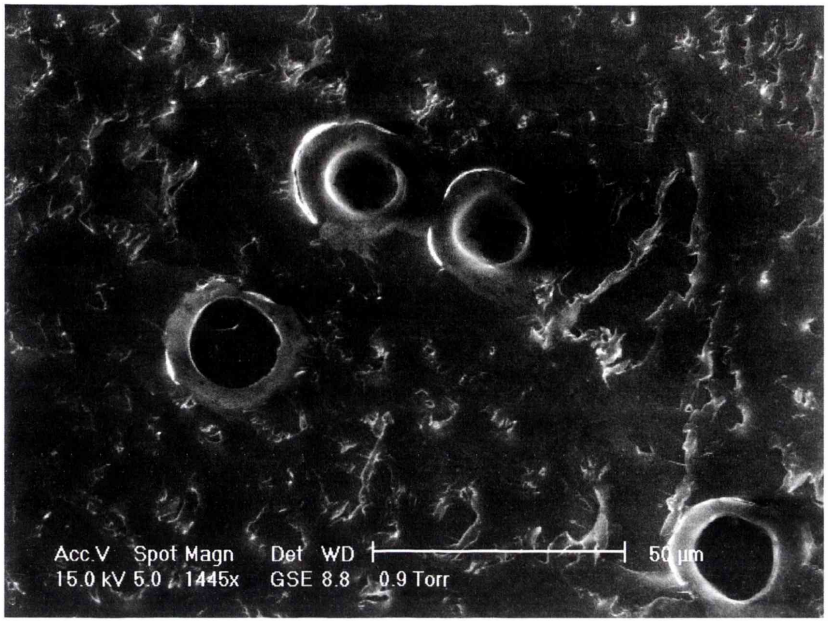

Figure 3.7: *Cross-section image of Trevira 256 (Trevira) sheath-core bicomponent fibres obtained using environmental scanning electron microscopy (ESEM).*

3.3.2 Infrared Spectral Imaging

A number of different sampling methods were used to analyse the bicomponent fibre samples. It was found that normal transmission analysis and the use of a diamond anvil cell produced good quality infrared spectra for the nylon type fibres, Monvelle (Monsanto) and Cantrece (DuPont); however, problems were encountered when analysing the acrylic bicomponent fibres. Interference fringing, which appears as a sinusoidal wave in the baseline, was seen in many of the spectra obtained, along with sloping baselines. This is not uncommon in the single-point infrared analysis of acrylic fibres in general. There are a number of reasons why interference fringing can occur, such as if fibre samples are flattened on a smooth surface to produce a thin film (due to internal reflections of the infrared beam within the sample), and they can also occur when using a diamond anvil cell accessory (due to multiple reflections occurring at the diamond faces) (19). To overcome these problems, the fibre samples

were flattened using a roughened metallic hand-roller for transmission analysis, to avoid obtaining a thin smooth sample, and infrared spectra were acquired through only one diamond face (as is the normal practice), to reduce reflections occurring between the diamond faces. Several other attempts were made to overcome this interference fringing including: (i) the addition of paraffin oil to the diamond anvil cell to remove air gaps and thus reduce refractive index differences (19, 107); and (ii) the use of an attenuated total reflectance (ATR) microscope accessory.

The first option, which involved the addition of a drop of paraffin oil to the diamond anvil cell, did reduce the amount of interference fringing seen in the infrared spectra. This is due to the refractive index of paraffin being higher than that of air. The large difference in refractive index between diamond (2.42) and air (1.003) (or the sample in question), contributes to interference fringing. The addition of paraffin oil (1.48) reduces the overall difference in refractive indices, which in turn reduces reflection at the diamond interface, and this leads to less interference fringing (19, 107). Paraffin oil was chosen because, although it will contribute to the infrared spectra of the fibre sample, paraffin has very few infrared bands and therefore its contribution can be easily monitored and, if desired, spectrally subtracted prior to library searching for fibre identification. Another option would be the use of potassium bromide (KBr) powder, which is not quite as convenient as paraffin to use in this way, but has the advantage of having no infrared peaks.

The second option, in which a germanium micro-ATR accessory was used to analyse the fibres side-on, was able to produce very good quality infrared spectra without

interference fringing. There are, however, a number of drawbacks when using micro-ATR imaging, including that a much higher number of co-added scans were required to obtain an acceptable signal-to-noise ratio. At least 1024 scans are recommended, which takes a total time of 25 minutes (at 8 cm^{-1} resolution), compared with 5-6 minutes for the 256 scans required to analyse the fibres in transmission. Another difference between micro-ATR imaging and the transmission methods tested is the image size possible. With micro-ATR imaging, due to the high refractive index of the ATR crystal, a field of view of only around 80 μm x 80 μm is obtained (53, 108). For the analysis of many of the bicomponent fibre samples, which ranged from 10 μm to around 80 μm in diameter, this image size is still satisfactory. However, for all of the bicomponent samples tested in this research, side-on analysis using micro-ATR imaging was only able to image one component, and therefore did not reveal any of the fibres as being bicomponent. This is because micro-ATR imaging is a surface-preferenced technique, which means for side-on analysis of the fibres, the technique would most likely not detect a sheath-core configuration, as only the sheath material would be imaged by the ATR crystal. This was the case with the known sheath-core bicomponent fibre Trevira 256, in which micro-ATR imaging of the fibre side-on revealed a spectrum of only the polyethylene sheath component. Unfortunately, the spatial configurations (i.e. sheath-core or side-by-side) for the majority of samples analysed in this research were generally unknown, with the fibre reference libraries identifying these samples only as being bicomponent. From previous studies and results obtained from this study, some of the fibre samples were known to be side-by-side bicomponent fibres, and theoretically could have been identified as such by micro-ATR imaging (14). It

may be that, by chance, the ATR crystal was only making optical contact with one component of the side-by-side fibres. For this reason, multiple samples were prepared and many repeat tests were conducted; however, micro-ATR imaging still failed to detect any second component present in the known side-by-side bicomponent fibre samples. For the reasons discussed previously, infrared analysis using either normal transmission mode or the use of a diamond anvil cell is recommended as the most suitable and practical sampling methods. If major problems are encountered with interference fringing and sloping baselines, then side-on analysis using micro-ATR imaging may assist in obtaining better quality spectra of at least one component.

Overall, infrared spectral imaging had varied success in identifying the presence of two chemically distinct regions in each bicomponent fibre sample. Published classification schemes, including Grieve's (1995) acrylic fibre identification key, were used in conjunction with other references (Grieve, 1988; Kirkbride & Tungol 1999) to identify the chemical compositions of the fibres (14, 17, 19). In seven of the twelve samples examined, two side-by-side or sheath-core components could be clearly distinguished and in most cases these components could be characterised (see Table 3.2).

FIBRE	MANUFACTURER	POLYMER COMPOSITION	SPATIAL CHARACTERISATION
Cashmilon G4K	Asahi Chemical Co.	PAN-MA-AA/PAN-MA	Side-by-side
Acrilan B57	Monsanto	PAN/VA	No
Acrilan B94	Monsanto	PAN/VA	No
Monsanto X-24	Monsanto	PAN/VA based (with minor spectral variations in range 1000-1300 cm^{-1} that concur with Grieve's spectrum 1995)	No
Monvelle	Monsanto	PA/PU	Side-by-side
Velicren bicomponent	Snia	PAN/MA/Sulphonate + DMF	No
Beslon F040	Toho Rayon	PAN-MA-AA/PAN-MA	Side-by-side
Orlon 21	DuPont	PAN/PAN-SS	Side-by-side
Cantrece	DuPont	Nylon 6,6/Unknown polyamide component	Side-by-side
Creslan 68	American Cyanamid Co.	PAN/MMA (without DMF solvent)	No
Dralon K	Bayer	PAN/MA/Sulphonate + DMF	Side-by-side
Trevira 256	Trevira	PE/PET	Sheath-core

Key: PAN: Pure Acrylonitrile; MA: Methylacrylate; AA: Acrylamide; VA: Vinyl Acetate; DMF: Dimethylformamide; PA: Polyamide; PU: Polyurethane; SS: Styrene Sulphonate; MMA: Methylmethacrylate; PE: Polyethylene; PET: Polyethylene Terephthalate.

Table 3.2: *Polymer compositions of fibre samples determined by the author using published classification schemes and the Microtrace Fibre Reference Collection.*

An example where two side-by-side components could be characterised is the Monvelle (Monsanto) fibre, which is identified in the Microtrace Fibre Reference Collection as containing polyamide and polyurethane components. Fig. 3.4 shows the visible light image of the sample, in which only a faint division line can be seen, possibly indicating that the sample is a bicomponent fibre. However, infrared spectral images, formed by imaging the integrated spectral intensity under peaks centred near 1641 cm^{-1} (amide I in polyamide) and 1735 cm^{-1} (carbonyl stretch in polyurethane), clearly reveal not only that this sample is bicomponent, but also show its spatial configuration to be that of a side-by-side bicomponent fibre (Figs. 3.8(a) and 3.8(b)). The two components are clearly distinguished, and the infrared spectra for each component can be easily obtained from the appropriate pixels. These spectra are shown in Figs. 3.8(c) and 3.8(d), where the peaks used to form the corresponding spectral images are highlighted.

An example where the core and sheath components could be characterised is the Trevira 256 (Trevira) fibre, which is known to contain polyethylene (PE) and polyethylene terephthalate (PET) components. Fig. 3.9(a) shows the visible light image of the fibre sample flattened in the diamond anvil cell, in which it appears division lines between the core and sheath components can be seen, indicating that the sample is a sheath-core bicomponent fibre. The infrared spectral image, formed by imaging the integrated spectral intensity under the peak centred near 2916 cm^{-1} (C-H stretch in polyethylene), clearly shows this sample is bicomponent, and reveals its spatial configuration to be that of a sheath-core bicomponent fibre (Fig. 3.9(b)). The infrared spectral image shows the outer sheath component as red (i.e. high

intensity of the infrared band 2916 cm^{-1}) and the middle of the fibre as green (i.e. medium intensity, as both the core and sheath components are contributing to the spectra obtained). The two components are clearly distinguished, and through spectral subtraction, the infrared spectra for both the core and sheath components can be easily obtained. By selecting a pixel from the edge of the fibre, an infrared spectrum of the polyethylene sheath is obtained (Fig. 3.9(c)). The infrared spectrum obtained from the centre of the fibre image is a combined spectrum of both the sheath (PE) and core (PET) components (Fig 3.9(d)). Through spectral subtraction, a spectrum of the PET core component can be obtained (Fig 3.9(e)).

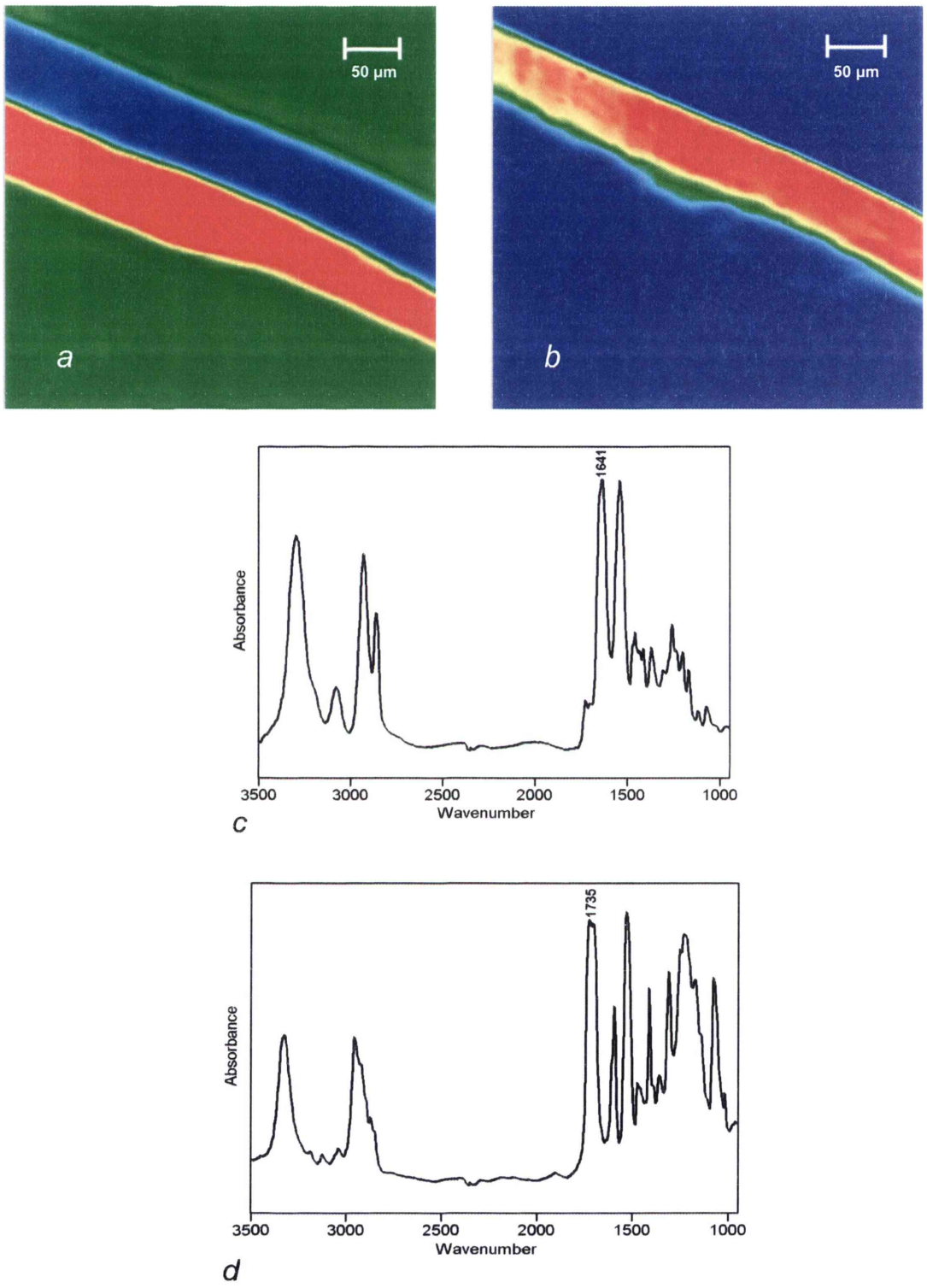

Figure 3.8: *Infrared spectral image of Monvelle (Monsanto) formed by imaging at (a) 1641 cm^{-1} and (b) 1735 cm^{-1}. Infrared spectrum of (c) bottom component, identified as nylon, and (d) top component, identified as polyurethane, from Monvelle (Monsanto).*

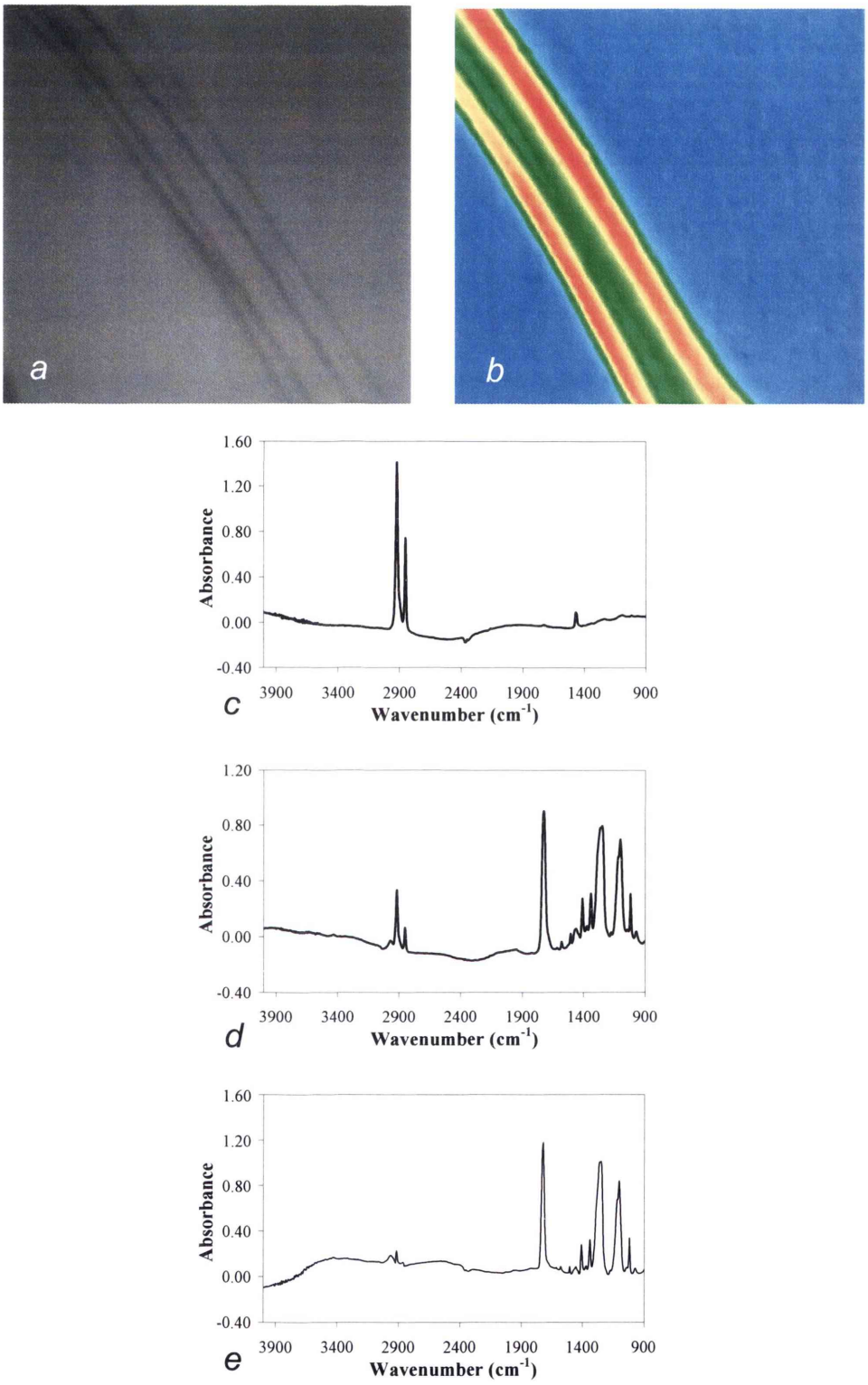

Figure 3.9: *(a) Visible image of Trevira 256 fibre and (b) infrared spectral image of Trevira 256 formed by imaging at 2916 cm^{-1}. Infrared spectra of (c) sheath component, identified as PE (d) combined core and sheath components (PE and PET) and (e) core component, identified as PET, from Trevira 256.*

Two other samples that were revealed to be of side-by-side configuration were Beslon F040 (Toho Rayon) and Cashmilon G4K (Asahi Chemical Co.), both of which have previously been identified by the Microtrace Fibre Reference Collection as containing PAN-MA-AA/PAN-MA (see Table 3.2 for abbreviations). Acrylamide can be added to one side of a bicomponent fibre to produce a different shrinkage potential in that side, which generates a permanent crimp in the fibre (17). It was possible to distinguish the two components in these fibres by imaging on the characteristic amide I (C=O) peak for acrylamide at 1684 cm^{-1} (integrated intensities under peaks are used for all images in this chapter). As similar images and spectra were obtained for these fibre samples, the results for Beslon F040 only are shown here. The first infrared spectral image shown, Fig. 3.10(a), was formed by imaging on a peak that is common to both acrylic components, the nitrile (C≡N) functional group at 2244 cm^{-1}. As this peak is common to both components, the entire width of the fibre is highlighted (i.e. both components can be seen and appear the same). However, by imaging on an infrared peak present in only one of the components (1684 cm^{-1} due to acrylamide), only that component is highlighted (Fig. 3.10(b)). As noted previously, it is easy to obtain the infrared spectrum from each component simply by selecting a pixel from each component (Fig. 3.10(c)).

As can be seen with the above examples, there were two possible ways the spectral images could be formed to highlight the spatial configuration of the components. With Monvelle (Monsanto) the two components could be clearly imaged independently as there were infrared bands present in each component that were characteristic of only that component. However, as could be seen for Beslon F040,

only one side of the fibre contains a polymer (acrylamide in this case) that enables it to be imaged independently. In these cases, the spatial configuration is revealed by imaging the entire fibre width, and comparing this with the image of the side containing the distinctive component.

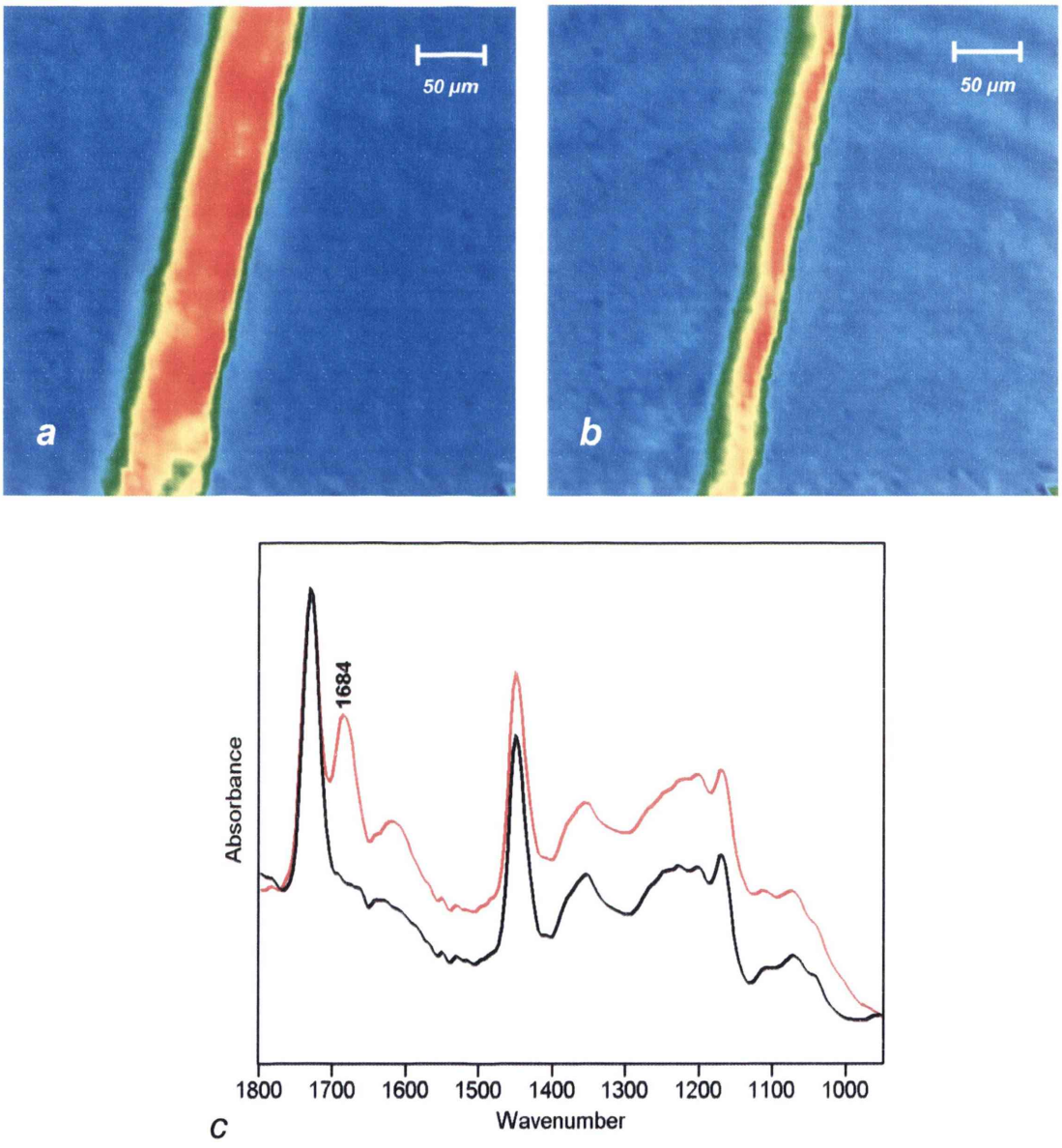

Figure 3.10: *Infrared spectral image of Beslon F040 (Toho Rayon) formed by imaging using the peak area at (a) 2244 cm^{-1} and (b) 1684 cm^{-1}. c) Infrared spectra of the two components in Beslon F040 (Toho Rayon). Spectra have been truncated for Figs. 3.10 – 3.13 to allow minor differences to be seen more clearly.*

The three remaining samples for which two side-by-side regions could be distinguished, i.e. Orlon 21 (DuPont), Cantrece (DuPont) and Dralon K (Bayer), gave images that were similar to those already shown. For Orlon 21 (DuPont), which has previously been identified as containing PAN/PAN-SS, the entire width of the fibre is highlighted by imaging on the common acrylic peak at 2244 cm^{-1} (Fig. 3.11(a)). The component containing styrene sulphonate is highlighted by imaging on either one of the characteristic doublet peaks at 1011 and 1036 cm^{-1}, which have been assigned to, respectively, in-plane bending of the benzene ring and a symmetric vibration of the SO_3^- group (Fig. 3.11(b)) (109). Another peak that could be used to image the PAN-SS component was a shoulder at 1191 cm^{-1} (antisymmetric SO_3^- vibration) (109). The infrared spectra of the two components are shown in Fig. 3.11(c), in which the peaks that can be used to image the PAN-SS component are indicated. Similar images were obtained for Dralon K, which was found to contain PAN/MA/Sulphonate + DMF, according to Grieve's classification scheme (17). The entire width of the fibre was highlighted by imaging on the acrylic peak (2244 cm^{-1}) as shown in Fig. 3.12(a), however it was found that one side appeared to contain a higher amount of methylacrylate, due to the increased peak intensity at 1730 cm^{-1} (the carbonyl group from the ester) (17). By imaging on this peak, only half the fibre width is highlighted (Fig. 3.12(b)). The infrared spectra of the two components are shown in Fig. 3.12(c), where the increased peak intensity at 1730 cm^{-1} is indicated, and also minor differences can be seen between 1250 – 1170 cm^{-1}. It has been reported that the amount of methylacrylate is significant as it influences the shrinking capacity of the fibre, and therefore the addition of extra methylacrylate to only one side of the bicomponent fibre can generate a differential shrinkage potential, leading

to a permanent crimp in the fibre (17). Images similar to those shown for Monvelle (Monsanto) were obtained for the Cantrece (DuPont) fibre sample. Cantrece (DuPont) contains nylon 6,6 and another unknown polyamide component. The exact identification of the other component was not possible, however minor but reproducible spectral differences between the components could be used to image each side-by-side component, with one side containing a shoulder at 1246 cm^{-1} (Fig. 3.13(a)), and the other side exhibiting increased intensity of a peak at 1201 cm^{-1} (Fig. 3.13(b)). Figure 3.13(c) shows the infrared spectra and the characteristic infrared peaks used to form the spectral images that reveal the side-by-side configurations.

In some of these successful cases, some attempts failed to spatially characterise the two distinct regions, i.e. only one (apparently combined) infrared spectrum could be seen throughout the entire width of the fibre. A possible reason for this is that one component may have been flattened over the other, and hence the infrared beam passed through the two components at the same time, producing a mixed spectrum of the two components. For this reason multiple samples were prepared and analysed. This scenario may lead to potential problems in actual casework, where there may only be limited sample available to analyse. Where possible, it is recommended that repeat preparations (i.e. flattening of the fibre) and analyses of samples is undertaken, to ensure that the extra spatial information is not lost due to the way that the fibre is flattened.

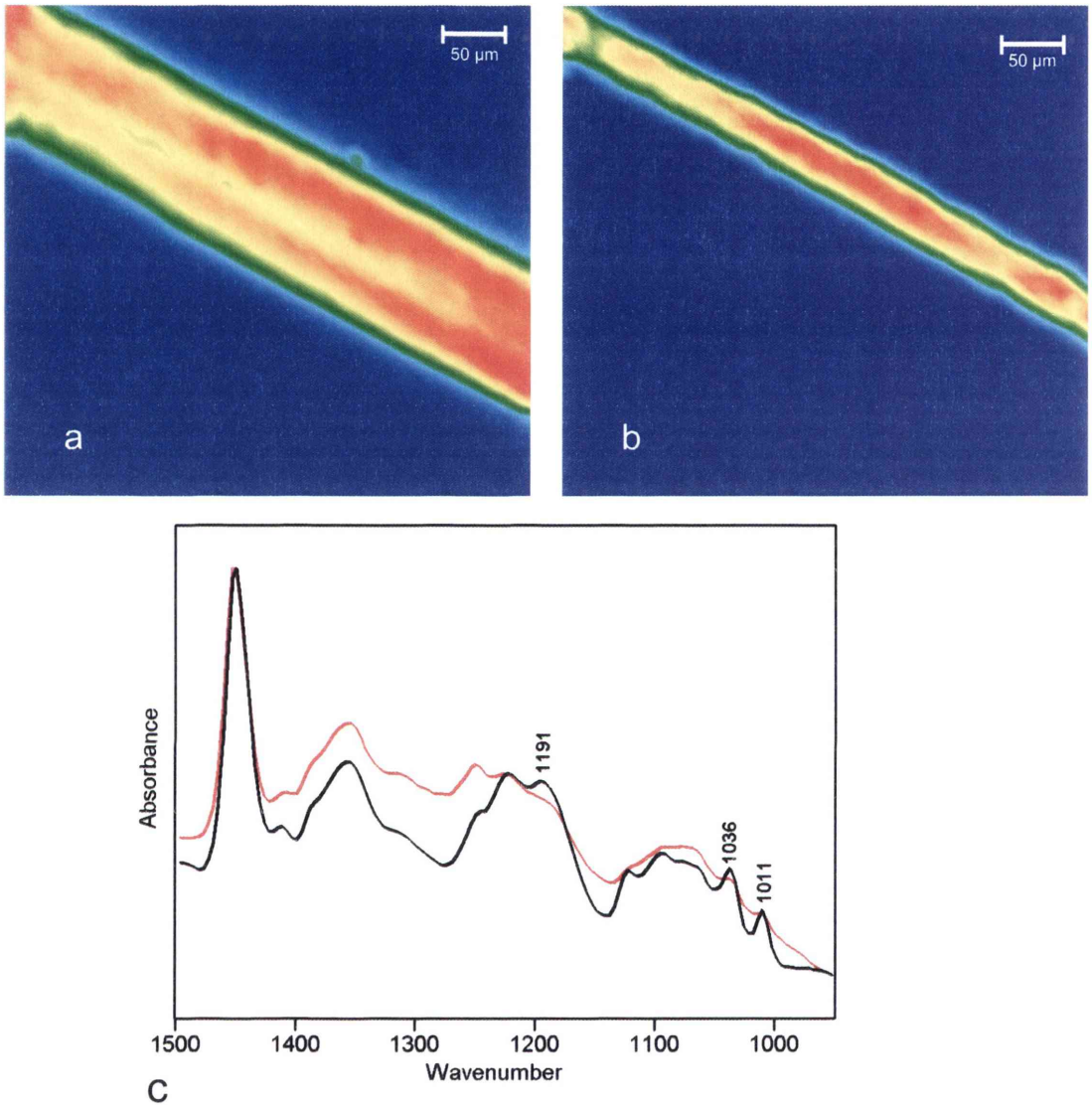

Figure 3.11: *Infrared spectral image of Orlon 21 (DuPont) formed by imaging using the peak area at (a) 2244 cm^{-1} and (b) 1036 cm^{-1}. (c) Infrared spectra of the two components in Orlon 21 (DuPont).*

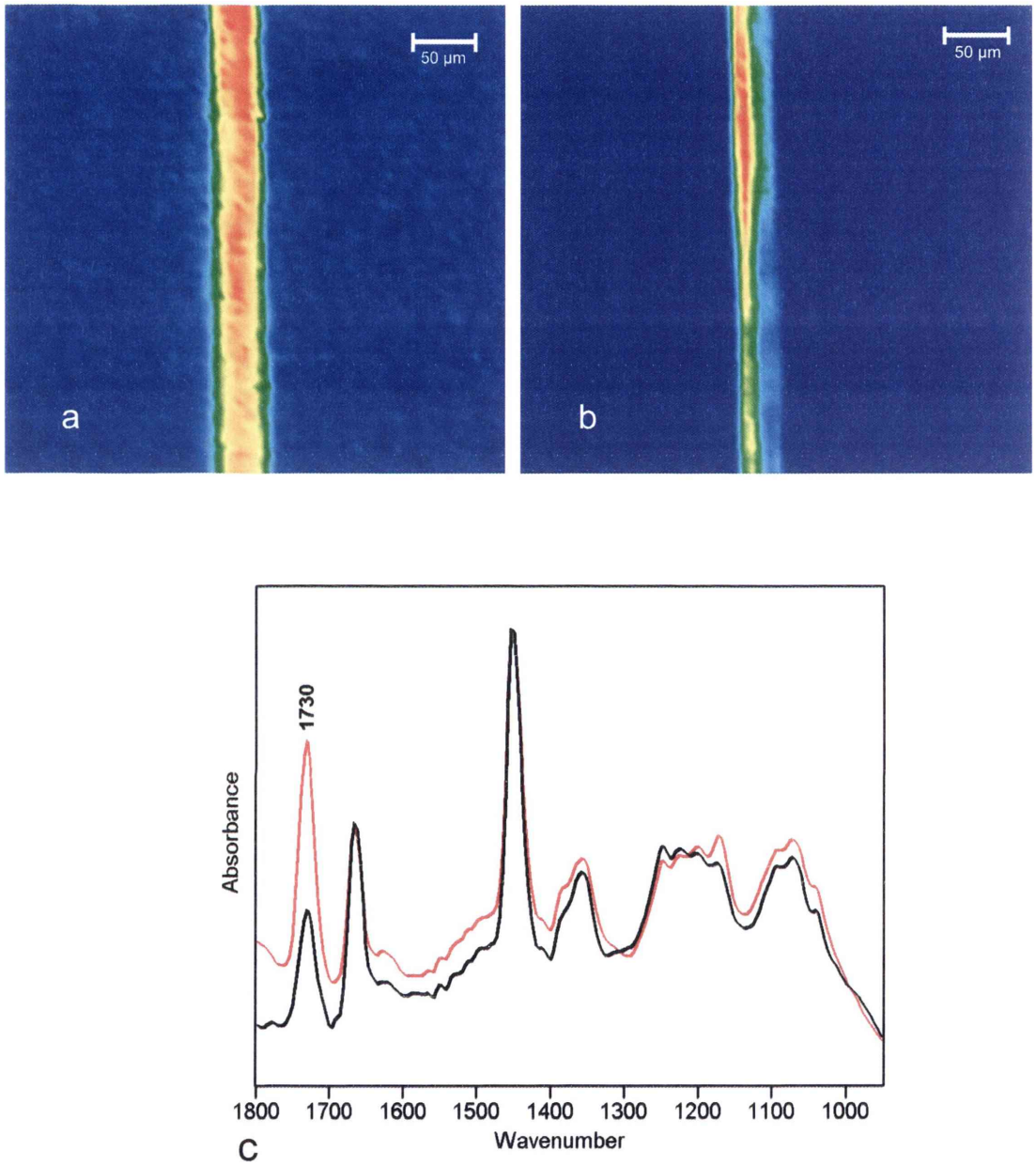

Figure 3.12: *Infrared spectral image of Dralon K (Bayer) formed by imaging using the peak area at (a) 2244 cm^{-1} and (b) 1732 cm^{-1}. (c) Infrared spectra of the two components in Dralon K (Bayer), with the increased peak intensity indicated at 1730 cm^{-1}.*

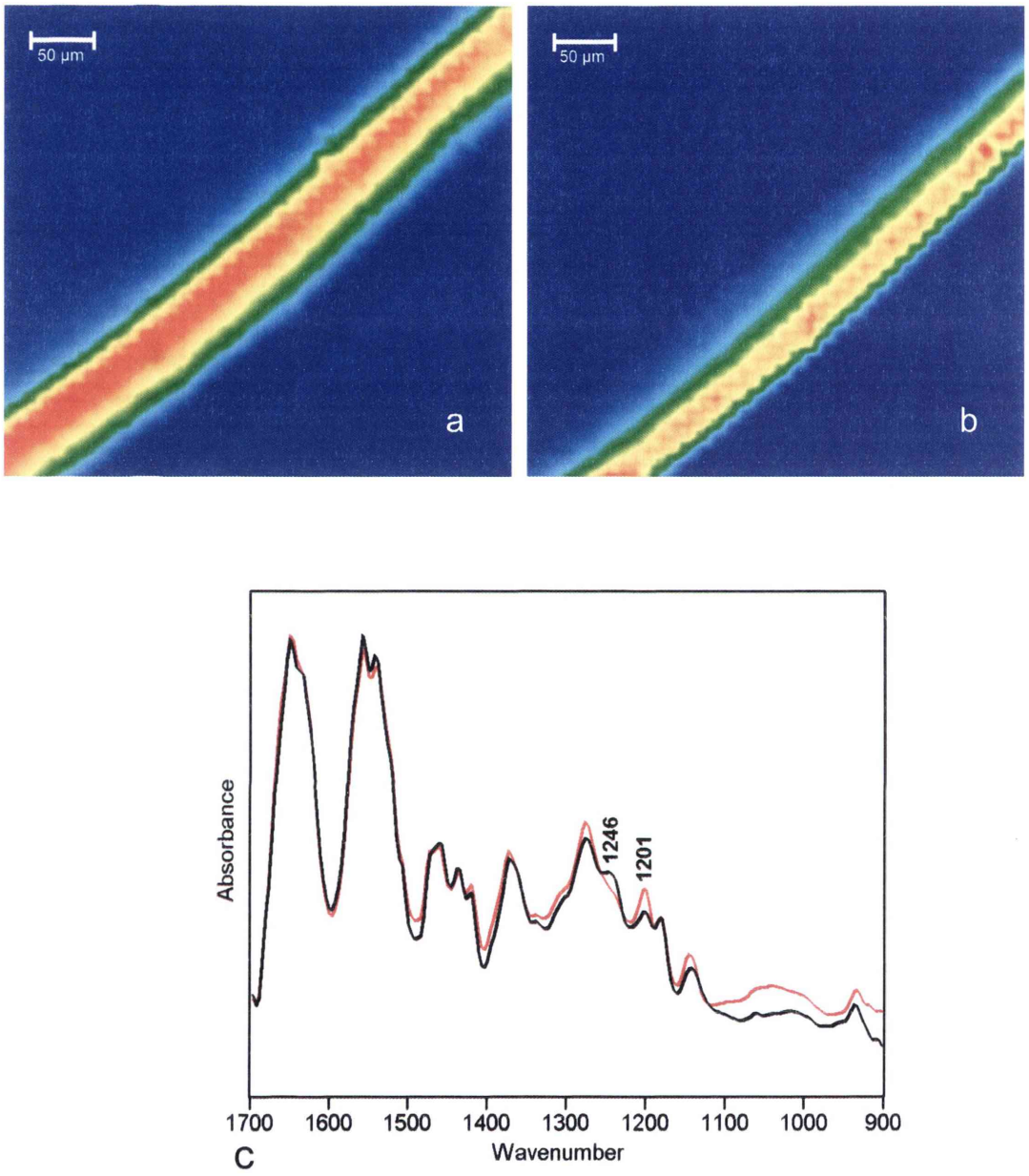

Figure 3.13: *Infrared spectral image of Cantrece (DuPont) formed by imaging using the peak area at (a) 1246 cm^{-1} and (b) 1201 cm^{-1}. (c) Infrared spectra of the two components in Cantrece (DuPont).*

For the rest of the five samples, infrared spectral imaging failed to spatially recognise more than one distinct region being present in each sample. This may have been due to the spectral differences between each component being very minor and hard to detect, a problem that is exacerbated by the presence of interference fringing or sloping baselines, both of which were common in the infrared spectra of the acrylic-based bicomponent fibres. Creslan 68 (American Cyanamid Co.) is an example of a fibre that is identified in a fibre reference library as being bicomponent (acrylic/acrylic), but in which the two components may be so chemically similar that spectroscopic differences are either undetectable or masked by interference fringing.

Another possibility is that the samples, although referred to as bicomponent samples, may indeed contain only one component. It was reported by Grieve et al that the chemical composition of random bicomponent fibres, such as Acrilan B94 (Monsanto), Creslan 68 (American Cyanamid Co.) and Beslon F040 (Toho Rayon), can vary through all possibilities from 100% of one polymer to 100% of the other polymer (14). Obviously the examination of fibres at the extremes of these composition ranges will be particularly difficult. It is possible that some of the random bicomponent samples examined in this study did contain close to 100% of one polymer, explaining why the spectrum of only one polymer was detected. It may also be possible that the size of the regions of one component may be too small to be spatially resolved by infrared spectral imaging. As mentioned previously, a spatial resolution of around 15 μm is possible with the 'normal' field of view (or around 5 μm with micro-ATR imaging). Therefore, if regions of one component are smaller than the best spatial resolution possible, this component would either go undetected

by infrared spectral imaging, or its spectra would be averaged with those of the other component. The composition of the polymers contained in the fibres were still able to be determined using the infrared spectra obtained, and by following the classification schemes previously mentioned (see Table 3.2).

Cross-sectional analysis of the fibres was fairly tedious and time-consuming. Unfortunately, the majority of commercially available embedding resins are purposely designed to be colourless, to allow for the correct orientation of samples within the resin, and for microtoming. It was therefore necessary to dye the resin material to overcome the initial difficulties in locating the white-to-colourless fibres in the colourless resins. Once the resins were dyed purple, it was a much simpler task locating the fibre cross-sections for imaging. Excellent results were obtained with transmission analysis for Monvelle (Monsanto), with the two side-by-side components clearly visible in the infrared spectral image of the fibre cross-section (Fig. 3.14). Unfortunately, the resins appeared to infiltrate the rest of the fibre samples (most of which were acrylic-based) and no remedy for this was found in this study. Attempts were made to image the cross-section of the fibres using a germanium ATR crystal. As for the transmission cross-sectional analysis, micro-ATR imaging was found to only be successful for imaging the cross-section of the Monvelle (Monsanto) bicomponent fibre (Fig. 3.15). The use of an ATR crystal to image the fibre cross-sections has a number of advantages, including the higher spatial resolution relative to transmission analysis that is achieved (53), and it avoids the need for thin sections to be microtomed, as the fibre cross-section is analysed whilst remaining in the resin block. There were, however, a number of difficulties

encountered with the ATR technique. It was difficult to align the ATR crystal so that it made contact exactly with the fibre cross-section because the germanium ATR crystal is optically opaque and does not necessarily engage or lock into the exact same position when it is inserted into the microscope objective. In addition, the sample would occasionally move slightly when the ATR crystal was placed in contact with the resin block. At this stage, the micro-ATR imaging technique for examining the fibre cross-sections would not be practical in a forensic laboratory setting due to the time-consuming aspects of aligning the ATR crystal exactly on the correct location on the sample. It may be worthwhile testing a different type of ATR crystal which is not optically opaque and has a flat surface (e.g. diamond) or to conduct the testing on another instrument, which may not suffer from some of the alignment problems which were encountered in this research. The difficulties in locating the colourless fibre cross-sections in the resin also exacerbated the problems in aligning the ATR crystal.

Even though there were difficulties encountered with the technique, cross-sectional analysis of possible bicomponent fibres using infrared spectral imaging would be the ideal approach where possible and convenient, as it would remove the ambiguities inherent to side-on analysis, particularly for sheath-core fibres and would overcome the occasional problems (indicated above) caused by the flattening of side-by-side fibres.

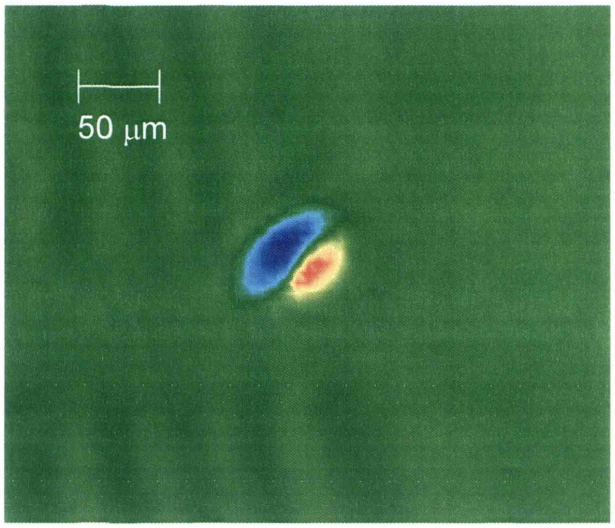

Figure 3.14: *Transmission infrared spectral image (1648 cm^{-1}) of a fibre cross-section from Monvelle (Monsanto).*

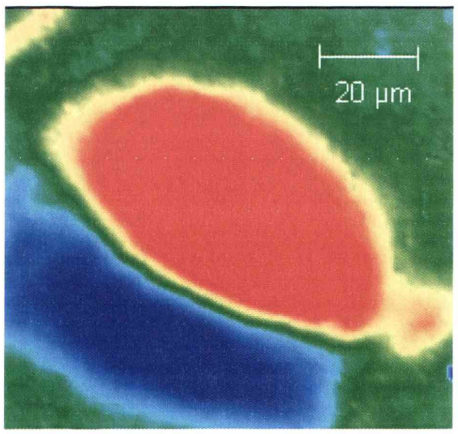

Figure 3.15: *ATR infrared spectral image (1648 cm^{-1}) of a fibre cross-section from Monvelle (Monsanto).*

Overall, infrared spectral imaging was shown to be a technique that can provide spatially resolved chemical information on bicomponent fibres as long as detectable spectral differences exist between the two components. The common conventional techniques were shown to occasionally detect and spatially characterise side-by-side and sheath-core bicomponent fibres; however, unlike infrared spectral imaging, such techniques fail to provide chemical information on the components present. Unfortunately, no one technique examined was shown to work for all of the types of bicomponent fibres analysed in this research. Although infrared spectral imaging will not identify/analyse bicomponent fibres with success in all cases, it does improve significantly upon the standard methods of analysis, and would be an asset when used in conjunction with these.

Infrared spectral imaging fits into the current examination sequence for fibre analysis, and can easily replace the conventional infrared spectroscopic analyses for fibres, since for side-on analysis it requires the same sample preparation as for conventional analysis (e.g. flattened and analysed in a diamond anvil cell). The technique has the advantage that it can be used for both sheath-core and side-by-side bicomponent fibres and can also be used for obtaining hundreds of spectra within single-component fibres, and therefore can completely replace conventional infrared analysis. In addition, as infrared spectral imaging allows for hundreds of spectra to be simultaneously obtained, rather than just a handful of single averaged spectra, as is the case in single-point infrared analysis, confidence in the results is greatly increased. If spectral differences are detectable, infrared spectral imaging may be able to detect other heterogeneities present within the fibre samples, such as surface

treatments, dye components etc. Using the traditional forensic analysis techniques (including conventional IR analysis), Grieve et al failed to detect bicomponent fibres in a garment encountered in actual casework that was known to contain Monsanto bicomponent fibres (14). Using infrared spectral imaging for analysing fibres instead of conventional infrared techniques allows for the greatest possibility that a bicomponent fibre will be detected if encountered in routine casework.

A disadvantage of infrared spectral imaging is that it does take longer than conventional IR analysis, taking 5-6 minutes per fibre as opposed to a collection time of approximately 30 seconds with conventional IR analysis. Even though the difference in analysis time sounds quite large, especially when considering the large workload of trace evidence laboratories, there is a substantially greater amount of information obtained from each fibre sample, and the potential evidential value gained when a bicomponent fibre is detected should outweigh any concerns regarding analysis time. It should also be noted that the most time-consuming aspect of a forensic fibre examination is the searching and collection of evidential fibres and also sample preparation, and therefore, an additional five minutes spent conducting infrared imaging analysis is fairly inconsequential when the whole forensic fibre examination time is considered.

3.4 Conclusions

In summary, infrared spectral imaging has been demonstrated as a technique that can be used to both recognise and provide spatially resolved chemical information for those bicomponent fibres where it is possible to detect spectral differences between

the two components present. It is a relatively rapid technique (5-6 min for 256 scans at 8 cm^{-1} resolution) that provides a large wealth of information, which includes not only the spectral signatures of the chemical components of a sample, but also their locations within the sample. As demonstrated, results can be visualised in numerous different ways, including the forming of spectral images, which allow the spatial distribution of the two components in the fibre sample to be clearly seen, an obvious advantage for displaying results to a layperson such as a jury member. While it was not successful in providing spatial information for certain samples examined in this research (where the two components were chemically very similar), the potential of infrared spectral imaging has clearly been demonstrated, with its ability to reveal both a fibre's chemical composition and spatial configuration with a single measurement. Few other techniques (apart from perhaps Raman spectral imaging) would be capable of providing this information without any prior knowledge of the fibre's bicomponent nature and the configuration of its components, although more research is required prior to introducing this method into a routine case-working environment, particularly with the cross-sectional analysis. When the method reaches its potential, the case-working analyst will require advanced skills to conduct the imaging and spectral interpretation.

As found with the paint chip work, one of the most time-consuming and difficult steps in the whole process was that of sample preparation. For side-on analysis, where the fibre remains intact and only needs to be flattened prior to analysis, the only difficulties encountered included those of interference fringing and sloping baselines (which are also inherent in conventional IR analysis), and

recommendations were given as to ways to overcome some of these problems. Cross-sectional analysis would be most beneficial for sheath-core fibres, as it would allow for pure spectra to be obtained of each component and for their spatial arrangement to be clearly visualised. However, the preparation of cross-sections proved to be both tedious and time-consuming. Difficulties were found with locating the fibre cross-sections within the resins, even after the colourless resins had been dyed purple, and the resins also infiltrated and contaminated the fibre spectra. Attempts to avoid the microtoming step by using micro-ATR analysis on fibres while still embedded in the resin block were successful in one case, however problems with aligning the ATR crystal directly into contact with the fibre significantly impacted on the practicality of this technique.

Since recent patents report the use of materials such as polyethylene, polyester and nylon to produce bicomponent fibres (110), and since the use of bicomponent fibres is expected to increase in the future, infrared spectral imaging should grow in importance as a forensic tool for the detection and identification of such fibres where there is a measurable spectral difference between the two components.

3.5 Future Work Recommendations

As mentioned above, one of the greatest problems encountered during this work was due to the sampling methods, and specifically with the imaging of fibre cross-sections. As discussed previously in Section 2.5, there is a great need for the development of new resins which can be used for infrared purposes. Development of a resin that does not contaminate the infrared spectrum would greatly aid the analysis of bicomponent fibre cross-sections.

Further research should be conducted into the use of micro-ATR imaging for analysing fibre cross-sections. The micro-ATR technique has the advantage that no microtoming is required, and therefore would significantly cut-down on the time required for sample preparation. The micro-ATR technique can also achieve a higher spatial resolution in comparison to transmission analysis. As discussed previously, problems were encountered with placing the ATR crystal in direct contact with the fibre cross-section. This was due to a number of factors including that the germanium ATR crystal is optically opaque, the ATR microscope attachment did not always lock or engage into the same position when inserted into the microscope, and the sample would also occasionally move slightly when the ATR crystal was placed in contact with the resin block. Future research should be conducted to try overcome these problems, and should include testing with an optically transparent ATR crystal with a flat surface (such as a diamond ATR crystal), and testing should be conducted on another infrared spectral imaging instrument that may not suffer some of the alignment problems which were encountered with the instrumentation used in this research. It would be worthwhile testing the Perkin Elmer FT-IR Imaging ATR accessory, which was released in 2006, which allows for a larger area to be imaged than was achieved with the instrumentation used throughout this study (using the infrared microscope). The Perkin Elmer FT-IR Imaging ATR accessory contains a germanium ATR crystal with a 600 μm diameter sample area that can image a sample a few hundred microns across, at a high spatial resolution of around 3 μm (99). The use of this ATR accessory, with its capability to image a larger area whilst still achieving a high

spatial resolution, may overcome some of the problems described above for locating and analysing bicomponent fibre cross-sections using micro-ATR imaging.

It should be noted that in this research, only integrated peak intensities were used to attempt imaging of the bicomponent fibres. This requires the operator to examine the infrared spectra from across the fibre sample to assess whether there is more than one chemical component present, and then choose a suitable peak to form images of the two components. In some of the bicomponent fibres examined, there were only extremely minor differences between the spectra of each component, and therefore these fibres could potentially be overlooked during a case scenario. Future work could be conducted into using multivariate statistical techniques, such as hierarchical cluster analysis (HCA), which can be used to highlight small but consistent differences between the spectra (97). Alternatively, composite images based on spectral intensities at more than one wavelength could be constructed. The use of such techniques would however require a much greater level of operator expertise, and problems may be encountered applying multivariate statistical techniques when there are interference fringes present in the infrared spectra.

CHAPTER 4:

Examining Intersecting Lines Using ATR-FTIR Spectral Imaging

Chapter 4: Examining Intersecting Lines Using ATR-FTIR Spectral Imaging

4.1 Introduction

4.1.1 Questioned Documents

Documents play a major role in our everyday life. A document can be defined as 'any material containing marks, symbols, or signs that convey meaning or a message to someone' (111). A questioned document is one which is 'suspected of being fraudulent or whose source is unknown or background is disputed' (111). There are a large number of documents that may be used in criminal activities such as wills, birth certificates, contracts, cheques, licences, logbooks, to name just a few. Criminal activities involving documents can cost billions of dollars per year (112). Examples of crimes which could potentially involve questioned documents includes kidnapping (ransom notes), identity fraud, business fraud such as altering contracts, wills, medical malpractice (doctored notes), counterfeiting money and the list goes on.

Questioned documents can be completely forged, or a genuine document may be altered. There are a number of ways in which a genuine document can be altered – these include:

- erasures – writing material is removed through chemical means or by abrasion/scraping.
- obliterations – the original text is covered up by some opaque material and cannot be read.

- additions – material is inserted so as to potentially alter the meaning of the original document. The addition may be an interlineation, where the added text does not overlap with the original material on the document; or it may be overwriting, where a portion of the added text overlaps with the original text. It is the latter type of addition, where a portion of the text overlaps with the original text, which is examined in this research.

4.1.2 Writing and Printing Materials

A variety of writing and printing materials can be used to produce documents, such as ballpoint pens, laser & ink-jet printing. A brief overview of the materials examined throughout this research is given here.

4.1.2.1 Ballpoint Pens

Ballpoint pens are by far the most common type of pen used for handwritten documents (113). The ballpoint pen was developed in Europe in the mid to late 1930s. By 1946 several million Reynolds ballpoint pens were distributed in the United States. The ballpoint pen design was a completely new way of placing ink on paper. The way a ballpoint pen works is through a small steel ball, located at the end of a tube. The ball is contained in a housing that allows it to rotate freely, and whilst the pen is in motion across the paper surface, the ball rotates and delivers ink from the reservoir above it to the paper (113, 114). Most ballpoint pen inks contain three components, these being dyes, resins and volatiles. Unlike many other fluid writing inks, ballpoint point pen ink is a highly viscous, paste-like substance with a glossy appearance. The viscosity in ballpoint pen inks is due to the high dye content, as

much as 50% of the whole ink formulation (112). Ballpoint pen ink dries rapidly once deposited onto the paper, and is only partly absorbed into the paper surface. This is in contrast to the fluid inks in many other types of pens, such as roller-ball, felt-tip and gel pen inks, which absorb into the paper (113, 114). There are a number of materials that can be found in ballpoint pen inks including synthetic dyes (sometimes with carbon or graphite added to assist with permanence) in various solvents (often glycol or benzyl alcohol), fatty acids (as a lubricant), resins, surface active ingredients, corrosion control ingredients, and viscosity adjustors. Prior to the 1950s, ballpoint pen inks were made with oil-based solvents (e.g. mineral oil, linseed oil, glycerin monoricinoleate). Post-1950 ballpoint pen inks are often called glycol-based inks, due to the use of ethylene glycol or glycol derivatives as the solvents; however benzyl alcohol is also commonly used (112).

4.1.2.2 Porous-tip Pens

There are a number of names which can be used when referring to this class of pen including porous-tip, fibre-tip, and felt-tip pens. This type of pen was developed in Japan around 1962 by Pentell. Instead of using a small rotating ball to deliver the ink, these pens deliver ink by a capillary action from the ink reservoir through the porous writing point of the pen, and onto the paper surface (113). The writing point can be made up of compressed dense fibres (fibre-tip), less dense fibre bundles (felt-tip) or some companies even use a hard, perforated plastic tip (hard-tip) (114). The inks used in these pens are water or xylene-based and contain dyes which are water-soluble or acidic dye salts. Other ingredients that may be found include formamide and/or glycol additives, which are added to stop the writing tip from drying out

(112). The aqueous ink is absorbed into the paper when the writing tip makes contact.

4.1.2.3 Roller Ball Pens

Roller ball pens were first sold in Japan in the late 1960s. The roller-ball pen design is the same as the ballpoint pen (i.e. the ink is transferred through a rotating metal ball), however instead of using a viscous paste-like ink, the roller-ball pen uses a water-based fluid ink similar to that used in porous-tip pens. As with the porous-tip pens, the fluid ink generally saturates the paper (114).

4.1.2.4 Gel Pens

Gel pens were first developed in 1984 by the Sakura Color Products Corporation (Japan). The concept behind the invention of gel pens was to produce an environmentally friendly pen which did not contain volatile organic components. These pens operate in the same way as ballpoint and roller ball pens, but use different inks. The gel pens were initially produced using a highly viscous pigment-based ink, however modern gel pens use both dye-based and pigment colouring. These pens are very popular with children and artists, due to the wide variety of colours available and the ability to yield ink strokes with a metallic appearance (114).

4.1.2.5 Ink-jet Printing

Ink-jet printing is a non-impact method of printing, in that it does not touch the surface in order to create an image. Ink-jet printers work by projecting small

droplets of ink onto the receiving surface, such as paper. Unlike traditional typewriters, in which the entire character image is produced on the paper in one stroke, ink-jet printers produce the characters through a series of dots. Ink-jet printing works through the use of a print head containing a series of nozzles that spray single droplets of ink onto the paper in order to build up the desired image. There are two main ink-jet technologies that are commonly used, thermal (bubble) and piezoelectric systems. In a thermal ink-jet printer (also known as bubble-jet), voltage pulses are sent to a heating element, and this heats the ink to its boiling point to create a bubble. The force of the expanding bubble causes some of the ink to be pushed out of the nozzle onto the paper. Typically, a bubble jet print head has 300 or 600 tiny nozzles, all of which can fire a droplet simultaneously. The more nozzles the print head contains, the higher the quality of printing. Piezoelectric technology was patented by Epson, and involves the use of piezo crystals. These crystals are located at the back of each ink reservoir of each individual nozzle. When an electric charge is applied to the crystals, this causes the crystals to vibrate. The vibration forces a small amount of ink out of the nozzle onto the paper. Ink-jet printer inks can be water-based, pigment-based or dye-based (113, 115, 116).

4.1.2.6 Laser Printing

Laser printing technology uses electrostatic imaging to transfer toner to the paper surface. In general, an electrostatic charge is applied to a photosensitive drum, and then partially discharged by laser in the areas where printing is required. Positively charged toner (fine black powder) is then applied to the drum. Typically, the areas of the drum that have been discharged attract the toner, and the charged background

area repels the toner. Blank paper is then fed through the imaging drum, and the paper is given an electrostatic charge so that it can pull the toner away from the drum. The toner is transferred to the paper surface and fused to its surface through heat and/or pressure. There are variations to this method, in which the system can operate on the reverse electrical charges to those described above (also known as print-white process). The toner material is a fine black powder that may contain some of the following components: binding agents (typically organic resins, e.g. styrene/acrylate copolymer), pigment (carbon black), additives (fused silica), carrier (spherical ferrite) (113, 116, 117).

4.1.3 Forensic Document Examination – Intersecting Lines

Forensic document examiners are often called upon to determine the sequence of intersecting lines. An example of where it may be important to determine the order of strokes could be in a document such as a will or contract. The addition of an extra clause or paragraph could dramatically alter the terms of the agreement. If the added text overlaps, or intersects, with the signature on the document, then the alteration may be detected by examining the order of the strokes.

There are two main types of line intersections, homogeneous and heterogeneous. A homogeneous line intersection is defined as one where the line crossings have been produced using the same type of writing instrument or printing device, for example line crossings produced using two ballpoint pens. A heterogeneous line intersection is one where two different types of writing instruments and/or printing devices have been used to produce the line crossings, such as a laser printer and a ballpoint pen, or

even a ballpoint pen and a gel pen (118). In this research, both types of line crossings are examined.

Many of the techniques used in forensic laboratories to examine line crossings are based on optical examination and observation of physical characteristics. These have the advantage of being non-destructive, but they do suffer some drawbacks. One of the biggest disadvantages of many techniques currently used is that they are subject to human interpretation. Optical microscopy is the most widely used technique in determining the sequence of intersecting lines (119). The drawback of this technique is that optical illusions can occur; for example, a heavier or darker pen stroke may appear to be on top of a lighter pen stroke, regardless of the actual order of strokes (111, 120). It has also been reported that with line intersections, 'there is a tendency to see what one perceives to be the correct sequence' (121). It may be that two document examiners examine the same intersection, and come to different conclusions regarding the order of strokes, as demonstrated later in this chapter.

A number of techniques are available to examine intersecting line samples, and the choice of technique depends on a number of factors such as the writing tools used to produce the intersecting lines, and whether a non-destructive technique is required over a destructive one. For forensic analysis, a non-destructive technique is always preferred over a destructive one, and therefore destructive techniques, such as the scraping technique (121), where part of the toner material can be scraped away to reveal whether the ink deposit is below or above the toner, may not be suitable in many cases. A comprehensive review of the techniques available was conducted by

Poulin in 1996, in which thirty different sequence of stroke techniques were examined (118). Some of the techniques examined include optical microscopy (with various lighting techniques), Scanning Electron Microscopy (SEM), Video Spectral Comparator (VSC) examination, various lifting techniques such as wax or Kromekote lifting, and various chemical reactions. Each of the available techniques has various advantages and disadvantages. Too many techniques have been reported in the literature to mention all of them here, but some of the major techniques reported will be discussed.

Forensic document examiners often rely on visual examination of various physical and optical characteristics in order to determine the sequence of strokes. Such examinations include, among others, the observation of specular reflectance when ballpoint ink is applied over toner material (122), examination of infrared luminescence for pen crossings (only successful if one of the two pens luminesces) (123), the examination of groove configurations (most successful for different coloured pen line crossings) (124), the examination of track lines ('railway effect') produced when two ballpoint pen strokes intersect (125), the examination of the stroke width of the pen lines at the point of intersection, and various other physical characteristics including ink smearing, paper tearing or disturbed paper fibres, skipping (e.g. if an water-based ink is used over a oil-based ink), gaps and striation patterns within ballpoint pen strokes (118). Various lifting techniques have also been explored such as the Kromekote lifting technique (125-127), in which a piece of glossy Kromekote paper is placed over the ballpoint pen intersection and rubbed with enough pressure to remove the edge markings, which can then be observed under a

microscope for the continuity of the track lines, to determine which stroke was applied last. The main disadvantages of many of these techniques is that they are subjective, and there are a number of factors, such as the pen pressure used and the quality and surface of the paper the intersection is on, that can greatly affect the accuracy of results. It is reported with the Kromekote technique that if the first pen stroke was applied at a pressure 2.5 times greater than the second stroke, incorrect results will be obtained in the sequence of stroke determination (125).

Scanning Electron Microscopy was first reported as a method for examining stroke crossings by Waeschle in 1979 (128). Since then, there have been a number of articles published regarding the use of an SEM for line crossing determinations (129-132), and also SEM in combination with various lifting techniques (133, 134). Scanning electron microscopy has been shown to be successful for viewing most heterogeneous intersections involving ink deposits that do not absorb into the cellulose fibres of the paper (such as ballpoint pens, laser printing). One of the initial drawbacks of this method was that it was partially destructive, in that the area containing the line intersection had to be cut from the document and some form of conductive coating applied prior to analysis in the SEM to overcome charging effects. Difficulties have also been encountered examining some felt-tip pen ink, ballpoint pen inks, stamp pad and writing pen inks when only a light writing pressure is used, so that they deposit only a thin layer onto the paper surface (134). The accurate positioning of the line crossing has also been reported to be difficult, and the potential for analysing the wrong area has been highlighted (119). Feasibility studies on the use of Atomic Force Microscopy (AFM) (119) and Environmental Scanning

Electron Microscopy (ESEM) (135, 136), have shown promise. These techniques overcome the original drawbacks of the conventional SEM technique, avoiding the need to cut-out and coat the specimen prior to analysis. Currently, the AFM technique has been shown to be successful for intersections produced using black ballpoint pens and laser and ink-jet printers. Initial studies, using the ESEM technique for line crossings, have shown promise for intersections produced using black ballpoint pens and laser printers, but the technique was not successful for examining ink-jet printer / ballpoint pen intersections. Both Kasas et al. and Stitt et al. indicate that further extensive testing needs to be conducted on the AFM and ESEM techniques (119, 135).

In recent years, there has been a trend towards research examining non-destructive techniques that can provide an objective method of analysis for line crossings, and hence remove the ambiguities encountered when using subjective techniques. Recently examined techniques include FTIR-ATR microscopy for crossed printed text and ballpoint pen lines (discussed further below) (137), and 3D laser profilometry for homogeneous pen line crossings (only useful for writing materials which leave a profile on the paper) (138). These studies outline the potential of these techniques for the examination of line intersections, using only a small range of writing material configurations, and therefore further extensive research into these techniques is required. Research into the use of Raman spectroscopy for examining crossed ink lines, and ink and ink-jet printer crossed lines has also been conducted. The feasibility study by Claybourn et al. (2000) found the technique to be promising for sequencing ballpoint pen line crossings, although they only examined a small

number of line crossings (139). Further investigation into the use of Raman spectroscopy for sequencing crossed ink lines and ink and ink-jet printed lines was conducted by Fabianska et al. (2003). Raman spectroscopy was found not to be an effective or reliable technique for determining the sequence of intersecting lines, with correct sequence determinations in only 54.9% of heterogeneous intersections and 29.1% of homogeneous intersections (140). Time-of-flight secondary ion mass spectroscopy (ToF-SIMS) has recently been investigated for determining the sequence of different coloured ballpoint pen ink and fountain pen ink line crossings (141). Line crossings produced using three different coloured ballpoint pens (black, blue and green) and two different coloured fountain pens (black and green) were examined, and by forming images based on characteristic ions for the different coloured pens, the authors were able to successfully determine the sequence order of different coloured ballpoint pens. Intersections produced using fountain pens were more difficult, and the authors found that often the two different fountain pen inks smeared or mixed with each other and also with the ballpoint pen inks. To successfully image the correct sequence order of line intersections produced using a fountain pen, it was necessary to wait one and a half hours before applying the second ink line, to avoid the effects of mixing or smearing (141). To date, ToF-SIMS has only been demonstrated to be useful for examining ink line crossings where two different coloured inks are used to produce the line crossings. Currently there is no one technique that is suitable for examining all types of line intersections encountered, and the majority of the techniques currently used by document examiners are subjective and can lead to ambiguous results. There is therefore a

need for research into techniques which provide the most objective results possible, for a variety of material configurations.

4.1.4 Infrared Spectroscopic Imaging for Examining Line Crossings

As discussed previously, the ideal technique for determining the sequence of intersecting lines is one which is non-destructive, and can provide an objective method of analysis for a variety of material configurations. Infrared spectroscopy is an objective, non-destructive technique, and is widely accepted for the analysis of many types of forensic evidence. FTIR spectroscopy has been used to analyse various materials encountered when examining intersecting lines, such as paper (25), ballpoint pen ink (26-28), and photocopy and printer toners (23, 24, 142). Even though FTIR spectroscopy has been used to analyse many of the materials commonly encountered in intersecting line samples, at the time of completing this PhD research it had not been used to determine the sequence of strokes. Recently, a feasibility study using conventional FTIR spectroscopy to examine the sequence of strokes was published in the online non-peer reviewed forensic magazine, Global Forensic Science Today (GFST). Gal et al. (2007) used FTIR-ATR microscopy to successfully determine the sequence of crossed printed text and ballpoint pen ink lines (137). They prepared crossed line samples using three black laser printers and three black ballpoint pens. Using a germanium ATR crystal, they obtained spectra at the point of intersection, and by determining the chemical composition of the upper layer, were able to identify the order in which the materials were applied. Their findings were in agreement with those reported later in this chapter, in that when the toner was over the ink, there were no ink peaks seen in the infrared spectrum;

whereas when the ink was above the toner, a combined spectrum was obtained. The major drawback of using FTIR-ATR microscopy is the difficulty in accurately placing the ATR crystal on the centre of the line intersection (especially with an optically opaque germanium ATR crystal), and thus it has the potential to be misaligned, and inaccurately determine the sequence order. There are a number of advantages of using FTIR-ATR infrared imaging over conventional FTIR-ATR microscopy, and these are discussed later on.

If the conventional FTIR-ATR microscopy technique were to obtain both spectral and spatial information from a line intersection, the time-consuming process of infrared mapping would need to be employed. This involves obtaining numerous infrared spectra, one-by-one, at each point on a grid across the sample. Using micro-FTIR-ATR infrared imaging, it would be possible to simultaneously collect thousands of spectra over an area of around 80 μm x 80 μm. However, the typical size of a line intersection is in the order of mm. It is therefore necessary to use a macro-ATR FTIR spectral imaging technique, which can simultaneously obtain both spectral and spatial information from a larger area in rapid collection times (53). Using macro-ATR FTIR spectral imaging it is possible to image an area of 3.0 x 2.3 mm, which allows an entire 12-point (Times New Roman) printed character to be imaged (see Results and Discussion).

As discussed previously, with infrared spectral imaging it is possible to visualise different chemical components in a sample by imaging at particular frequencies corresponding to the vibrations of chemical functional groups. It is hoped in this

research that by choosing functional groups specific to the materials commonly encountered in intersecting line samples e.g. paper, ink and toner, spectral images showing their spatial distribution can be formed, and that they will provide information as to the order in which the line crossings were applied.

4.1.5 Overall Aims

In this chapter, the use of infrared spectral imaging as an objective, non-destructive method for determining the sequence of intersecting lines is investigated. Both homogeneous and heterogeneous line crossings produced using a range of writing materials are examined. The techniques attempted in this work are infrared reflectance microspectroscopic imaging and macro-ATR (attenuated total reflectance) infrared imaging (53, 108). Since ATR is a surface-preferenced technique, and has been used successfully in conventional (non-imaging) analysis of inks and toner on paper (23, 143), ATR imaging holds the greater promise for sequencing of line crossings on paper.

4.2. Materials and Methods

4.2.1. Sampling

A variety of writing materials was used to produce homogeneous and heterogeneous intersecting line samples including black ballpoint pens, gel pens, fluid ink pens, felt-tip pens, and laser and ink-jet printers. The materials tested are listed in Tables 1-4. The line crossings sequences were known for all samples examined, apart from the blind sample set. All intersections, apart from the blind samples, were drawn on white EXP800 Laser/Copy Paper. For ease of analysis, an area roughly 2 x 2 cm in size, containing the line intersection to be imaged, was cut out of the document. It is

possible, however, to manoeuvre an A4 page so that the intersection does not have to be cut from the document to be imaged.

4.2.2. Infrared Spectral Imaging

The intersections were examined using the Digilab Stingray® FT-IR imaging system described previously in Chapter 2. The system at UTS also has the optional Digilab LS large sample accessory, which allows for imaging of macrosamples. Images collected using this accessory had a spatial resolution of 44 μm, and a spectral resolution of 8 cm^{-1}. Images and spectra were collected and processed using Digilab Win-IR Pro 3.4.2.025 Software. The spectral range collected was 900 – 4000 cm^{-1}, as the FPA detector cannot collect data below 900 cm^{-1}.

4.2.3. Feasibility Study and Optimisation of the Sampling Method

An initial feasibility study was conducted to determine the capabilities of the technique and also to optimise the sampling parameters. The feasibility study focused on heterogeneous intersections produced using four black ballpoint pens and two laser and ink-jet printers (see Table 4.1). The samples were imaged using two different sampling methods, these being reflection analysis using the microscope, and macro-ATR analysis using a zinc selenide ATR crystal in the large sampling accessory.

BLACK BALLPOINT PENS	LASER PRINTERS	INK-JET PRINTERS
Papermate Kilometrico (M)	Epson AcuLaser C1900	Epson Stylus Photo 700
Uni SA-S (M)	HP LaserJet 1000	Canon Bubble-Jet BJC200
Staedtler Stick 430 (M)		
Sanford Suregrip (M)		

Table 4.1: *Intersecting lines feasibility study samples*

For reflection analysis, the samples were imaged using the "expanded field of view" mode on the microscope in which each individual image tile is approximately 700 μm x 700 μm. It is possible using a motorised stage to stitch together or "mosaic" several image tiles to form a larger image of up to 2 x 2 cm. To obtain a large enough image size to examine an intersection, four (2 x 2) image tiles were collected, giving a total area imaged of ~ 1.4 x 1.4 mm. The infrared spectra within each image tile were collected at 8 cm^{-1} resolution, using up to 1024 co-added scans. Background images were collected from infrared-reflective metal oxide-coated glass slides (Kevley Technologies).

For ATR imaging, due to the size of the intersections, it was necessary to use a macro ATR crystal in the large sampling accessory. A FastIR horizontal / single bounce ATR accessory (Harrick Scientific) was used, which allowed for images roughly 3.0 x 2.3 mm in size to be collected. Initially a zinc selenide (ZnSe) ATR crystal was used, however the results obtained (see Results and Discussion) led to the

investigation of a germanium (Ge) ATR crystal as well. For both ATR crystals, infrared spectra were collected at 8 cm^{-1} resolution, using 256 co-added scans. Background images were collected from the vacant ATR crystal surfaces.

Attempts were made to image both homogeneous and heterogeneous ink-ink intersections produced using the various different writing pens listed in Table 4.2. This testing was conducted using both the ZnSe and Ge ATR crystals in the large sampling accessory, under the parameters previously described.

4.2.4. Validation Study and Blind Testing

Validation studies were conducted using the optimal imaging method, i.e. using a ZnSe ATR crystal in the large sampling accessory. Five black ballpoint pens and five laser printers were used to produce known intersections where the ballpoint pen ink was variously applied before and after printing (see Table 4.3 for details).

Tests were conducted to determine whether ageing of the samples, and the pressure applied when producing the intersecting lines, affected the accuracy and quality of the results obtained. Ballpoint pen and laser printer line crossings were prepared for the ageing experiments using three black ballpoint pens (Sanford Suregrip, Staedtler and Uni S-AS) and two laser printers (Epson AcuLaser C1900 and Minolta Magicolour 2200). The samples were aged up to 12 months, and were imaged at various time intervals along the way. These ages were 0 days, 1 day, 3 days, 1 week, 2 weeks, 1 month, 3 months, 6 months and 12 months. The samples were stored in the dark in a drawer at room temperature. The same set of samples was imaged at

each age, along with replicate samples of the same age that had not previously been imaged (in case the original samples had been affected by being clamped repeatedly onto the ATR crystal). Pressure tests were also conducted on intersecting black ballpoint pen and laser printing lines, which were prepared using two black ballpoint pens (Papermate Kilometrico and Sanford Suregrip) and an Epson AcuLaser C1900 printer. A SpectraTech Contact Alert system was used to monitor the pressure used when applying the ballpoint pen ink lines, both before and after printing. The line crossings were prepared using a pressure indicator of 4, 7 and 10 (arbitrary scale) when applying the ballpoint pen ink lines.

BALLPOINT PENS	**GEL PENS**	**ROLLER BALL PENS**	**FELT-TIP PENS**
Sanford Suregrip (M)	BIC Intensity Clic	Staedtler Cool Roller	Artline 220 Superfine
Uni SA-S (M)	Hybrid Gel Grip DX	Uni-ball Micro	Pilot Drawing Ink (pigment ink)
Reynolds (F)	Zebra Sarasa	Bic Exact-Tip Roller	Staedtler Triplus Fineliner
Biro (F)	Pentel Energel (liquid gel ink)		
Staedtler Stick 430 (M)			
Bic Cristal (M)			
Ohto Gripper (F)			
Papermate Kilometrico (M)			

Table 4.2: *Ink-ink intersection samples*

BALLPOINT PENS	LASER PRINTERS
Biro (F)	Epson C1900 AcuLaser
Pentel BKL10	Minolta Magicolour 2200
Artline (M)	HP LaserJet 1000
Sanford Suregrip (M)	Ricoh Aficio 1060 RPCS
Reynolds (F)	Kyocera FS-1000

Table 4.3: *Intersecting lines validation study samples*

Blind tests were performed, in which the order of strokes was unknown prior to imaging. Four volunteers prepared twenty-one blind samples using various ballpoint pens and laser printers, and were asked to sign their name, neatly print a passage of writing and write a paragraph in their normal style of writing, either before or after printing. This protocol was used to ensure there was a variety of pen pressures and angles within the samples through the different styles of writing (see Table 4.4 for sample details). The results obtained using infrared spectral imaging were directly compared with those obtained by eight experienced forensic document examiners, who used methods they would use in casework (see Table 4.5 for details). The forensic document examiners were asked to independently examine the same set of blind samples and come to one of the following findings – ink over toner, ink under toner or inconclusive.

The intersecting line samples were photographed under white light illumination using a Video Spectral Comparator (VSC) 2000 (Foster and Freeman, UK) or a Sony

DSC-W1 Cyber-shot digital camera and a Leica MS5 microscope with a Leica CLS50E light source.

SAMPLE ID	BALLPOINT PEN TYPE	LASER PRINTER TYPE	PAPER TYPE
BS1	Zebra	Canon LBP-810	EXP
BS2	Biro	Canon LBP-810	EXP
BS3	Sanford Suregrip	Canon LBP-810	EXP
BS4	Sanford Suregrip	Canon LBP-810	EXP
BS5	Schmidt	Apple Laserwriter 16/600PS	EXP
BS6	Pilot BP-S	Epson C1900 Aculaser	HP
BS7	Pilot BP-S	Epson C1900 Aculaser	HP
BS8	Uni SA-S	Xerox Docucolour 3535	Unknown
BS9	Schmidt	Ricoh Aficio 1060 RPCS	Canon
BS10	Papermate	Konika	PPC
BS11	Ohto	Konika	PPC
BS12	Bic	HP Laserjet	Xerox
BS13	Schmidt	HP Laserjet	Xerox
BS14	Reynolds	HP Laserjet	Xerox
BS15	Sanford Suregrip	Panasonic KX-P7305	HP
BS16	Sanford Suregrip	Panasonic KX-P7305	HP
BS17	Zebra	Canon LBP-810	Reflex
BS18	Biro	Ricoh Aficio 1060 RPCS	Reflex
BS19	Staedtler Stick	Minolta Magicolour 6100 DeskLaser	EXP
BS20	Staedtler Stick	Lexmark T522	EXP
BS21	Staedtler Stick	Brother MFC-8840D	EXP

Table 4.4 *– Intersecting lines blind sample details*

FORENSIC DOCUMENT EXAMINER (FDE)	TESTING PERFORMED
FDE 1	Visual observation through stereomicroscope & ring light illumination (looking for 'bronzing' of the ink)
FDE 2	Incident lighting at 100x mag. Polarising microscope using reflected light.
FDE 3	Light stereomicroscope.
FDE 4	All intersections examined using polarizing microscope with reflected light, which gave colour contrast between ink / toner.
FDE 5	Visual inspection using magnification. VSC2000 – infrared, ultraviolet examinations.
FDE 6	Oblique and vertical lighting, spectral reflectance.
FDE 7	All binocular microscope (x6.5 – 40), F.O. lighting – specular reflectance.
FDE 8	Microscope

Table 4.5 *– Techniques used by forensic document examiners to examine blind samples*

4.3. Results and Discussion

4.3.1. Feasibility Study

An initial feasibility study was conducted to examine the potential of infrared spectral imaging for determining the sequence of intersecting lines. As mentioned previously, the infrared spectral imaging data can be viewed in a number of ways. Infrared spectra can be extracted from specific points on the sample to potentially identify individual components, and data can also be viewed as a series of images,

each produced by mapping the spectral intensity at a given frequency across the sample. By choosing an infrared band specific to a given material, it is possible to view the spatial distribution of the chosen material across the sample. In order to successfully determine the sequence of intersecting lines, the following three criteria need to be fulfilled:

- the various writing materials (as printed on the paper) must yield infrared spectra that can be resolved from the paper background;
- each writing material must have at least one characteristic infrared band that allows it to be independently imaged; and
- there must be a consistent pattern of results for the two possible line crossing situations (i.e. material A on material B or vice versa); this means that there must be no physical mixing of the two materials and that it must be possible to detect the spectrum of the uppermost material without interference from the other material in at least one of the two situations mentioned.

Intersections produced using ballpoint pens and laser and ink-jet printers were initially examined using two different infrared sampling methods. With reflection analysis, as mentioned previously, it is possible to image larger areas (up to 2 x 2 cm) by stitching together or "mosaicking" multiple image tiles collected using an automated stage. Reflection imaging using up to 1024 scans at 8 cm^{-1} resolution was attempted, and while it was possible to image a laser-printed toner character, the ballpoint pen ink and ink-jet printer spectra seemed to be swamped by the paper's spectral contribution (from cellulose and inorganic constituents within the paper), and so it was not possible to image any of the ballpoint pen inks or ink-jet printers

tested. Spectral subtraction of the paper component was not possible as the paper spectrum varies greatly from point to point, due to the heterogeneous nature of paper. Another disadvantage of reflection imaging is that the time needed to scan an entire 12 point toner character (an image area of ~ 1.4 x 1.4mm) took over an hour and a half.

It was therefore necessary to try another sampling method. Imaging with an ATR crystal was thought to be suitable since the IR penetrates a short distance into the sample from the surface. It was hypothesised that the infrared spectra collected would contain less contribution from the paper background and allow for the ballpoint ink and ink-jet printing spectra to be seen.

Macro-ATR infrared imaging, using the ZnSe ATR crystal in the large sampling accessory, was found to successfully image laser toner and ballpoint ink crossings. Around six minutes was required to collect an image 3.0 x 2.3 mm in size (with 256 co-added scans at 8 cm^{-1} resolution). By choosing an infrared band present only in either the toner spectrum or the ink spectrum, separate spectral images showing the spatial distribution of these materials could be obtained. An example of the spectral images formed can be seen in Fig. 4.1. Figure 4.1(a) shows the visible light image of a line crossing produced with a black Staedtler ballpoint pen and an Epson AcuLaser printer. Figures 4.1(b) and 4.1(c) show the infrared spectra of the toner and ink materials, respectively. Figure 4.1(d) shows the infrared image of the toner material, and has been formed using the integrated intensity under the peak at 1724 cm^{-1}, which has previously been assigned as a carbonyl band in some major resins

typically found in toner, such as polystyrene-co-acrylate or epoxy plus acrylate (142). Figure 4.1(e) is an infrared image of the ink material, which has been formed using the integrated peak intensity under 1584 cm^{-1}. The peak at 1584 cm^{-1} is characteristic of the ballpoint pen ink, and has previously been assigned to a skeletal vibration of triarylmethane dye and the C=C stretch vibration of epoxy resin (27). In this work, the actual identification of the peaks used to form the images is not vital; it is only necessary that the peaks are characteristic of the ink or toner materials and allow for them to be independently imaged, so that their respective distributions within the sample can be viewed.

The third criterion for the infrared spectral imaging technique to be successful in determining the sequence of intersecting lines was that a consistent pattern needed to be observed when one material was lying above or below the other material. The preliminary results indicated that examining the toner spectral image was not particularly useful in determining the sequence of intersecting lines. No consistent changes or breaks were seen in the toner image at the point of intersection to indicate whether the ink line was present above or below the toner. However, when examining the ink spectral image, a consistent trend was observed. When the ink was underneath the toner, there was a gap in the ink image where the toner had passed over the ink (see Fig. 4.1). When ink was present over toner, no break was seen in the ink line where it crossed over the toner line (see Fig. 4.2). This can be explained by noting that the toner material absorbs strongly in the infrared, and blocks the infrared light from penetrating through to the ink material, causing a gap in the image where the ink lies under the toner. When the ink lies on top of the toner,

the ink spectrum is stronger, as there is less spectral contribution from the cellulose in the paper. In this case, no gap is seen in the ink line, and generally the image is stronger at the point of intersection (i.e. closer to a red colour (high intensity) in the image than green-blue (lower intensity)). The toner material generally gives a strong spectrum, and most of the time could be seen in the toner infrared images regardless of whether the ink lay above or below the toner. It therefore does not appear to help in determining the sequence order of the strokes.

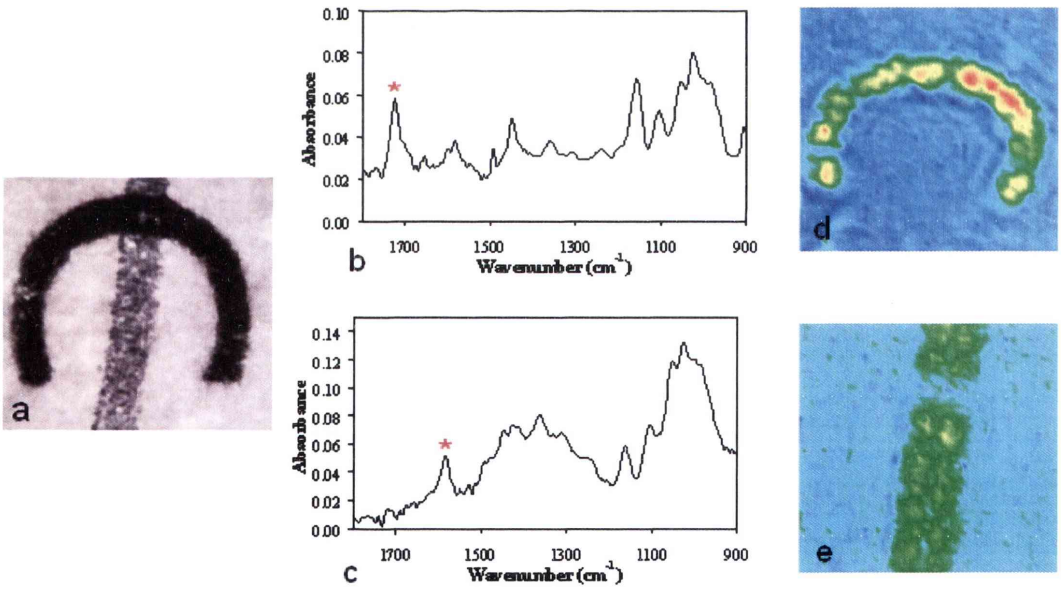

Figure 4.1 *- Example of ballpoint pen ink under laser printing showing a) visible image of intersection; b and c) infrared spectra of laser printing and ballpoint pen ink; d and e) infrared spectral images of laser printing and ballpoint pen ink formed by imaging at 1724 cm^{-1} and 1584 cm^{-1}.*

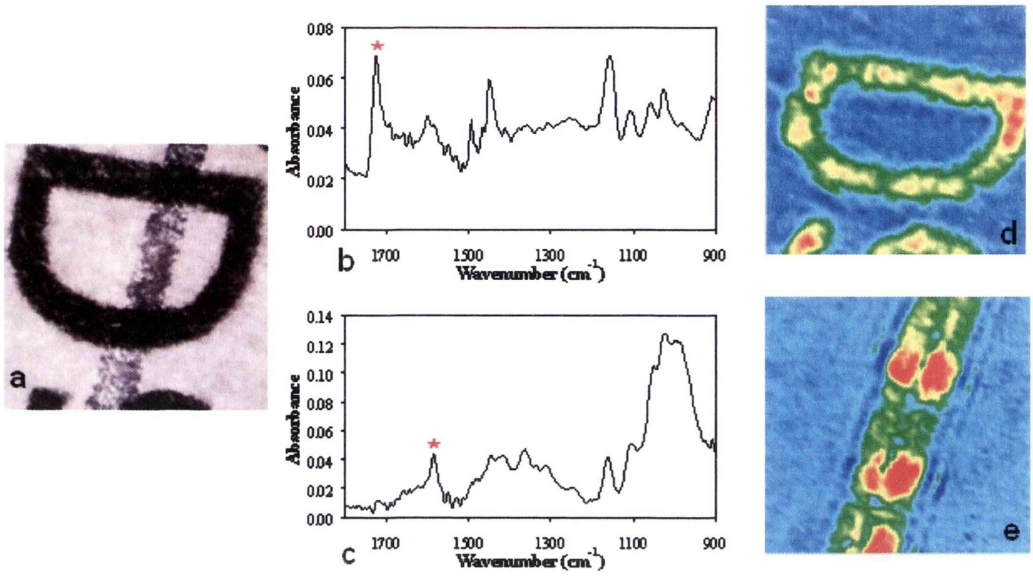

Figure 4.2 *– Example of ballpoint pen ink over laser printing showing a) visible image of intersection; b and c) infrared spectra of laser printing and ballpoint pen ink; d and e) infrared spectral images of laser printing and ballpoint pen ink formed by imaging at 1724 cm^{-1} and 1584 cm^{-1}.*

Overall the preliminary study indicated great potential for infrared spectral imaging in determining the sequence of intersecting ballpoint pen ink and laser printer toner lines. However, infrared spectral imaging was unable to image either brand of ink-jet printer ink on paper, with the weak ink-jet spectrum being swamped by strong paper spectral interference. Therefore it was necessary to look at further sampling methods to see if any improvement could be made to the technique to make it more sensitive to ink-jet printing and/or less sensitive to the underlying paper. One approach was to investigate the use of a different ATR crystal material. The higher the refractive index of the ATR crystal, the shorter the distance the evanescent wave penetrates into the sample. Therefore germanium, which has a refractive index of 4.0, gives a lower depth of penetration into the sample than the zinc selenide crystal, which has a refractive index of 2.4. It is possible to calculate the actual depth of

penetration (d_p) into the sample using each of the ATR crystals, using the following equation:

$$d_p = \frac{\lambda}{2\pi n_1 [\sin^2 \theta - (n_2/n_1)^2]^{0.5}}$$

where λ is the wavelength, θ is the angle of incident radiation, n_1 is the refractive index of the ATR crystal and n_2 is the refractive index of the sample (52). At a wavelength of 1000 cm^{-1}, with a 45° angle of incident radiation, and assuming a typical organic sample has a refractive index of 1.5, light from the zinc selenide ATR crystal will penetrate approximately 2 μm into the sample, whereas light from the germanium ATR crystal will only penetrate approximately 0.66 μm (52). The expected downside from using a crystal with a higher refractive index is that the overall signal from the sample would be reduced, but it was hoped that using the germanium crystal would reduce the spectral contribution from the paper substrate relative to that of the ink, and thus enable the imaging of ink-jet printed characters on the paper surface.

Attempts were made to image the feasibility sample set using a germanium ATR crystal in place of the ZnSe crystal. Unfortunately, it was still not possible to image either brand of ink-jet printing using the germanium ATR crystal. This is possibly due to the mechanism of printing. With laser printing, the toner material, which consists of fine black particles, is fused to the paper surface through the action of heat or pressure. However, with ink-jet printing, the liquid ink droplets are simply sprayed onto the paper, and absorb into it (144, 145).

Overall the results obtained with the ZnSe ATR crystal were far superior to those obtained using the Ge ATR crystal, including for the laser printed samples. This is demonstrated in Fig. 4.3, where the differences in results between the two types of ATR crystals are depicted. The Ge ATR crystal struggled to image the toner and ink materials, whereas the ZnSe ATR gave very good images of these materials. A further disadvantage of using the Ge ATR crystal was that its sensitivity was so poor that it was difficult to see if the line intersection was clamped down onto the correct location on the ATR crystal prior to imaging. With the ZnSe ATR crystal, it was possible to push the sample onto the crystal surface using a finger, and by viewing the 'real time' infrared window (which shows the integrated intensity response of the detector in real time), instantly tell whether the line intersection of interest was in the correct position on the crystal for imaging (see Fig. 4.4(c)). However, with the Ge ATR crystal, no image could be seen in the 'real time' infrared window, so there was a lengthy trial and error process to get the intersection onto the correct position on the crystal (see Fig. 4.4(b)).

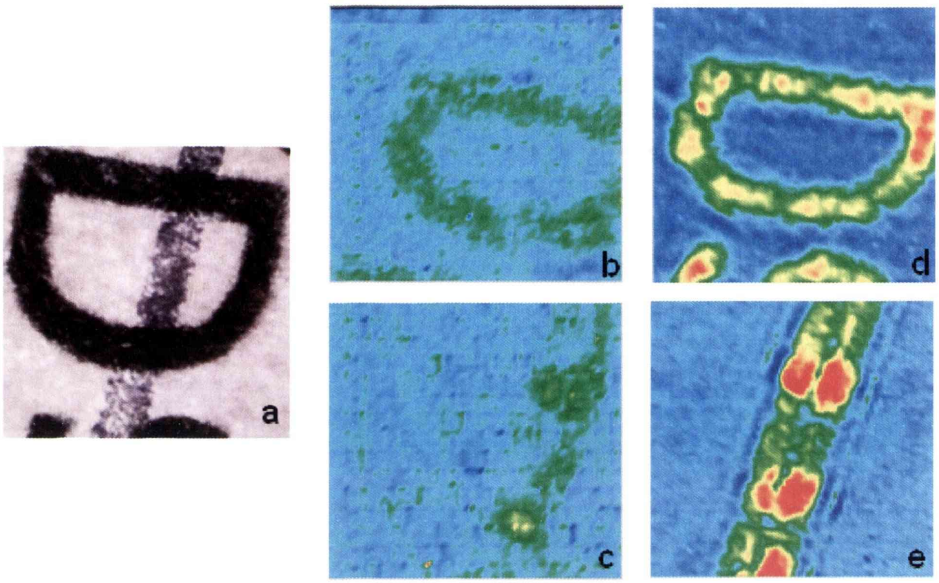

Figure 4.3 *– Comparison of the quality of infrared spectral images obtained when using different ATR crystals. Visible image of ink over toner shown in (a); (b-c) shows the toner and ink spectral images obtained using a Germanium ATR crystal; (d-e) shows the toner and ink spectral images obtained when using a Zinc Selenide ATR crystal.*

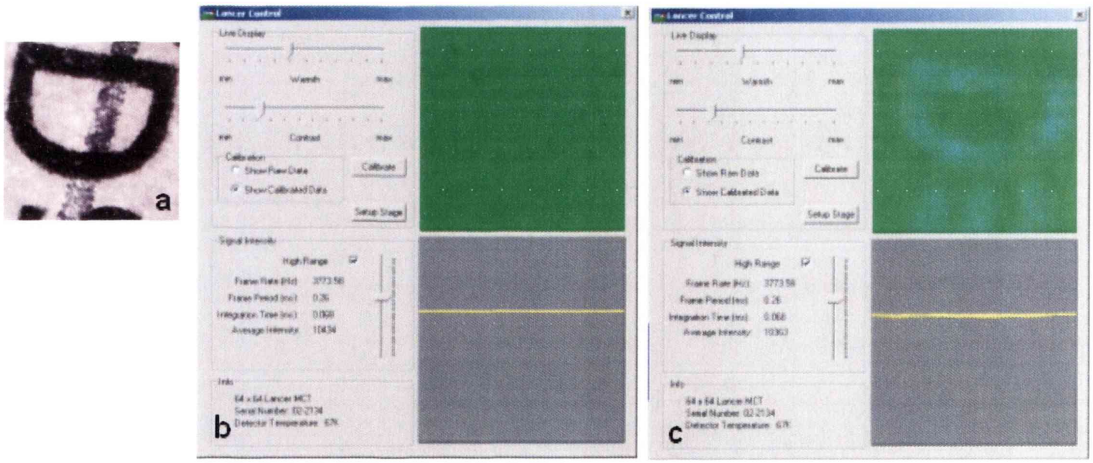

Figure 4.4 *– 'Live infrared window display' (total integrated intensity) of line intersection (a) produced when using the (b) Germanium and (c) Zinc Selenide ATR crystal.*

4.3.2. Ink-Ink Intersections

Attempts were made using both the germanium and zinc selenide ATR crystals to image various ink-ink intersections. Four different types of writing pens were tested, these being ballpoint pens, gel pens, roller ball pens and felt-tip pens. Unfortunately, the technique failed to give infrared spectra of the ink from gel pens, roller ball pens and felt-tip pens on paper. It appeared that as for the ink-jet printing, the spectra were swamped by the paper spectrum. The only pen type that could be imaged was the ballpoint pens. As with the ink-jet printing, this can be explained by the different ways in which these inks deposit onto the paper surface. Ballpoint pen ink is a viscous paste-like material that smears onto the surface of the paper, and is only partly absorbed into the paper, whereas the other types of pens, such as the felt-tip and roller ball pens, contain water-based inks that are more readily absorbed into the paper material (113, 146).

Line intersections produced using a number of different ballpoint pens were examined, and even though spectra of the inks could be obtained, the peaks allowing the formation of spectral images were common to all types of ballpoint pens encountered. The major ink peaks observed in the spectra occurred at 1584, 1360 and 1176 cm^{-1}, and are characteristic of triarylmethane dyes (27). Any minor differences in the ballpoint pen ink spectra that may exist between the different pen brands were swamped by the paper spectral contribution. This meant that, even though it was possible to form images showing the spatial distribution of the ink lines, these images gave no information as to which line lay on top of the other, as can be seen in Fig. 4.5. In a previous study by Wang et al., over 100 blue ballpoint

pens were analysed by FTIR spectroscopy (27). They found two major categories of ink spectra, as shown in Fig. 4.6. One of the categories is the typical ballpoint pen ink spectrum that was encountered in this study, where the major peaks were due to the triarylmethane dyes (1584, 1360 and 1176 cm^{-1}). However, the other type of spectrum was quite different, with the major peaks occurring at 1730 and 1285 cm^{-1}. It is possible that infrared images of a line crossing produced using the two different types of ballpoint ink might be used to determine the order of the strokes, if the inks do not mix significantly at the intersection. Unfortunately in this study only one of these two types of ballpoint pen spectrum was encountered, and so this hypothesis could not be tested.

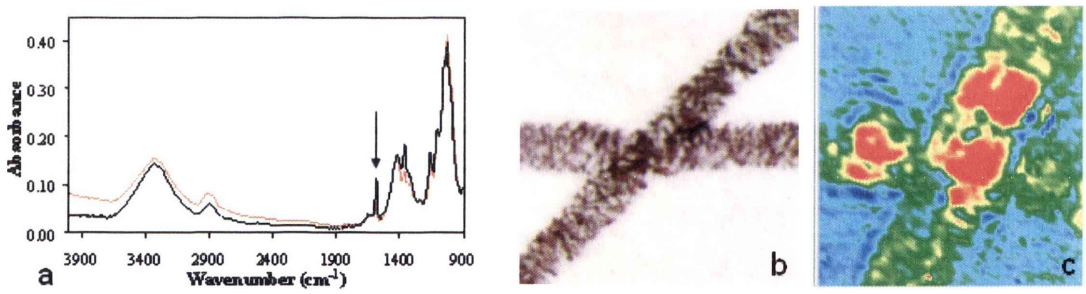

Figure 4.5 *– Example of ink-ink intersection showing (a) visible image of two intersecting ballpoint pen lines; (b) infrared spectra of two ballpoint pens and (c) infrared spectral image of ink lines formed using the integrated peak intensity under 1584* cm^{-1}.

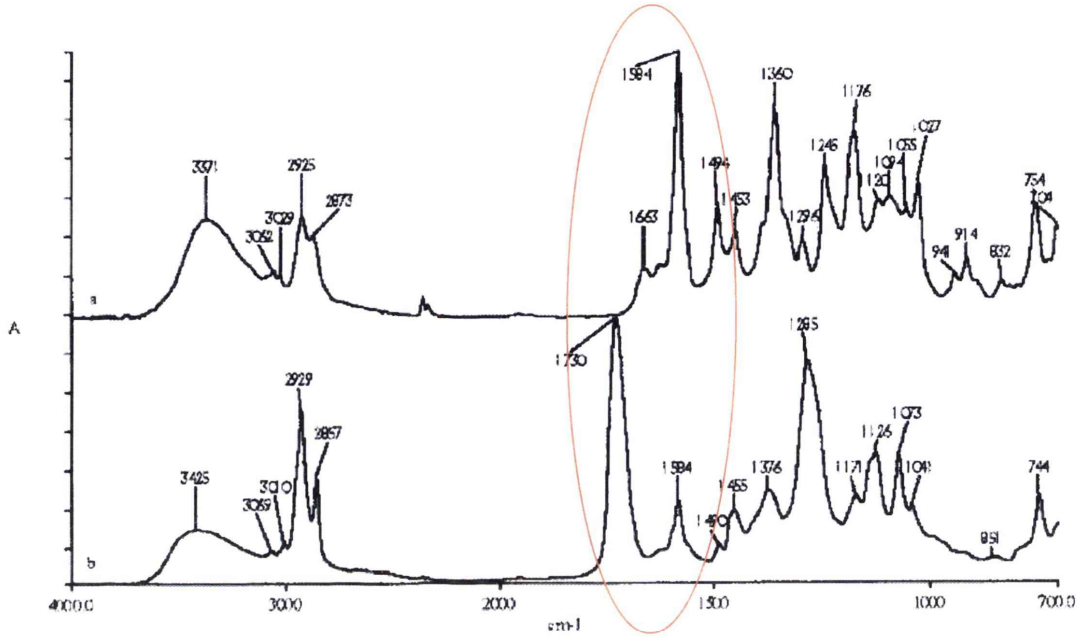

Figure 4.6 *– Infrared spectra of two main types of ballpoint pen ink found in Wang et al. (2001) study (27) (Reprinted, with permission, from the Journal of Forensic Sciences, Vol. 46, Issue 5, copyright ASTM International, 100 Barr Harbor Drive, West Conshohocken, PA 19428).*

4.3.3. Validation Study for Ink / Toner Intersecting Lines

In the validation study, over 100 intersections produced using five brands of ballpoint pens and five laser printers were examined. Similar results were obtained to those found in the feasibility study, and the technique could accurately identify the sequence of all of the line crossings. A consistent pattern was observed in the ink spectral images, in that if the ink was above the toner material, no gap was seen in the ink line at the point of intersection, but if the ink was below the toner material, then a gap could be seen. The peaks used to form the spectral images were the same across the different brands of writing materials, i.e. 1584 cm^{-1} for the ballpoint pen inks and 1724 cm^{-1} for the toner materials.

In the validation study it was observed that the spectral images were horizontally stretched in comparison with the visible light images such that the sample area imaged was 3.0 x 2.3 mm. This is due to the elliptical imaging area formed on the crystal surface when the circular beam of light hits it at 45°. A detailed explanation of the phenomenon can be found in Chan and Kazarian (53). It would be possible to convert the image back to an un-stretched version using image processing software, but this was unnecessary for this study. For presentation at court it may be worthwhile un-stretching the image, or otherwise explaining why it appears slightly different to the visible image so as to avoid any confusion.

The aged samples were successfully imaged up to the age of 12 months, and the ink spectral images could still be used to correctly determine the order of strokes. At the age of 12 months, the general pattern of a gap in the ink image at the point of intersection if the ink was underneath the toner and no gap when the ink was lying on top of the toner could still be seen. A study by Wang et al, found that when ballpoint pen ink samples were artificially aged (through heating to 50-150 ^{0}C and exposure to UV irradiation), the intensity of the 1584 cm^{-1} peak decreased (27). In this study, no consistent trend in the intensity of the peak at 1584 cm^{-1} over time was observed, and this peak could still be used to form images showing the spatial distribution of the ink materials at an age of 12 months.

Pressure testing was conducted to determine whether the pressure used when applying the ballpoint pen ink, either before or after laser printing, affected the accuracy of the technique in determining the correct sequence of strokes. The pen

pressure applied ranged from heavy to light. The results showed that, even with the varied pen pressure, there was still a consistent pattern in the ink images which could be used to accurately identify whether the ink was above (no gap at the point of intersection) or below (with a gap at the point of intersection) the laser printing. A notable finding was the effect the pen pressure had on the toner images produced. As stated previously, there was no consistent pattern in the toner images to indicate whether the ink was above or below the toner. More often than not, no gap was seen where the ink was lying on the top of the toner, leading to the earlier hypothesis that this was due to the strong toner spectrum produced. However, with the heaviest pen pressure (pressure indicator of 10), there was a gap in the toner image at the point of intersection with the ink (see Fig. 4.7(d)), at the medium pen pressure there was a small gap seen at the point of intersection (see Fig 4.7(e)), and at the weakest pen pressure, there was no gap seen in the toner image (see Fig. 4.7(f)). Observation of the toner spectral image may therefore help in some cases to reinforce the determination of the order of strokes; however the main focus should remain on the more reliable pattern seen in the ink spectral images, i.e. whether or not there is a gap in the ink line at the point of intersection. It is also important to examine the infrared spectra around the point of intersection to confirm whether toner or ink peaks are present, in addition to viewing the infrared images.

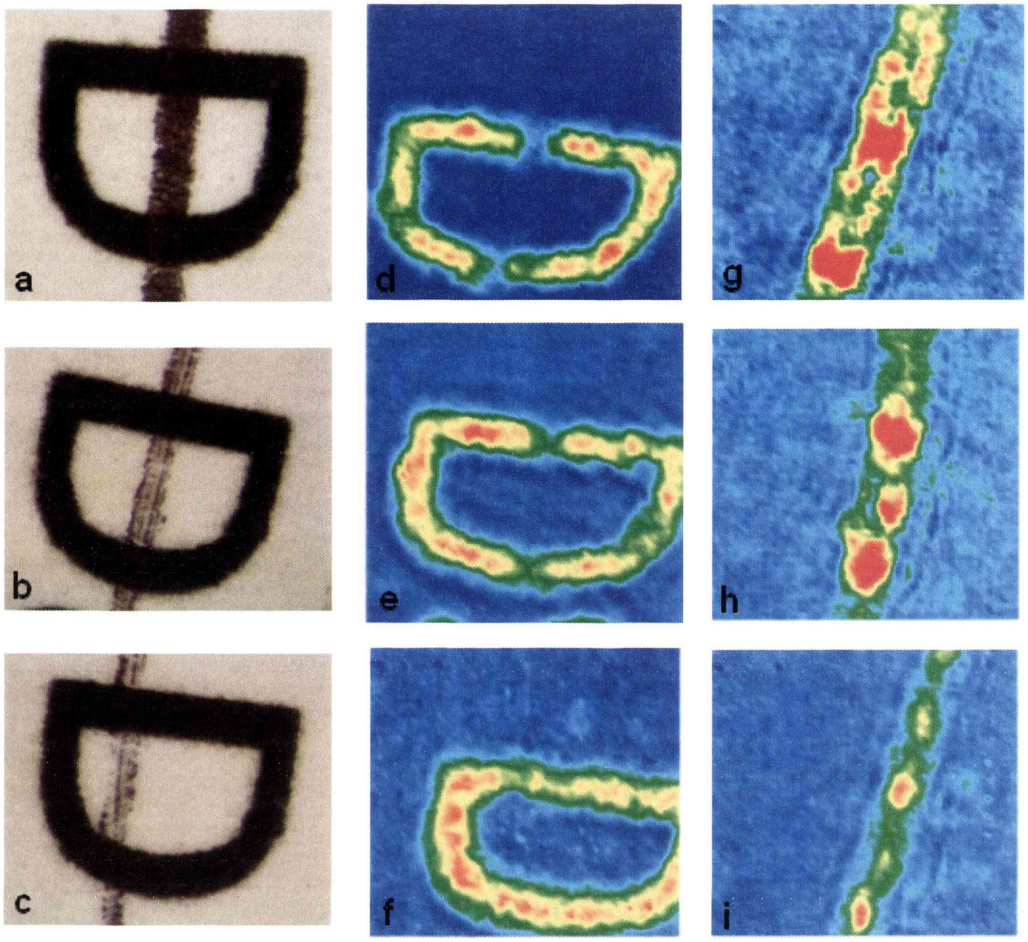

Figure 4.7 *– Example showing results obtained when different pen pressures used. (a-c) shows the visible light images of Sanford ink over Epson toner using pressure indicators of 10, 7 and 4 respectively; (d-f) the respective toner spectral images formed using the integrated peak intensity under 1724 cm^{-1}; (g-i) the respective ink spectral images formed using the integrated peak intensity under 1584 cm^{-1}.*

4.3.4. Blind Testing for Ink / Toner Intersecting Lines

Twenty one blind tests, where the order of strokes was unknown prior to examination, were conducted. The results obtained using the infrared spectral imaging technique were directly compared to those obtained by eight experienced forensic document examiners, using techniques they would employ in casework

(refer to Table 4.5 for details). The infrared spectral imaging technique was the most successful in determining the correct sequence order of the line crossings, with a 100% success rate. The results obtained by the document examiners can be seen in Table 4.6; the majority of the document examiners got most sequences correct or made an inconclusive determination. However, there were two samples (BS1 and BS16) for which an incorrect determination was made by some of the document examiners. The samples where there were differing opinions among the document examiners were more difficult intersections, where the ink line was fairly heavy underneath the toner character (BS16) or where there was a fairly light ink line over the toner (BS1). This emphasises the need for a technique which does not rely on visual interpretation, as optical illusions can occur. The infrared spectral imaging results for BS1 are shown in Fig. 4.8. One document examiner incorrectly assigned the order of strokes, and four document examiners came to inconclusive results. Examination of the ink spectral image (Fig 4.8(c)) shows that the ink is clearly over the toner (as there are no gaps at the point of intersection with toner). The infrared imaging results for BS16 are shown in Fig. 4.9. For this sample two document examiners incorrectly assigned the order of strokes, and two document examiners came to inconclusive results. By examining the ink spectral image (Fig. 4.9(c)) it is very clear from the gaps seen at the points of intersection that the ink was under the toner. These two examples highlights the effectiveness of the imaging technique, and the advantages of producing images based on chemical differences, rather than relying on visual observations, which can be subject to optical illusions and varied human perceptions.

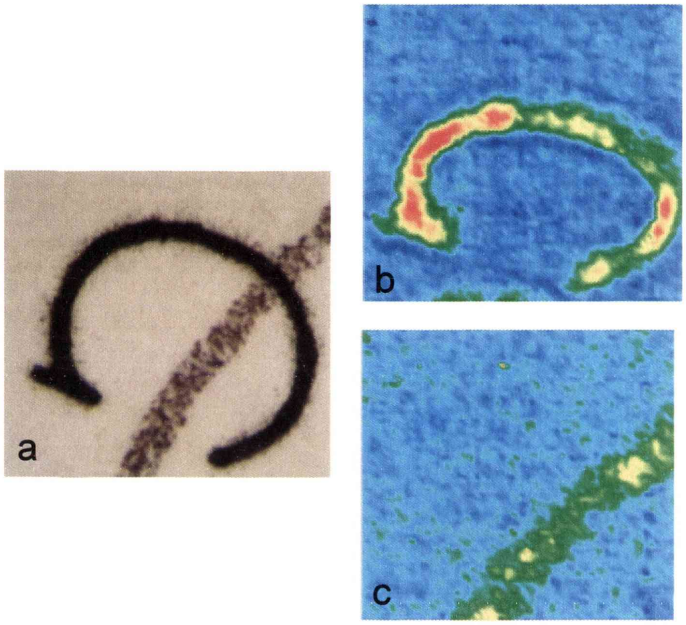

Figure 4.8 *– Infrared spectral image results for blind sample 1, with the visible light image shown in (a), the toner spectral image formed using the peak intensity at 1724* cm^{-1} *in (b) and the ink spectral image formed using the peak intensity at 1584* cm^{-1} *in (c).*

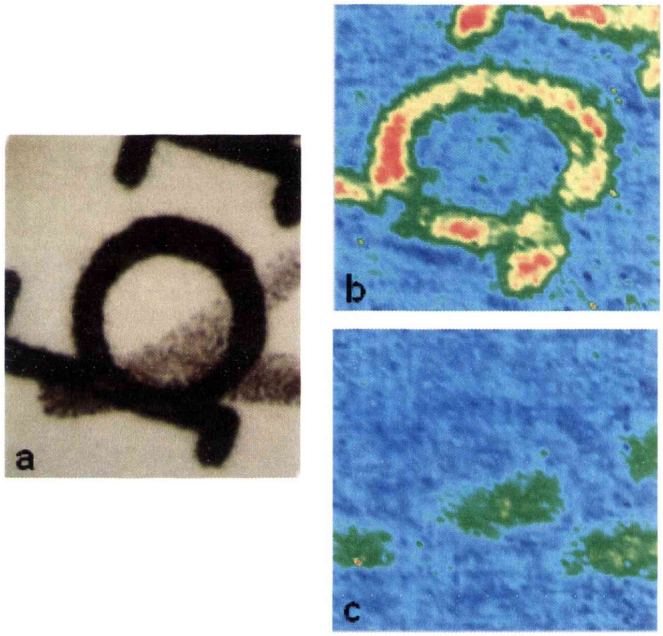

Figure 4.9 *– Infrared spectral image results for blind sample 16, with the visible light image shown in (a), the toner spectral image formed using the peak intensity at 1724 cm^{-1} in (b) and the ink spectral image formed using the peak intensity at 1584 cm^{-1} in (c).*

BLIND SAMPLE	CORRECT ORDER	IR IMAGING	FDE 1	FDE 2	FDE 3	FDE 4	FDE 5	FDE 6	FDE 7	FDE 8
BS1	Ink over toner	✓	✓	✓	×	✓	I	I	I	I
BS2	Ink over toner	✓	✓	✓	✓	✓	I	✓	✓	✓
BS3	Ink under toner	✓	✓	✓	✓	✓	I	✓	✓	✓
BS4	Ink under toner	✓	✓	✓	✓	✓	I	✓	✓	✓
BS5	Ink over toner	✓	✓	✓	✓	✓	I	✓	✓	✓
BS6	Ink under toner	✓	✓	✓	✓	✓	I	✓	✓	✓
BS7	Ink under toner	✓	✓	✓	✓	✓	I	✓	✓	✓
BS8	Ink over toner	✓	✓	✓	✓	✓	I	✓	✓	✓
BS9	Ink under toner	✓	✓	✓	I	✓	I	✓	I	✓
BS10	Ink over toner	✓	✓	✓	✓	✓	✓	✓	I	I
BS11	Ink over toner	✓	I	✓	✓	✓	✓	✓	✓	I
BS12	Ink over toner	✓	✓	✓	✓	✓	I	✓	✓	✓
BS13	Ink over toner	✓	✓	✓	✓	✓	I	✓	✓	✓
BS14	Ink over toner	✓	✓	✓	✓	✓	I	✓	✓	✓

BS15	Ink under toner	✓	✓	✓	✓	✓	I	✓	✓	✓
BS16	Ink under toner	✓	✓	×	I	×	I	✓	✓	✓
BS17	Ink under toner	✓	✓	✓	✓	✓	I	I	I	I
BS18	Ink over toner	✓	✓	✓	✓	✓	I	✓	✓	✓
BS19	Ink over toner	✓	I	✓	I	✓	I	I	I	I
BS20	Ink over toner	✓	✓	✓	✓	✓	I	✓	✓	✓
BS21	Ink over toner	✓	✓	✓	✓	✓	I	✓	✓	✓
Overall % Correct		100	90	95	81	95	10	86	76	76
Overall % Inconclusive		0	10	0	14	0	90	14	24	24
Overall % Incorrect		0	0	5	5	5	0	0	0	0

KEY: ✓ Correct sequence determination

I Inconclusive sequence determination

× Incorrect sequence determination

Table 4.6 – *Intersecting lines blind testing results*

For the majority of the blind samples, the sequence order of the strokes was fairly apparent upon visual examination, and in those cases the use of the more advanced technique of infrared spectral imaging may not be warranted. However, for more borderline intersections, or ones where an inconclusive determination is made, it would be worthwhile to examine the intersection using infrared spectral imaging, where available, to ensure that no errors are made in determining the sequence of line crossings. A further advantage of infrared spectral imaging over the conventional optical methods of examination is that images are formed that can clearly convey the results to a layperson, such as a jury member. The forensic document examiners were asked to provide photographic proof, if possible, to demonstrate why they came to the particular conclusion regarding the sequence of the line crossings. Only two out of the eight document examiners provided photographs, and both apologised for the poor quality of the photos, stating that the physical and optical characteristics they were looking for were much easier seen in person than in the photographs. In a court setting, images such as those obtained with infrared spectral imaging will be much more easily understood by a jury member than a verbal explanation of a phenomenon observed by a document examiner (such as bronzing of the ink when it lies above the toner material).

4.4. Conclusions

Overall, the infrared spectral imaging technique, using a ZnSe ATR crystal in the large sampling accessory, was found to be very successful in determining the sequence of intersecting ballpoint pen and laser printer lines. The chief advantages of the technique are that it is an objective method of analysis, and relies on chemical

differences in the samples rather than simply visual differences that are subject to human interpretation. The technique is relatively fast, taking only six minutes to analyse a sample, and is non-destructive as long as the document can be manoeuvred so that the line crossing of interest is placed in contact with the ATR crystal. The results are also displayed in a way that makes them more easily understood by a layperson, such as a jury member. Using the macro-ATR imaging technique, an entire 12-point character can be imaged, an obvious advantage over conventional ATR-FTIR microscopy in which there is the potential for erroneous conclusions if the ATR crystal is not perfectly aligned on the point of intersection.

The disadvantages of the technique include its inability to image a number of writing materials on paper, including ink-jet printing, and various pens such as gel pens, roller ball pens and felt-tip pens. The instrumental requirements are more demanding than infrared microscopic imaging: it is necessary to have the optional large sampling accessory, and also a large enough focal plane array detector to collect an image of a line intersection.

4.5 Future Work Recommendations

There are a number of avenues for future research. In this study, only one general type of ballpoint pen ink was encountered, and therefore infrared spectral imaging failed to determine the sequence of intersecting ballpoint pen lines. A previous study by Wang et al found two general types of ballpoint pen spectra, with a number of significant spectral differences between the two types (27). Future work should be conducted using infrared spectral imaging to examine intersecting ballpoint pen lines

produced using pens that contain ink of these two types. Problems may still be encountered if the two inks mix at the point of intersection.

Previous work has been conducted by Ricci et al (2007) using variable-angle ATR analysis as a means to reduce spectral interference from a background surface and also for depth profiling (74). This technique may assist in determining the sequence of intersecting lines since imaging at different depths into the sample may lead to a reduction in the paper's spectral contribution and may provide additional information regarding the sequence of strokes by looking at different depth profiles. Further work investigating the suitability of other ATR crystal types may also assist in reducing the paper spectral contribution, or may provide better results than those obtained using a zinc selenide ATR crystal e.g. diamond may allow higher pressure to be applied between the crystal and the sample.

Further work could be conducted regarding environmental exposure and ageing of the line intersection samples. During this research project, the ageing experiments were conducted by placing the samples in a drawer, as this is what would happen with many of the documents where the sequence order is contested, such as wills and contracts. Ageing the samples in direct sunlight, and exposing them to environmental elements, may affect the accuracy of infrared spectral imaging in correctly determining the order of strokes, and therefore should be investigated.

The use of multivariate data analysis techniques such as hierarchical cluster analysis (HCA) could be explored in the future, as they may allow for small differences to be

highlighted. One problem envisaged with this approach is that the paper background is heterogeneous, and so cluster analysis techniques may highlight differences in the paper background before say, differences between two fairly similar ballpoint pens. Nevertheless, it may still be worth exploring techniques other than simply using the integrated peak intensities to image the line intersections.

CHAPTER 5:

Overall Discussion

Chapter 5: Overall Discussion

Overall, it can clearly be seen that infrared spectral imaging has a number of advantages for forensic analysis. There are a number of ways in which infrared spectral imaging can be applied, including for:

- pure visualisation purposes e.g. intersecting lines (147), fingerprint enhancement (35, 71, 72, 74),
- visualisation and chemical identification of materials e.g. paint and bicomponent fibres (148, 149),
- classification/discrimination using multivariate statistical methods e.g. cluster analysis of paint images (148), and
- automation of single-point spectroscopy analysis e.g. analysing drug/explosive particles within a latent fingerprint deposit (67, 76, 150, 151).

A key advantage is that the technique of infrared spectroscopy is already a widely accepted technique for use in forensic studies. This means that it should not require much additional user training for forensic scientists to be able to use the technique, and it should not be too much of a leap for it to gain acceptance for use in a forensic laboratory. The associated multivariate classification techniques may, however, require a significant amount of further user training in order for the processes involved to be completely understood and applied properly.

As has been highlighted above, infrared spectral imaging has the ability to simultaneously provide both spectral (i.e. chemical) and spatial (i.e. visualisation of components) information in rapid analysis times. In comparison to other chemical

imaging techniques currently gaining applications for forensic studies, such as UV-visible chemical imaging, infrared spectral imaging has a much higher chemical specificity and, together with Raman imaging, is one of the only spectral imaging techniques which can allow for the functional group mapping of a surface. An infrared spectrum for most molecules will exhibit a high number of narrow infrared bands, compared with the small number of broad overlapping peaks which are generally seen in a UV-visible spectrum. This means that with infrared spectral imaging there is a higher chance of isolating an individual peak which can be used to map the distribution of a specific component in a sample, and the spectra obtained can be used to identify exactly which chemical components are present. Infrared spectral imaging also has a high spatial resolution (of around 15 μm and better for micro-ATR imaging), and is not restricted by the use of apertures, as is the case for conventional single-point infrared analysis (53, 108).

As has been illustrated with the paint chips, bicomponent fibres and the sequence of intersecting lines results, the infrared spectral image data can be presented in visually appealing displays which allow for simpler ways for results to be explained to a layperson such as a juror member, and should make results much easier to comprehend. Information from the entire paint chip and fibre sample can be obtained simultaneously in one experiment, and due to the large amount of data obtained, confidence in the results is increased. For bicomponent fibres, infrared spectral imaging was successful in identifying the chemical composition and spatial configuration in over 50% of the samples analysed. In comparison, the conventional microscopy techniques were only successful in identifying 33% of the bicomponent

fibres as being bicomponent, and these techniques do not provide chemical information. For the best chance that a bicomponent fibre will be detected and fully characterised in casework, infrared spectral imaging, in combination with the various microscopy techniques, should be employed.

One of the major limitations encountered throughout this research was the sample preparation involved to prepare thin cross-sections of multi-layered paint chips for transmission analysis, and also the preparation of cross-sections of bicomponent fibres. This problem is inherent to both conventional infrared spectroscopy and infrared imaging. A variety of resins were investigated, and a new method was proposed for the preparation of thin sections of multi-layered paint chips. However this method was only found useful for good quality paint chips, and cannot be used on older, more crumbly paint chips. This problem was not remedied in this study, and for the true potential of infrared spectral imaging to be realised, a new sample preparation method needs to be developed (such as an embedding resin suitable for IR analysis that can support an older crumbling sample), or alternative sampling approaches need to be investigated. One such sampling approach is the use of micro-ATR imaging. Micro-ATR imaging was briefly investigated for the analysis of cross-sections of bicomponent fibres, but problems were encountered in aligning the ATR crystal directly onto the area of interest. For the analysis of paint samples, the micro-ATR attachment available for the Stingray infrared instrumentation was not suitable, due to the small sampling area (approximately 80 μm x 80 μm). The FTIR ATR imaging accessory released by Perkin Elmer in 2006 may overcome the difficulties encountered with sample preparation for paint chips, and potentially for

bicomponent fibres. The ability to image a larger area (the Perkin Elmer Ge ATR crystal accessory has a ~600 μm diameter), at a high spatial resolution of around 3 μm, by simply placing the paint chip in direct contact with the ATR crystal (i.e. no sample preparation), would be an ideal solution for the sampling difficulties encountered throughout this research.

Infrared spectral imaging was demonstrated to be a successful, non-destructive and objective technique for determining the sequence of intersections produced using ballpoint pens and laser printers, and was shown to have a 100% success rate in blind tests. It was originally hoped that infrared spectral imaging could be used for imaging many different materials encountered in line intersections. Unfortunately this was not the case; infrared spectral imaging was not successful in imaging ink-jet printing, gel pens, roller ball pens or felt-tip pens. A major problem was the significant spectral contribution made by the paper background, which seemed to swamp any infrared peaks from the writing materials mentioned above. Attempts to overcome this problem were largely unsuccessful. The technique was also unsuccessful in determining the sequence of homogeneous ballpoint pen intersections.

Other limitations of infrared spectral imaging include that the array detector may have a more limited spectral range than conventional detectors, and is essentially instrument-dependent e.g. the Digilab (now Varian) instruments have a lower detector cut-off of 900 cm^{-1} whereas the Perkin Elmer system's cut-off is slightly lower at 700 cm^{-1}. Another instrument-specific limitation will be the array detector

size available and also the sampling area possible. For example, the Digilab system used in this research has a large sampling accessory which allows for larger images to be collected. Before a forensic laboratory purchases an infrared spectral imaging instrument, appropriate research must be conducted to decide what types of applications the instrument will be used for. If the instrument is intended for, say, paint and fibre analysis alone, then a system such as the Perkin Elmer Spotlight series would be suitable, but if the sequence of intersecting lines is to be determined, then it is necessary to have a large sampling accessory and also a large enough array detector (64 x 64 pixel or larger) for this application. Initially the cost of infrared spectral imaging instrumentation was fairly high, but as more companies are now manufacturing this type of instrument, the prices have started to drop substantially, and with some companies there is also the possibility of simply purchasing an add-on imaging (FPA) detector if a laboratory already has a compatible bench-top FTIR microscope system.

There are many further potential forensic applications yet to be discovered, including those which improve upon single-point infrared analysis and those which are yet to have been explored. The past five years has seen a great increase in forensic applications of infrared spectral imaging, and it is anticipated that many more will be discovered in the next decade, and that infrared spectral imaging will find a regular place in forensic laboratories.

CHAPTER 6:

References

Chapter 6: References

1. Skoog, D.A., and J.J. Leary, Principles of Instrumental Analysis, 4th Edition, Saunders College Publishing, USA, 1992.

2. Stuart, B., W.O. George, and P.S. McIntyre, Modern Infrared Spectroscopy, John Wiley & Sons, New York, 1996.

3. Suzuki, E.M., Forensic Applications of Infrared Spectroscopy, in *Forensic Science Handbook, Volume III*, edited by R. Saferstein, Prentice-Hall, New York, 1993, pp. 71-195.

4. Bartick, E.G., and M.W. Tungol, Infrared Microscopy and Its Forensic Applications, in *Forensic Science Handbook, Volume III*, edited by R. Saferstein, Prentice-Hall, New York, 1993, pp. 196-252.

5. Compton, S., and J. Powell, Forensic Applications of IR Microscopy, *American Laboratory* 23:41-51 (1991).

6. Roux, C., P. Maynard, and M. Dawson, FTIR Spectroscopy Applications in Forensic Science, *Chemistry in Australia* 66:11-15 (1999).

7. Bartick, E.G., Applications of Vibrational Spectroscopy in Criminal Forensic Analysis, in *Handbook of Vibrational Spectroscopy*, edited by J.M. Chalmers and P.R. Griffiths, John Wiley & Sons Ltd, Chichester, 2002, pp. 2993-3004.

8. Stoecklein, W., and M. Gloger, FT-Infrared Spectroscopy of Automobile Paints Using Infrared Microscopy, *FT-IR Spectral Lines* 9:2 (1988).

9. Wilkinson, J., J. Locke, and D. Lang, The Examination of Paints as Thin Sections Using Visible Microspectroscopy and Fourier Transform Infrared Microscopy, *Forensic Science International* 38:43-52 (1988).

10. Suzuki, E.M., Forensic Science Applications of Diffuse Reflectance Infrared Fourier Transform Spectroscopy (DRIFTS). IV. Direct Analysis of Metallic Paints - Sampling Considerations, *Journal of Forensic Sciences* 34:164-179 (1989).

11. Ryland, S., Infrared Microspectroscopy of Forensic Paint Evidence, in *Practical Guide to Infrared Microspectroscopy*, edited by H. Humecki, Marcel Dekker, inc., New York, 1995, pp. 163-243.

12. Zieba-Palus, J., Application of Transmittance and Reflectance FT-IR Microscopy to Examination of Paints Transferred Onto Fabrics, *Mikrochimica Acta, Supplement* 14:361-362 (1997).

13. Beveridge, A., T. Fung, and D. MacDougall, Use of Infrared Spectroscopy for the Characterisation of Paint Fragments, in *Forensic Examination of Glass and Paint*, edited by B. Caddy, Taylor & Francis, Inc., 2001.

14. Grieve, M.C., J. Dunlop, and T.M. Kotowski, Bicomponent Acrylic Fibers - Their Characterization in the Forensic Science Laboratory, *Journal of the Forensic Science Society* 28:25-33 (1988).

15. Grieve, M.C., Fibres and Their Examination in Forensic Science, in *Forensic Science Progress*, edited by A. Maehly and R.L. Williams, Springer-Verlag, Berlin, Heidelberg, New York, 1990, pp. 41-125.

16. Tungol, M.W., E.G. Bartick, and A. Montaser, Analysis of Single Polymer Fibres by Fourier Transform Infrared Microscopy: The Results of Case Studies, *Journal of Forensic Sciences* 36:1027-1043 (1991).

17. Grieve, M., Another Look at the Classification of Acrylic Fibres, Using FTIR Microscopy, *Science & Justice* 35:179-190 (1995).

18. Tungol, M.W., E.G. Bartick, and A. Montaser, Forensic Examination of Synthetic Textile Fibers by Microscopic Infrared Spectrometry, in *Practical Guide to Infrared Microspectroscopy*, edited by H.J. Humecki, Marcel Dekker Inc., New York, 1995, pp. 245-285.

19. Kirkbride, K.P., and M.W. Tungol, Infrared Microspectroscopy of Fibres, in *Forensic Examination of Fibres*, edited by J. Robertson and M. Grieve, Taylor & Francis, 1999, pp. 179-222.

20. Suzuki, E.M., Fourier Transform Infrared Analysis of Some Particulate Drug Mixtures Using a Diamond Anvil Cell with a Beam Condenser and an Infrared Microscope, *Journal of Forensic Sciences* 37:467-487 (1992).

21. Wielbo, D., and I.R. Tebbett, The Use of Microcrystal Tests in Conjunction with Fourier Transform Infra Red Spectroscopy for the Rapid Identification of Street Drugs, *Journal of Forensic Sciences* 37:1134-1148 (1992).

22. Zitrin, S., Analysis of Explosives by Infrared Spectrometry and Mass Spectrometry, in *Forensic Investigation of Explosives*, edited by A. Beveridge, Taylor & Francis, London, 1998, pp. 267-314.

23. Merrill, R.A., E.G. Bartick, and W.D. Mazzella, Studies of Techniques for Analysis of Photocopy Toners by IR, *Journal of Forensic Sciences* 41:264-271 (1996).

24. Andrasko, J., Microreflectance FTIR Techniques Applied to Materials Encountered in Forensic Examination of Documents, *Journal of Forensic Sciences* 41:812-823 (1996).

25. Kher, A., M. Mulholland, B. Reedy, and P. Maynard, Classification of Document Papers by Infrared Spectroscopy and Multivariate Statistical Techniques, *Applied Spectroscopy* 55:1192-1198 (2001).

26. Wang, J., S. Sun, and G. Luo, Examination of Blue Ball Point Writing Ink by Micro ATR Technology, in *Proceedings of the 57th Annual Meeting of the American Society of Questioned Document Examiners (ASQDE)*, Los Angeles, 1999.

27. Wang, J., G. Luo, S. Sun, Z. Wang, and Y. Wang, Systematic Analysis of Bulk Blue Ballpoint Pen Ink by FTIR Spectrometry, *Journal of Forensic Sciences* 46:1093-1097 (2001).

28. Merrill, R.A., and E.G. Bartick, Analysis of Ball Point Pen Inks by Diffuse Reflectance Infrared Spectrometry, *Journal of Forensic Sciences* 37:528-541 (1992).

29. Lennard, C.J., and W.D. Mazella, A Simple Combined Technique for the Analysis of Toners and Adhesives, *Journal of the Forensic Science Society* 31:365 - 371 (1991).

30. Merrill, R.A., and E.G. Bartick, Analysis of Pressure Sensitive Adhesive Tape: 1. Evaluation of Infrared ATR Accessory Advances, *Journal of Forensic Sciences* 45:93-98 (2000).

31. Cox, R.J., H.L. Peterson, J. Young, C. Cusik, and E.O. Espinoza, The Forensic Analysis of Soil Organic by FTIR, *Forensic Science International* 108:107-116 (2000).

32. Kalasinsky, K.S., J. Magluilo, Jr., and T. Schaefer, Hair Analysis by Infrared Microscopy for Drugs of Abuse, *Forensic Science International* 63:253-260 (1993).

33. Kalasinsky, K.S., Drug Distribution in Human Hair by Infrared Microscopy, *Cellular and Molecular Biology* 44:81-87 (1998).

34. Coates, J., and J. Reffner, Have FTIR ... Will Travel, *Spectroscopy* 15:19 - 29 (2000).

35. Tahtouh, M., J. Kalman, C. Roux, C. Lennard, and B. Reedy, The Detection and Enhancement of Latent Fingermarks Using Infrared Chemical Imaging, *Journal of Forensic Sciences* 50:64-72 (2005).

36. Exline, D.L., C. Wallace, C. Roux, C. Lennard, M.P. Nelson, and P.J. Treado, Forensic Applications of Chemical Imaging: Latent Fingerprint Detection Using Visible Absorption and Luminescence, *Journal of Forensic Sciences* 48:1047-1053 (2003).

37. Reich, G., Potential of Attenuated Total Reflection Infrared and Near-Infrared Spectroscopic Imaging for Quality Assurance/Quality Control of Solid Pharmaceutical Dosage Forms, *Pharmazeutische Industrie* 64:870-874 (2002).

38. Treado, P.J., and M.P. Nelson, Raman Imaging, in *Handbook of Raman Spectroscopy From the Research Laboratory to the Process Line*, edited by I.R. Lewis and H.G.M. Edwards, Marcel Dekker Inc., New York, 2001, pp. 191-249.

39. Koenig, J.L., S.-Q. Wang, and R. Bhargava, FTIR Images, *Analytical Chemistry* 73:360A-369A (2001).

40. Newbury, D.E., C.E. Fiori, R.B. Marinenko, R.L. Myklebust, C.R. Swyt, and D.S. Bright, Compositional Mapping with the Electron Probe Microanalyzer: Part I, *Analytical Chemistry* 62:1159A (1990).

41. Newbury, D.E., R.B. Marinenko, R.L. Myklebust, and D.S. Bright, Quantitative Compositional Mapping with the Electron Probe Microanalyzer, *Electron Probe Quantitation*:335-369 (1991).

42. Payne, G., B. Reedy, C. Lennard, B. Comber, D. Exline, and C. Roux, A Further Study to Investigate the Detection and Enhancement of Latent Fingerprints Using Visible Absorption and Luminescence Chemical Imaging, *Forensic Science International* 150:33-51 (2005).

43. Payne, G., C. Wallace, B. Reedy, C. Lennard, R. Schuler, D. Exline, and C. Roux, Visible and Near-Infrared Chemical Imaging Methods for the Analysis of Selected Forensic Samples, *Talanta* 67:334-344 (2005).

44. Exline, D.L., M.P. Nelson, and P.J. Treado, Forensic Examination of Synthetic Fibers Using Raman Chemical Imaging, in *52nd Pittsburgh Conference on Analytical Chemistry and Applied Spectroscopy*, New Orleans, LA, 2001.

45. Wolfe, J., and D.L. Exline, Characterization of Condom Lubricant Components Using Raman Spectroscopy and Raman Chemical Imaging, *Journal of Forensic Sciences* 48:1065-1074 (2003).

46. Chan, K.L.A., S.G. Kazarian, A. Mavraki, and D.R. Williams, Fourier Transform Infrared Imaging of Human Hair with a High Spatial Resolution Without the Use of a Synchrotron, *Applied Spectroscopy* 59:149 - 155 (2005).

47. Bhargava, R., B.G. Wall, and J.L. Koenig, Comparison of the FT-IR Mapping and Imaging Techniques Applied to Polymeric Systems, *Applied Spectroscopy* 54:470-479 (2000).

48. Wilson, J., Infrared Imaging: An Advance in Infrared Microscopy, *American Laboratory News* 34:10-12 (2002).

49. Miseo, E.V., and N.A. Wright, Developing a Chemical-Imaging Camera, *The Industrial Physicist* 9:29-32 (2003).

50. Kidder, L.H., A.S. Haka, and E.N. Lewis, Instrumentation for FT-IR Imaging, in *Handbook of Vibrational Spectroscopy* edited by J.M. Chalmers and P.R. Griffiths, John Wiley & Sons Ltd, Chichester, UK, 2002, pp. 1386-1404.

51. Lewis, E.N., and I.W. Levin, Real-Time, Mid-Infrared Spectroscopic Imaging Microscopy Using Indium Antimonide Focal-Plane Array Detection, *Applied Spectroscopy* 49:672-678 (1995).

52. Griffiths, P.R., and J.A. de Haseth, Fourier Transform Infrared Spectrometry, John Wiley & Sons, Inc., Hoboken, New Jersey, 2007.

53. Chan, K.L.A., and S.G. Kazarian, New Opportunities in Micro- and Macro-Attenuated Total Reflection Infrared Spectroscopic Imaging: Spatial Resolution and Sampling Versatility, *Applied Spectroscopy* 57:381-389 (2003).

54. Marcott, C., and R.C. Reeder, Industrial Applications of FT-IR Microspectroscopic Imaging Using a Mercury-Cadmium-Telluride Focal-Plane Array Detector, *Proceedings of SPIE-The International Society for Optical Engineering* 3436:285-289 (1998).

55. Chalmers, J.M., N.J. Everall, M.D. Schaeberle, I.W. Levin, E. Neil Lewis, L.H. Kidder, J. Wilson, and R. Crocombe, FT-IR Imaging of Polymers: An Industrial Appraisal, *Vibrational Spectroscopy* 30:43-52 (2002).

56. Kidder, L.H., V.F. Kalasinsky, J.L. Luke, I.W. Levin, and E.N. Lewis, Visualization of Silicone Gel in Human Breast Tissue Using New Infrared Imaging Spectroscopy, *Nature Medicine* 3:235-237 (1997).

57. Lasch, P., W. Haensch, D. Naumann, and M. Diem, Imaging of Colorectal Adenocarcinoma Using FT-IR Microspectroscopy and Cluster Analysis, *Biochimica et Biophysica Acta* 1688:176-186 (2004).

58. Kidder, L.H., A.S. Haka, P.J. Faustino, D.S. Lester, I.W. Levin, and E.N. Lewis, Infrared Spectroscopic Imaging as a Tool for Pathology, *Proceedings of SPIE-The International Society for Optical Engineering* 3257:178-186 (1998).

59. Buice, R., L. Cassis, and R. Lodder, Near-IR and IR Imaging in Lipid Metabolism and Obesity, *Cellular and Molecular Biology* 44:53-64 (1998).

60. Chan, K.L.A., S.V. Hammond, and S.G. Kazarian, Applications of Attenuated Total Reflection Infrared Spectroscopic Imaging to Pharmaceutical Formulations, *Analytical Chemistry* 75:2140-2146 (2003).

61. Kazarian, S.G., and K.L.A. Chan, Applications of ATR-FTIR Spectroscopic Imaging to Biomedical Samples, *Biochimica et Biophysica Acta* 1758:858-867 (2006).

62. Atti, E., S. Gomez, S.M. Wahl, R. Mendelsohn, E. Paschalis, and A.L. Boskey, Effects of Transforming Growth Factor-Beta Deficiency on Bone Development: A Fourier Transform-Infrared Imaging Analysis., *Bone* 31:675-684 (2002).

63. Marcott, C., R.C. Reeder, J.A. Sweat, D.D. Panzer, and D.L. Wetzel, FT-IR Spectroscopic Imaging Microscopy of Wheat Kernels Using a Mercury-Cadmium-Telluride Focal-Plane Array Detector, *Vibrational Spectroscopy* 19:123-129 (1999).

64. Van der Weerd, J., H. Brammer, J.J. Boon, and R.M.A. Heeren, Fourier Transform Infrared Microscopic Imaging of an Embedded Paint Cross-Section, *Applied Spectroscopy* 56:275-283 (2002).

65. Bhargava, R., and I.W. Levin, editors, Spectrochemical Analysis Using Infrared Multichannel Detectors, Blackwell Publishing Ltd, Oxford, UK, 2005.

66. Bartick, E.G., R. Schwartz, R. Bhargava, M. Schaeberle, D. Fernandez, and I.W. Levin, Spectrochemical Analysis and Hyperspectral Imaging of Latent Fingerprints, in *Proceedings of the 16th Meeting of the International Association of Forensic Sciences; 2002 September 2-7*, edited by E. Baccino, Monduzzi Editore, Bologna, Italy., Montpellier, France, 2002, pp. 61-64.

67. Bartick, E.G., R. Schwartz, R. Bhargava, M. Schaeberle, D. Fernandez, and I.W. Levin, Spectral Imaging of Latent Fingerprints, in *The Federation of Analytical Chemistry and Spectroscopy Societies, 29th Annual FACSS Meeting*, Providence, RI., 2002.

68. Botonjic, E., and C.W. Brown, Mid and Near-IR Spectral Comparison of Vein and Capillary Bloodstains, in *54th Pittsburgh Conference on Analytical Chemistry and Applied Spectroscopy*, Orlando, 2003.

69. Brown, C.W., S.W. Huffman, E. Botonjic, and M. Lamatagne, Spectra and Multispectral Images of Bloodstains, in *53rd Pittsburgh Conference on Analytical Chemistry and Applied Spectroscopy*, New Orleans, 2002.

70. Brown, C., and E. Botonjic, Moving Multispectral Image Data to Practical Solutions in the Forensic Laboratory, in *54th Pittsburgh Conference on Analytical Chemistry and Applied Spectroscopy*, Orlando, 2003.

71. Crane, N.J., E.G. Bartick, R. Schwartz Perlman, and S. Huffman, Infrared Spectroscopic Imaging for Noninvasive Detection of Latent Fingerprints, *Journal of Forensic Sciences* 52:48-53 (2007).

72. Tahtouh, M., P. Despland, R. Shimmon, J.R. Kalman, and B.J. Reedy, The Application of Infrared Chemical Imaging to the Detection and Enhancement of

Latent Fingerprints: Method Optimization and Further Findings, *Journal of Forensic Sciences* 52:1089 - 1096 (2007).

73. Ricci, C., K.L.A. Chan, and S.G. Kazarian, Combining the Tape-Lift Method and Fourier Transform Infrared Spectroscopic Imaging for Forensic Applications, *Applied Spectroscopy* 60:1013 - 1021 (2006).

74. Ricci, C., S. Bleay, and S.G. Kazarian, Spectroscopic Imaging of Latent Fingermarks Collected with the Aid of a Gelatin Tape, *Analytical Chemistry* 79:5771 - 5776 (2007).

75. Ricci, C., P. Phiriyavityopas, N. Curum, K.L.A. Chan, S. Jickells, and S.G. Kazarian, Chemical Imaging of Latent Fingerprint Residues, *Applied Spectroscopy* 61:514 - 522 (2007).

76. Chan, K.L.A., and S.G. Kazarian, Detection of Trace Materials with Fourier Transform Infrared Spectroscopy Using a Multi-Channel Detector, *The Analyst* 131:126-131 (2006).

77. Ricci, C., L. Nyadong, F.M. Fernandez, P.N. Newton, and S.G. Kazarian, Combined Fourier-Transform Infrared Imaging and Desorption Electrospray-Ionisation Linear Ion-Trap Mass Spectrometry for Analysis of Counterfeit Antimalarial Tablets, *Analytical and Bioanalytical Chemistry* 387:551-559 (2007).

78. Polsky, C.H., and E.V. Valkenburg, The Diamond Anvil Cell, in *Handbook of Vibrational Spectroscopy* edited by J.M. Chalmers and P.R. Griffiths, John Wiley & Sons Ltd, Chichester, UK, 2002, pp. 1352 - 1360.

79. Reffner, J.A., and P.A. Martoglio, Uniting Microscopy and Spectroscopy, in *Practical Guide to Infrared Microspectroscopy*, edited by E.G. Brame, Marcel Dekker Inc., New York, 1995, pp. 41-84.

80. Kazarian, S.G., and K.L.A. Chan, "Chemical Photography" of Drug Release, *Macromolecules* 36:9866 - 9872 (2003).

81. Scientific Working Group on Materials Analysis (SWGMAT) Forensic Paint Analysis and Comparison Guidelines *Forensic Science Communications* 1 (1999).

82. Percy, R., and R. Audette, Automotive Repaints: Just a New Look?, *Journal of Forensic Sciences* 25:189-239 (1980).

83. McEwen, D.J., and G.D. Cheever, Infrared Microscopic Analysis of Multiple Layers of Automotive Paints, *Journal of Coatings Technology* 65:35 - 41 (1993).

84. Allen, T.J., Paint Sample Presentation for Fourier Transform Infrared Microscopy, *Vibrational Spectroscopy* 3:217-237 (1992).

85. Tweed, F.T., R. Cameron, J.S. Deak, and P.G. Rodgers, The Forensic Microanalysis of Paints, Plastics and Other Materials by an Infrared Diamond Cell Technique, *Forensic Science* 4:211-218 (1974).

86. Derrick, M.R., Infrared Microspectroscopy in the Analysis of Cultural Artifacts, in *Practical Guide to Infrared Microspectroscopy*, edited by H. Humecki, Marcel Dekker, Inc., New York, 1995, pp. 286-322.

87. Petraco, N., and F. Gale, A Rapid Method for Cross-Sectioning of Multilayered Paint Chips, *Journal of Forensic Sciences* 29:597-600 (1984).

88. Cartwright, L., N. Cartwright, and P. Rodgers, A Microtome Technique for Sectioning Multilayer Paint Samples for Microanalysis, *Canadian Society of Forensic Science Journal* 10:7-12 (1977).

89. Chang, W.-T., T.-H. Chen, C.-C. Yu, and J.-Y. Kau, Comparison of Embedding Methods Used in Examining Cross-Sections of Automotive Paints with

Micro-Fourier Transform Infrared Spectroscopy, *Forensic Science Journal* 1:55-60 (2002).

90. Van der Weerd, J., R.M.A. Heeren, and J.J. Boon, Preparation Methods and Accessories for the Infrared Spectroscopic Analysis of Multi-Layer Paint Films, *Studies In Conservation* 49:193-210 (2004).

91. Nieznanska, J., J. Zieba-Palus, and P. Koscielniak, Physico-Chemical Study of Car Paints Coats, *Z Zagadnien Nauk Sadowych* 39:77-94 (1999).

92. Zieba-Palus, J., Selected Cases of Forensic Paint Analysis, *Science & Justice* 39:123-127 (1999).

93. Gothard, J., and P. Maynard, Evidential Value of Automotive Paint, in *Proceedings 13th International Symposium of the ANZFSS*, Sydney, 1996.

94. Woods, B., Personal Communication, Chemical Criminalist, Australian Federal Police, 2004.

95. Van der Weerd, J., Microspectroscopic Analysis of Traditional Oil Paint, PhD Thesis, University of Amsterdam, Amsterdam, 2002, p. 178.

96. Richards, J.A., and X. Jia, Remote Sensing Digital Image Analysis, Springer-Verlag, Berlin, 1999.

97. Brereton, R.G., Chemometrics: Data Analysis for the Laboratory and Chemical Plant, John Wiley, Chichester, 2003.

98. Lasch, P., Cytospec Software Manual, http://www.cytospec.com.

99. http://las.perkinelmer.com/News/News+Details/11142006.htm (accessed 02/01/2008).

100. Zapletalova, T., Introduction to Bicomponent Fibers, *International Fiber Journal* 13:20-24 (1998).

101. www.fibersource.com (accessed 20/1/05).

102. Miller, H., Keeping FIT with Bicomponents: Cha's Fiber Innovation Technology Fills Niche in Specialty Fibers, *International Fiber Journal* 13:44-47 (1998).

103. Thoennessen, F., and J. Dahringer, Trevira Bicomponent Fibers for Nonwovens, *Chemical Fibers International* 53:422-425 (2003).

104. Cho, L., J.A. Reffner, B.M. Gatewood, and D.L. Wetzel, Single Fiber Analysis by Internal Reflection Infrared Microspectroscopy, *Journal of Forensic Sciences* 46:1309-1314 (2001).

105. Tungol, M.W., E.G. Bartick, and A. Montaser, The Development of a Spectral Data Base for the Identification of Fibers by Infrared Microscopy, *Applied Spectroscopy* 44:543-549 (1990).

106. Nelson, W.G., and J.L. Woods, An Effective Method for Mounting Fibres to Allow Simple Processing, Embedding and Alignment for Sectioning, *Journal of Microscopy* 181:88-90 (1996).

107. Miyakawa, M., Method for Removing Interference Spectra in FT-IR Microspectroscopy, *Bunseki Kagaku* 43:57-60 (1994).

108. Sommer, A.J., L.G. Tisinger, C. Marcott, and G.M. Story, Attenuated Total Internal Reflection Infrared Mapping Microspectroscopy Using an Imaging Microscope, *Applied Spectroscopy* 55:252-256 (2001).

109. Yang, J.C., M.J. Jablonsky, and J.W. Mays, NMR and FT-IR Studies of Sulfonated Styrene-Based Homopolymers and Copolymers, *Polymer* 43:5125-5132 (2002).

110. Kihara, Y., Nonwoven Fabric Made of Core/Sheath Type Composite Fiber and Process for Producing the Same, Japan Patent WO2004035900 (2004).

111. Hilton, O., Scientific Examination of Questioned Documents, C.R.C Press, Boca Raton, Florida, 1982.

112. Brunelle, R.L., Questioned Document Examination, in *Forensic Science Handbook*, edited by R. Saferstein, Prentice-Hall, Inc., New Jersey, 1982, pp. 672-725.

113. Ellen, D., Scientific Examination of Documents: Methods and Techniques, CRC Press, Taylor and Francis Group, Boca Raton, FL, 2006.

114. Lindblom, B.S., Pens and Pencils, in *Scientific Examination of Questioned Documents*, edited by J.S. Kelly and B.S. Lindblom, CRC Press, Taylor & Francis Group, Boca Raton, FL, 2006, pp. 147-158.

115. Andreottola, M.A., Basic Ink Jet Technology: A Tutorial on the Method Behind Ink Jet Printing, *International Journal of Forensic Document Examiners* 5:285-289 (1999).

116. Flynn, W.J., The Examination of Computer-Generated Documents, in *Scientific Examination of Questioned Documents*, edited by J.S. Kelly and B.S. Lindblom, Taylor & Francis Group, CRC Press, Boca Raton, FL, 2006, pp. 191-216.

117. Totty, R.N., Analysis and Differentiation of Photocopy Toners, *Forensic Science Review* 2:2-23 (1990).

118. Poulin, G., Establishing the Sequence of Strokes: The State of the Art, *International Journal of Forensic Document Examiners* 2:16-32 (1996).

119. Kasas, S., A. Khanmy-Vital, and G. Dietler, Examination of Line Crossings by Atomic Force Microscopy, *Forensic Science International* 119:290-298 (2001).

120. Villanova, Establishing the Sequence of Superimposed Lines, *International Criminal Police Review* 24:214-220 (1969).

121. Hart, L.J., and B.B. Carney, Typewriting Versus Writing Instrument: A Line Intersection Problem, *Journal of Forensic Sciences* 34:1329-1335 (1989).

122. Planty, M.G., Determining the Relative Chronology of Intersecting Ball-Point Pen Lines and Laser Printed Document Marks - Linton Godown Revisited, *International Journal of Forensic Document Examiners* 3:31-34 (1997).

123. Radley, R.W., Determination of Sequence of Ballpoint Pen Writing Utilising Infrared Luminescence Techniques, *Journal of the Forensic Science Society* 22:373-375 (1982).

124. Strach, S.J., Establishing the Sequence of Intersecting Ball-Point Pen Strokes, *Forensic Science* 11:67-74 (1982).

125. Leung, S., and Y. Leung, A Systematic Study of the Lifting Techniques for Determining the Writing Sequence of Intersecting Ball Pen Strokes, *Science & Justice* 37:197-206 (1997).

126. Igoe, T.J., and B.L. Reynolds, A Lifting Process for Determining the Writing Sequence of Two Intersecting Ballpoint Pen Strokes, *Forensic Science International* 20:201-205 (1982).

127. Godown, L., Recent Developments in Writing Sequence Determination, *Forensic Science International* 20:227-232 (1982).

128. Waeschle, P.A., Examination of Line Crossing by Scanning Electron Microscopy, *Journal of Forensic Sciences* 24:569-578 (1979).

129. Baier, P.E., Technical Improvements of Scanning Electron Microscope Methods in Document Examination, *Forensic Science International* 22:265-278 (1983).

130. Nolan, P.J., M. England, and C. Davies, The Examination of Documents by S.E.M. and X-Ray Spectrometry *Scanning Electron Microscopy* 2:599-610 (1982).

131. Blueschke, A., and A. Lacis, Examination of Line Crossings by Low KV Scanning Electron Microscopy (SEM) Using Photographic Stereoscopic Pairs, *Journal of Forensic Sciences* 41:80-85 (1996).

132. Tollkamp, S., and H.G. Fackler, Use of Low Voltage SEM in the Detection of Forgeries, *International Journal of Forensic Document Examiners* 2:333-341 (1996).

133. Mathyer J, and P. R., The Determination of Sequence of Crossing Strokes by the 'Kromekote' Paper Lifting Process and by the Scanning Electron Microscope Method, *Forensic Science International* 24:113-124 (1984).

134. Koons, R.D., Sequencing of Intersecting Lines by Combined Lifting Process and Scanning Electron Microscopy, *Forensic Science International* 27:261-276 (1985).

135. Stitt, J., The Examination of Line Crossings by Environmental Scanning Electron Microscopy and Atomic Force Microscopy, Honours Thesis, Department of Chemistry, Materials and Forensic Sciences, University of Technology, Sydney, 2002, p. 105.

136. Stitt, J., M. Phillips, J. Brandi, and C. Roux, The Examination of Line Crossings by Environmental Scanning Electron Microscopy and Atomic Force Microscopy, in *Proceedings of the 3rd European Academy of Forensic Science*

Meeting, edited by P. Saukko, Forensic Science International, Istanbul, Turkey, 2003, p. 81.

137. Gal, T., J. Sandor, and A. Karoly, Determining the Sequence of Crossed Lines by FT-IR-ATR-Microscopy, in *Global Forensic Science Today*, 2007, pp. 8-11.

138. Spagnolo, G.S., Potentiality of 3D Laser Profilometry to Determine the Sequence of Homogeneous Crossing Lines of Questioned Documents, *Forensic Science International* 164:102-109 (2006).

139. Claybourn, M., and M. Ansell, Using Raman Spectroscopy to Solve Crime: Inks, Questioned Documents and Fraud, *Science & Justice: Journal of the Forensic Science Society* 40:261-271 (2000).

140. Fabianska, E., and M. Kunicki, Raman Spectroscopy as a New Technique for Determining the Sequence of Intersecting Lines, *Z Zagadnien Nauk Sadowych* 53:60-73 (2003).

141. He, A., D. Karpuzov, and S. Xu, Ink Identification by Time-of-Flight Secondary Ion Mass Spectroscopy, *Surface and Interface Analysis* 38:854-858 (2006).

142. Merrill, R.A., E.G. Bartick, and H.J. Taylor, III, Forensic Discrimination of Photocopy and Printer Toners. I. The Development of an Infrared Spectral Library, *Analytical and Bioanalytical Chemistry* 376:1272-1278 (2003).

143. Bartick, E.G., M.W. Tungol, and J.A. Reffner, A New Approach to Forensic Analysis With Infrared Microscopy: Internal Reflection Spectroscopy, *Analytica Chimica Acta* 288:35-42 (1994).

144. LaPorte, G.M., and R.S. Ramotowski, The Effects of Latent Print Processing on Questioned Documents Produced by Office Machine Systems Utilizing Inkjet Technology and Toner, *Journal of Forensic Sciences* 48:658-663 (2003).

145. Kemp, G.S., and R.N. Totty, The Differentiation of Toners Used in Photocopy Processes by Infrared Spectroscopy, *Forensic Science International* 22:75-83 (1983).

146. Bhagvati, C., and D. Haritha, Classification of Liquid and Viscous Inks using HSV Colour Space, in *Eighth International Conference on Document Analysis and Recognition*, Seoul, Korea, 2005, pp. 660-664.

147. Bojko, K., C. Roux, and B.J. Reedy, An Examination of the Sequence of Intersecting Lines using Attenuated Total Reflectance-Fourier Transform Infrared Spectral Imaging, *Accepted for Publication in Journal of Forensic Sciences* (2008).

148. Flynn, K., R. O'Leary, C. Lennard, C. Roux, and B.J. Reedy, Forensic Applications of Infrared Chemical Imaging: Multi-Layered Paint Chips, *Journal of Forensic Sciences* 50:832-841 (2005).

149. Flynn, K., R. O'Leary, C. Roux, and B.J. Reedy, Forensic Analysis of Bicomponent Fibers Using Infrared Chemical Imaging, *Journal of Forensic Sciences* 51:586-596 (2006).

150. Walker, S., Detection of Illicit Substances in Fingerprints by Infrared Chemical Imaging, Honours Thesis, Department of Chemistry, Materials and Forensic Sciences, University of Technology, Sydney, 2006, p. 91.

151. Ng, P.H.R., Methods for the Detection of Illicit Substances in Fingerprints by Infrared Chemical Imaging, Honours Thesis, Department of Chemistry, Materials and Forensic Sciences, University of Technology, Sydney, 2007, p. 121.